INHIBITION OF EUKARYOTIC TRANSLATION ELONGATION BY THE ANTITUMOR NATURAL PRODUCT AGELASTATIN A

by

Brandon T. McClary

A dissertation is submitted to the Johns Hopkins University in conformity with the requirements for the degree of Doctor of Philosophy

Baltimore, MD

October, 2016

Abstract

The goal of my PhD thesis research was to identify new potent and specific inhibitors of untargeted proteins that can be used as tools to study biology and serve as starting points for the development of new drugs down the road. I decided to focus on a recently discovered antitumor natural product known as agelastatin A (AglA), derived from the marine sponge *Agelas dendromorpha*. Using a systematic approach, I show that AglA selectively inhibits protein synthesis. Protein synthesis plays an essential role in cell growth and survival, especially in fast-proliferating cancer cells. Several inhibitors of eukaryotic protein synthesis have entered the clinical stage, establishing translation as a promising target for chemotherapy.

I have verified the inhibition of translation elongation by [^{35}S]-methionine labeling experiments, an *in vitro* HCV IRES dual luciferase assay, and a stress granule formation assay. AglA was found to act at an early stage of translation elongation, inhibiting dipeptide bond formation. Based on these findings, we predicted that AglA disrupts peptide bond formation by binding to the peptidyl transfer center (PTC) of the ribosome. Using a new chemical footprinting method, we initially identified the AglA to ribosomal A-site proximal to the C2821 25S rRNA residue in the 60S ribosomal subunit. X-ray crystallography was used to determine a high-resolution structure of 80S ribosomes from *Saccharomyces cerevisiae* in complexes with AglA, which validated the binding site originally determined by chemical footprinting. Not only is this promising for the discovery of new cancer therapeutics; perturbation of translation by AglA will provide further mechanistic insight into the eukaryotic ribosome and its components. In the future, we hope that these insights will establish further contrasts between prokaryotic ribosomes, contributing to greater promise of newly synthesized antibiotics.

Ph.D. DISSERTATION REFEREES FOR BRANDON MCCLARY

Dr. Jun O. Liu, Professor of Pharmacology and Oncology, Pharmacology and Molecular Sciences, Johns Hopkins School of Medicine (faculty sponsor)

Dr. Philip A. Cole, Director and Professor, Pharmacology and Molecular Sciences, Johns Hopkins School of Medicine (reader)

Acknowledgements

I would first like to thank my thesis adviser Dr. Jun Liu for giving me the opportunity to work in his laboratory. His cheerful attitude and excitement about new data is extremely refreshing and made it easy to work for him. I will always admire his strong enthusiasm for science, which constantly motivated me throughout my time in the lab. On the intellectual front, Dr. Liu has helped me to become a strong independent researcher by granting me complete freedom to design my own experiments, execute them and interpret the data before bringing it forth to him. I would like to thank the Pharmacology Department for support, and also the Biochemistry, Cellular, and Molecular Biology (BCMB) Program for believing in my potential, and extending the offer to come to the Johns Hopkins University for my graduate studies.

I would also like to thank the current and former members of the Liu laboratory for their help with this project and creating a great working environment in the laboratory. Many people within our laboratory aided my work, in particular Dr. Yongjun Dang, who previously worked with several translation inhibitors and provided helpful advice during the initial efforts of determining the molecular mechanism of Agelastatin A. I was fortunate to have a talented synthetic chemist, Dr. Daniel Romo from Baylor University as a close collaborator of this project; his former members Drs. JC Reyes and Morgan Jouanneau made a number of interesting synthetic analogs of Agelastatin for its SAR studies, which formed the foundation of my project. Completion of this project would have never been possible without the help of Dr. Rachel Green and the members of her lab Anthony Schuller and Dr. Boris Zinshteyn, who performed translation assays for monitoring the formation di-peptides and a novel assay for determining the binding site of Agelastatin within the ribosome, respectively. More helpful advice was provided by Drs. Philip Cole, Hal Dietz, and Jon Lorsch who served on my thesis committee.

I would like to thank the Meyerhoff Scholarship Program. My scientific journey was hugely impacted in the spring of 2006 when I received a large red envelope in the mail, notifying me of my acceptance into the Meyerhoff Scholarship Program at the University of Maryland, Baltimore County (UMBC). The program supports students who have interests in the STEM fields, with a focus on the advancement of underrepresented minorities in the sciences. After every Meyerhoff meeting, UMBC President Dr. Freeman Hrabowski reminded us of the importance of persistence, asking students to recite the Langston Hughes poem expressing that sentiment:

Hold fast to dreams,
For if dreams die
Life is a broken-winged bird
That cannot fly.
Hold fast to dreams,
For when dreams go
Life is a barren field
Frozen with snow.

-Langston Hughes

Remembering these words helped me push through during challenging times along my graduate school journey. Without the support of the Meyerhoff Program, I am not sure that I would be embarking on a career in biomedical sciences today.

To all my friends, I am grateful for the fact that there are too many names to list here, and I thank you for your emotional support, encouragement, and nights in Baltimore that I will never forget. Last but far from least, I would like to thank my family for their constant love and support throughout my life. Thank you for always being my personal cheerleaders.

Table of Contents

List of Figures

Chapter 1. Introduction

This thesis interpolates material from a paper by the author. Chapter 2 uses material from Jouanneau et al., 2016. Chapter 3 uses material from an unpublished manuscript. Some material from each of these sources has been incorporated into this introductory chapter.

Defined broadly, natural products are chemical compounds produced by biological sources including plants, animals, and microorganisms. Due to their biological activity, many natural products serve as the active components of traditional medicines and offer therapeutic benefit in treating diseases, particularly in cancer and microbial infection (Koehn and Carter, 2005). Historically, many drugs and bioactive small molecules, particularly natural products, were discovered based on their ability to exert pharmacological effects at the cellular or whole organismal level. Currently, the targets of many widely used drugs and bioactive natural products have been identified, leading to a deeper understanding of the physiological functions of the newly identified protein targets and opening gateways to the subsequent studies of the corresponding cellular processes.

In attempts to obtain new chemically diverse compounds that will be analyzed and evaluated in drug discovery bioassay screens, researchers travel around the world to biologically diverse environments and collect samples of microorganisms or plants. A crude extract from any one of these natural sources typically contains a range of structurally diverse and often novel chemical compounds with biological activity. Following isolation, purification, and identification through determination of the chemical structures, the active compounds can evolve to become discovery "leads." Indeed, some current medicines have been developed directly from those leads.

The approach of producing immense numbers of synthetic compounds by

combinatorial chemistry has largely failed in offering sufficient candidate compounds for developing new drugs (Ortholand and Ganesan, 2004) . The difficulties with these large synthetic libraries may also reflect on another advantage of molecules derived from natural sources: production of secondary metabolites requires a significant investment of energy and resources for the organism, but this investment becomes worthwhile when it creates a selective benefit to the host organism. For this very reason, natural product collections are essentially evolutionarily pre-screened, enhancing the likelihood of finding interesting compounds. This has an advantage in that they are novel compounds, but the chemical complexity also makes the synthesis of such compounds difficult. Instead, the compound may need to be extracted from its natural source, which can many times be a labor intensive, expensive and inefficient process. As a result, there is an advantage in designing simpler analogues. Fortunately, with the emergence of molecular technology, it is now possible to isolate the biosynthetic machinery responsible for natural product production. Furthermore, some synthetic analogs of natural products with improved potency and safety can be prepared through total/semisynthesis. This allows natural products to successfully serve as starting points for drug discovery (Beghyn et al., 2008; Hunter, 2008; Koehn and Carter, 2005), although, as discussed in Chapter 2, slight alterations of structures of natural products can also drastically alter their mechanisms and effects.

Agelastatin A

The majority of the current natural product-derived therapeutics has terrestrial origins. However, mining novel sources, such as the marine environment, is clearing the way for chemical and biological novelties as well. Recently, marine natural products have served as valuable sources for novel drugs (Montaser and Luesch, 2011). This project began with acquisition of marine natural products from the laboratory of Dr.

Daniel Romo at the Texas A & M, currently at Baylor University. One recently discovered antitumor natural product is the structurally unique brominated alkaloid Agelastatin A (AglA). Isolated from the marine sponge *Agelas dendromorpha* in 1993 from the coast of the Coral Sea, AglA belongs to the pyrrole-2-aminoimidazole alkaloid (PAI) family (D'Ambrosio et al., 1993). Since then, many efforts toward total synthesis of this natural product have been made (Dong, 2010a; Jouanneau et al., 2016; Reyes and Romo, 2012). AglA has shown potent activity against several human cancer cell lines (Han et al., 2013; Jouanneau et al., 2016; Stout et al., 2014). More recently, AglA and its analogues have displayed excellent blood-brain barrier penetration, making it an excellent candidate for brain cancer studies (Li et al., 2013). Previous reports identified AglA as an inhibitor of β-catenin, osteopontin-mediated malignant transformation, and glycogen synthase kinase-3β (Mason et al., 2008; Meijer et al., 2000). However, it remains unclear whether this inhibition is responsible for its underlying antiproliferative activity.

Target Identification of bioactive molecules

To identify the primary target of AglA, we took advantage of the two general target identification methods: the bottom-up and top-down approaches. The bottom-up approach, a target based approach, consists of methods that allow for the direct identification of a protein target using genetics or affinity based methods. We call this the "bottom-up" approach because the identification of a target protein serves as an initial base before building up to explain the phenotype through perturbation of the function of the target protein (Titov and Liu, 2012).

The top-down or phenotypic approach consists of methods that allow identification of the protein target by exploiting the existing knowledge of a given cellular process that is perturbed by a small molecule. We call this the "top-down" approach

because it allows one to systematically narrow down the possible targets based on a general understanding of cellular pathways that the small molecule perturbs, and the proteins known to be involved in the relevant processes (Titov and Liu, 2012).

This thesis will cover efforts to identify the primary target(s) of AglA using both bottom-up (Chapter 2) and top-down (Chapter 3) approaches.

Chapter 2. Derivatization of agelastatin A leading to bioactive analogs and a trifunctional probe

Introduction

(−)-Agelastatin A (**1**, AglA) is a tetracyclic member of the pyrrole-2-aminoimidazole alkaloid (PAI) family (Al-Mourabit et al., 2011; Forte et al., 2009). Since its isolation in 1993 by Pietra and co-workers from the sponge *Agelas dendromorpha* (D'Ambrosio et al., 1993; Guerriero et al., 1994), this family has grown to include six agelastatin congeners (A through F, Fig. 1a)(Hong et al., 1998; Tilvi et al., 2010). Weinreb (Stien et al., 1999) described the first total synthesis of AglA and since then several additional racemic (Domostoj et al., 2004; Duspara and Batey, 2013) and enantioselective (Movassaghi et al., 2010; Wehn and Du Bois, 2009) syntheses of AglA have been reported (Al-Mourabit et al., 2011; Dong, 2010b). Recently, Movassaghi developed an elegant and efficient bioinspired approach to AglA and all congeners that involved a late stage C4–C8 bond formation (Movassaghi et al., 2010). Our collaborator, Dr. Romo's group reported an alternative bioinspired approach that involved a final Npyrrole–C7 bond formation (Reyes and Romo, 2012). The reported bioactivities of this alkaloid are varied and include inhibition of β-catenin (Mason et al., 2008), suppression of osteopontin-mediated malignant transformation and inhibition of glycogen synthase kinase (Meijer et al., 2000). AglA and derivatives demonstrated good potency against 60 leukemia (Stout et al., 2014) and notably displayed excellent blood–brain barrier penetration (Li et al., 2013). These recent studies by Molinski and Yoshimitsu revealed that substitutions at C13 on the pyrrole ring are tolerated (Fig. 1c) with addition of a C13-trifluoromethyl and chloro substituent providing a marked increase in potency toward a leukemia and a breast cancer cell line, respectively. While AglA has been an attractive target for both synthetic and biological studies over two decades, a molecular level understanding of its effects in cells including cellular target(s) has not been described. Herein, we report expanded structure-activity relationship studies of agelastatin A

enabling the identification of an active chloro derivative and the design and synthesis of a bioactive, trifunctional cellular probe that could assist with cellular target identification.

Results

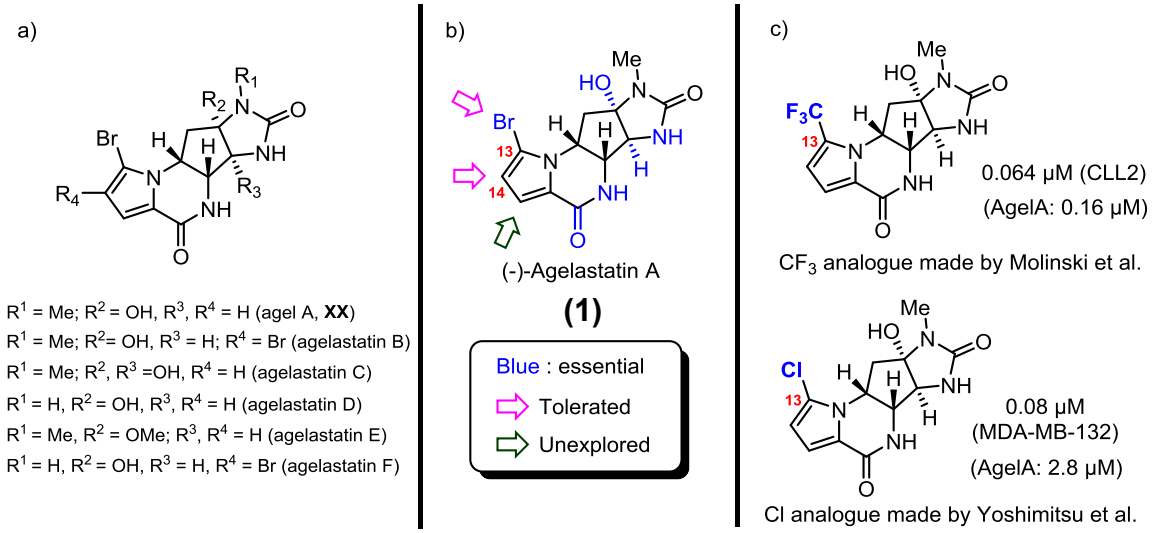

R^1 = Me; R^2 = OH, R^3, R^4 = H (agel A, **XX**)
R^1 = Me; R^2= OH, R^3 = H; R^4 = Br (agelastatin B)
R^1 = Me; R^2, R^3 =OH, R^4 = H (agelastatin C)
R^1 = H, R^2 = OH, R^3, R^4 = H (agelastatin D)
R^1 = Me, R^2 = OMe; R^3, R^4 = H (agelastatin E)
R^1 = H, R^2 = OH, R^3 = H, R^4 = Br (agelastatin F)

Fig. 1. (a) Agelastatin A **(1)** and congeners. (b) Structure–activity relationship (SAR) overview of agelastatin A **(1)**. (c) IC_{50} values of two known potent AglA derivatives.

Synthesis of agelastatin A analogs

Our derivatization of AglA focused on functionalization at C14 and C15 of the pyrrole ring given the lack or absence of investigations of these positions. Given the efficiency and scalability of the Movassaghi synthesis of all known agelastatins, we prepared (–)-agelastatin A **(1)** for our studies as described starting from D-aspartic acid in 9 steps in ~4% overall yield (95% ee) and all derivatives prepared herein began with this material (Movassaghi et al., 2010). Iodination with N-iodosuccinimide (NIS) promoted by $(InOTf)_3$ (Zhou et al., 2010) gave 14-iodo **2** in 74% yield (Scheme 1) which

enabled subsequent functionalization of C14 through chemoselective Pd-mediated reactions.

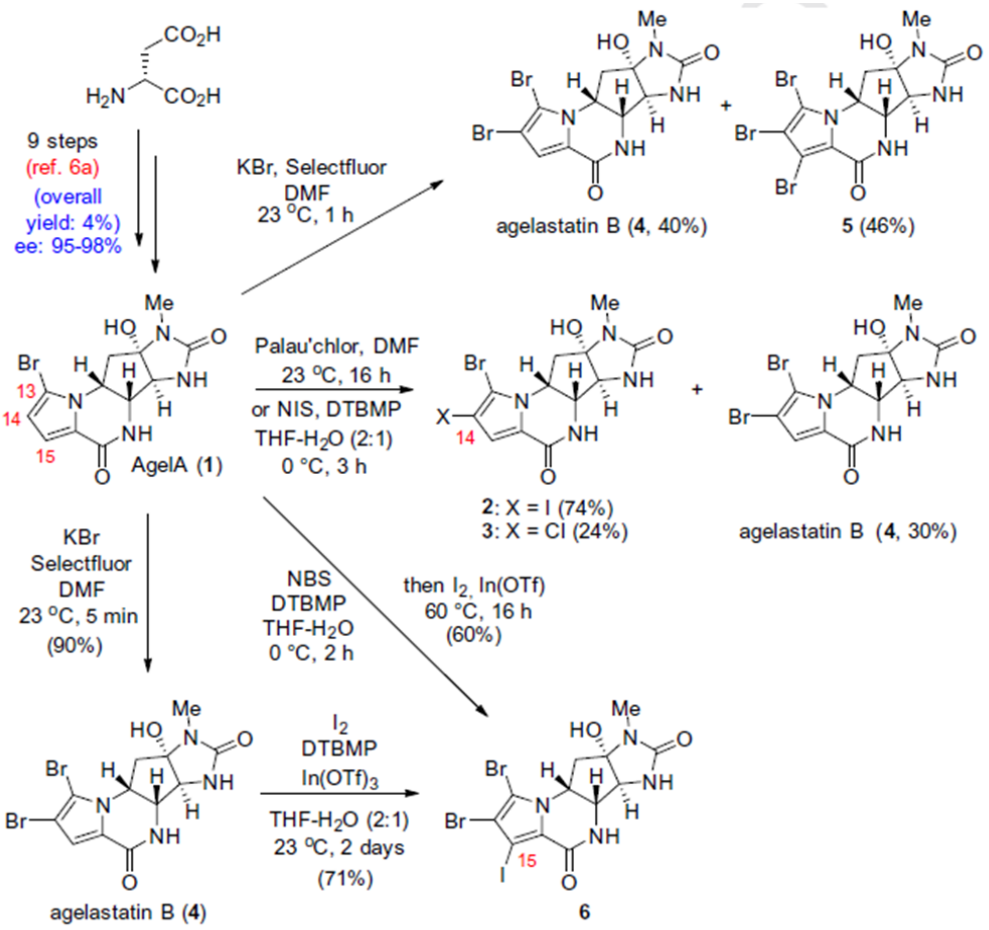

Scheme 1. Synthesis of halogenated AglA derivatives 2–6 by the Romo group.

Initial chlorination conditions employing standard conditions (NCS) gave complex mixtures, however chlorination of AglA with Palau'chlor® (Rodriguez et al., 2014) gave a mixture of the desired 14-chloro AglA **3** (24%) and AgelB 4 (30%) along with traces of C13,C14-dichlorinated derivative detected by LCMS. Modified reaction conditions allowed access to AgelB in 5 min using KBr and selectfluor®, as brominating agent

(Syvret et al., 2002; Ye and Shreeve, 2004). Longer reaction times (1 h) with excess brominating agent gave AgelB **(4)** with 15-bromoAgelB **(5)** in 46% yield, the first C15 functionalized AglA derivative. The 15-iodoAgelB **(6)** was synthesized from AgelB (**4**) employing a large excess of iodine in the presence of Lewis acid (Zhou et al., 2010) in 71% yield over extended periods (2 days). Alternatively, treatment of AglA with 1.5 equivalent of NBS followed by iodine at 60 °C for 16 h gave iodo derivative **6** in 60% yield.

With various halogenated pyrrole derivatives in hand, we studied methylation of the pyrrole ring to differentiate steric versus electronic effects in this heterocycle beginning with C15. Methylation at C15 was studied through both Stille and Suzuki conditions 100 (Scheme 2). Under Suzuki conditions, a mixture of the mono and dimethylated compounds **7**, **8** was obtained in favor of the dimethyl derivative. Stille conditions delivered only the monomethyl derivative **7** in 77% yield. Hydrogenolysis of bromide **7** gave 15-methyl-13,14-debromoAglA **(9)** in quantitative yield (Scheme 2).

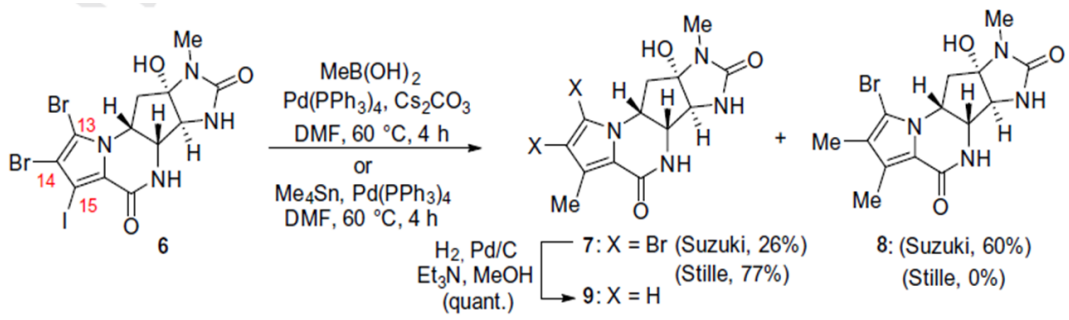

Scheme 2. Synthesis of methylated pyrrole AglA derivatives

Further substitutions on the pyrrole ring were investigated including arylation, alkynylation and acylation (Scheme 3). Suzuki coupling with phenylboronic acid gave a mixture of bis- and mono-arylation products providing 13,14-diphenyl derivative **10** and 14-phenyl derivative **11** derivatives in 23% and 19% yields, respectively. Stille coupling with tetramethyltin and tributylethynylphenyltin gave the 14-methyl derivative **12** and 14-ethynylphenyl derivative **14** in 26% and 55% yield, respectively. Stille coupling with an enol ether stannane followed by mild hydrolysis gave the C-acetylated derivative **13** in 46% yield over two steps.

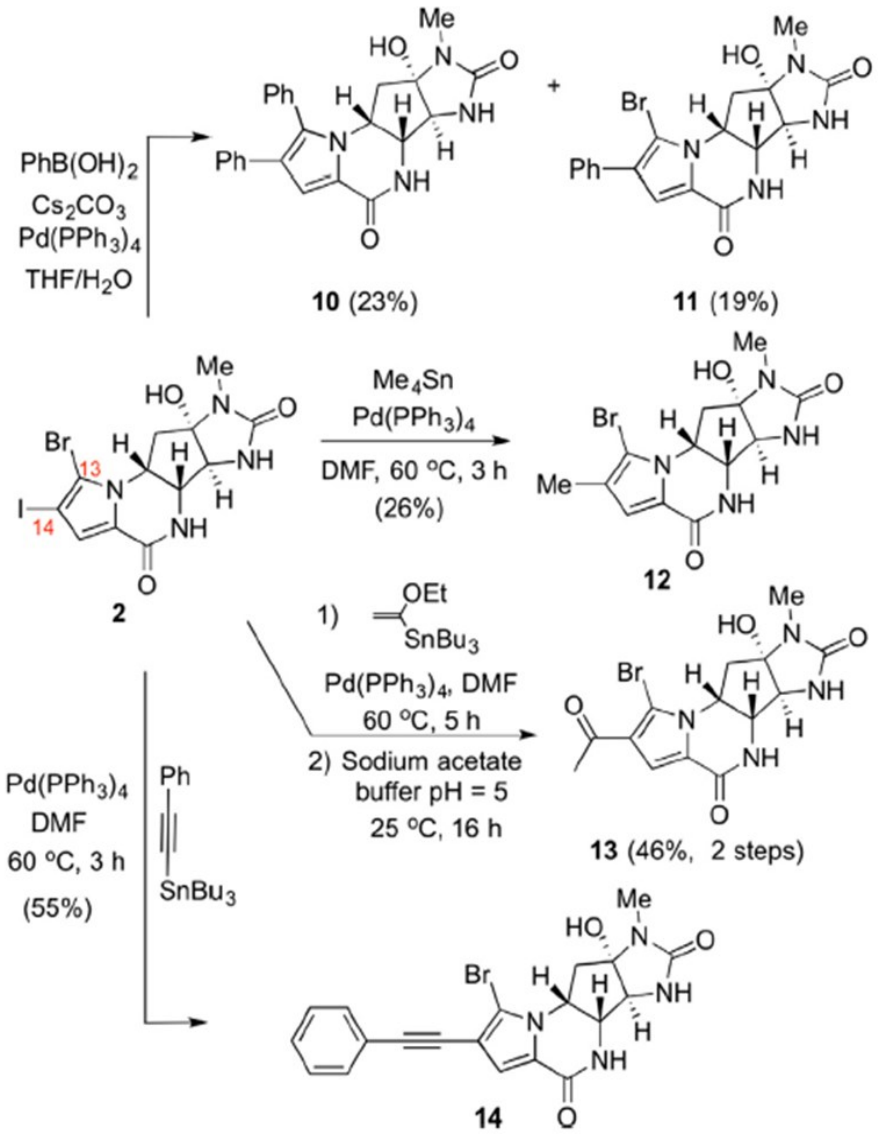

Scheme 3. Synthesis of various C14 AglA derivatives 10–14

Modifications of the C5 and N9 positions were also studied leading to several O- and N-substituted derivatives and a stable aminal derivative. Triazole amide derivative **15** was obtained via acid catalyzed C5 substitution with 4-pentyn-1-ol followed by Sharpless-Hüisgen cycloaddition with α-azido-N-benzylamide (**A**) to provide amide 15 in 46% (Scheme 4). Inspired by Pietra's work (D'Ambrosio et al., 1993), acetylation of the C5 carbinolamine enabled milder substitution conditions with nucleophiles such as 4-hydroxybutanone to provide the alkyl carbinolamine **17** or ammonia to give aminal **18** (Scheme 4). The presence of the amine was confirmed by HRMS and by changes in the ^{13}C chemical shift of C5; namely, a shift from 95.7 to 82.0 ppm supports formation of an aminal at C5. This derivative exhibited excellent stability in water. No trace of AglA by HPLC was detected after 30 days in water at pH = 7 at 37 °C.

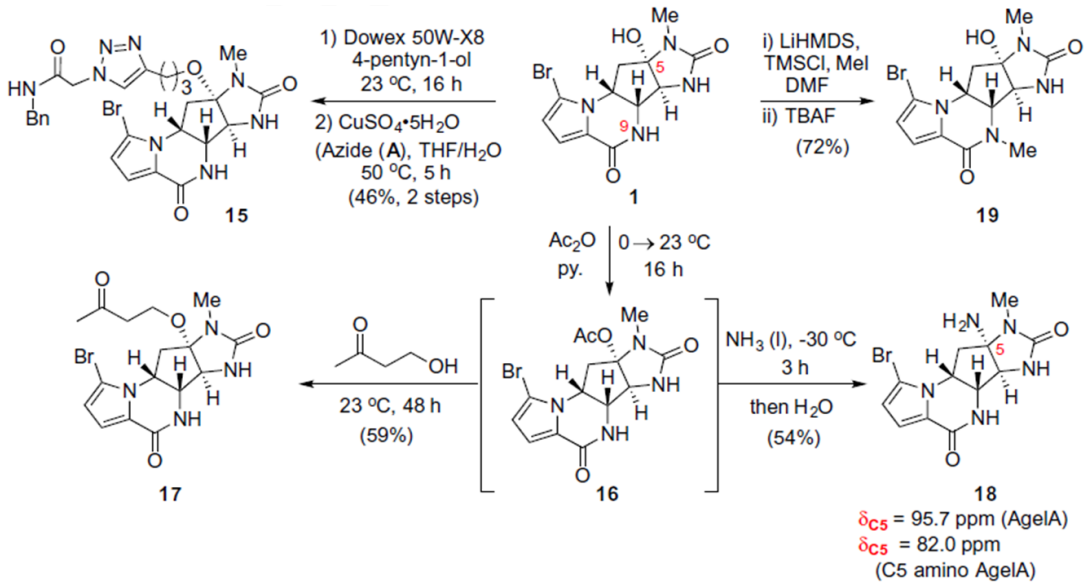

Scheme 4. Synthesis of O-substituted, N9 and aminal AglA derivatives 15, 17–19

To access the unknown methyl-substituted N9 derivative **19**, we took advantage of the differential acidity of protons in AglA (C5–OH > N9–H > N3–H). Addition of 1.0 equiv of LiHMDS, presumably led to initial deprotonation of the carbinolamine and addition of TMSCl gave an intermediate silylether derivative that was not isolated but directly treated with a second equivalent of LiHMDS followed by quenching with methyliodide. The silylether was then cleaved by direct addition of TBAF to provide the monomethylated compound **19** in good yield (72%). The regiose-lectivity of this methylation was confirmed through HMBC correlations.

Structure–activity relationship studies: anticancer activity of AglA derivatives

AglA derivatives **2–25** were screened against several cancer cell lines and primary chronic lymphocytic leukemia (CLL) cells. HeLa cells were studied for comparison to published cytotoxicity of previously described AglA derivatives. Among the C14 and C15 AglA derivatives, only 14-chloro AglA **(3)** and the 14-methyl derivative **(12)** retained activity toward CLL albeit with only μM activity (IC_{50} = 2.82 μM and 7.12 μM, respectively vs 0.71 μM for AglA, Table 1). Likewise, toward HeLa cells, the choro derivative had greater activity than the methyl derivative (IC_{50} = 0.479 μM and 4.53 μM, respectively). Furthermore, the 14-methyl compound **(12)** showed comparable potency when compared to AgelB **(4)** (HeLa, IC_{50} = 4.53 μM and 7.85 μM, respectively). Given that a bromine atom and a methyl group have similar steric size (VDW radii = 1.85 and 1.80 Å, respectively) (Wermuth et al., 2015) but different electronic properties, this result suggests that the size of the group at C14 is more important than electronic effects when considering activity toward HeLa cells. This was further substantiated by comparison to the C14-chloro derivative **3** for which the size decreases from 1.85 Å (Br) to 1.75 Å (Cl)

and the potency significantly increased (17X toward HeLa cells). However, introduction of electron-withdrawing groups at C14 such as acetyl derivative **(13)** resulted in loss of activity (>10 μM and >20 μM for CLL and HeLa, respectively, Table 1). While previous reports demonstrated that a phenyl group is tolerated at C13, for example toward triple-negative breast cancer cells (Li et al., 2013), the introduction of a phenyl **(11)** or ethynylphenyl **(14)** at C14 led to loss of activity (>10 μM and >20 μM for CLL and HeLa, respectively, Table 1). Similarly, the 13,14-diphenyl derivative **10** did not show significant activity against HeLa and CLL cell lines. The 15-bromo and 15-methyl derivatives, **5** and **7**, were inactive against HeLa cells (Table 1). Additionally, no activity was observed with the bis-methyl compound **8**. These results suggest that substitution at C15 is not tolerated for AglA derivatives.

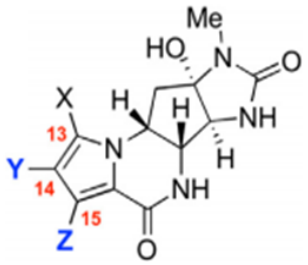

Compd	X	Y	Z	IC_{50} (μM)	
				CLL	HeLa
AglA (**1**)	Br	H	H	0.71 ± 0.10	0.084 ± 0.05
2	Br	I	H	NT	>20
3	Br	Cl	H	2.82 ± 1.07	0.479 ± 0.31
AglB (**4**)	Br	Br	H	>30	7.85 ± 1.12
5	Br	Br	Br	>10	>20
7	Br	Br	Me	NT	>20
8	Br	Me	Me	NT	>20
9	H	H	Me	NT	>20
10	Ph	Ph	H	>10	>20
11	Br	Ph	H	>10	>20
12	Br	Me	H	7.12 ± 1.44	4.53 ± 1.63
13	Br	Ac	H	>10	>20
14	Br	PhCC	H	>10	>20
25	Me	H	H	9.77 ± 4.48	>20

NT = not tested.

Table 1. Cytotoxicity of AglA derivatives 1–14 and 25 with pyrrole ring modifications toward CLL and HeLa **cell** lines

AglA derivatives **1, 3, 4** and **25** that displayed activity toward CLL were also assayed against various cancer cell lines (Table 2, CLL data included for comparison). The 14-chloro derivative **3** exhibited comparable activity to AglA while AgelB **4** was ~10x less potent than AglA toward all cell lines. Notably, compound **25** showed comparable activity to that of the parent natural product against Igrov and Ovcar3 (IC_{50} 0.306 and 0.276 μM, respectively) whereas against SJSA1, A3 and A431 the IC_{50} values were above 1 μM.

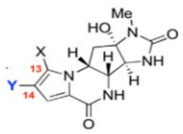

Compd			IC_{50} (μM)						
	X	Y	CLL	HeLa	Igrov	SJSA1	A3	A431	Ovcar 3
AglA (**1**)	Br	H	0.71 ± 0.10	0.084 ± 0.05	0.17 ± 0.00	0.44 ± 0.03	0.38 ± 0.05	0.46 ± 0.13	0.32 ± 0.09
3	Br	Cl	2.82 ± 1.07	0.479 ± 0.31	0.26 ± 0.06	0.56 ± 0.02	0.47 ± 0.03	0.34 ± 0.01	0.54 ± 0.09
AglB (**4**)	Br	Br	>30	7.85 ± 1.12	>1	>1	>1	>1	>1
25	Me	H	9.77 ± 4.48	>20	0.31 ± 0.02	>1	>1	>1	0.28 ± 0.00

CLL (primary human cells), HeLa, Igrov (human ovarian), SJSA1 (osteosarcoma), A3 (human acute T cell leukemia), A431 (epidermoid carcinoma) and Ovcar3 (ovarian carcinoma).

Table 2. Antitumor activities of AglA derivatives toward various cancer cell lines with pyrrole ring modifications

Consistent with previously reported SAR studies (Guerriero et al., 1994; Stout et al., 2014), O-alkylated compounds **15, 17 and 20** suffered from loss of activity toward HeLa and CLL cells (IC_{50} >10–20 μM, Table 3) with the exception of derivative **17**. However, we determined that AglA was slowly regenerated from alkoxy carbinolamine **17** in water ($t_{1/2}$ = 16 h at 25 °C) likely from β-elimination. This suggests that this and related alkoxycarbinolamine derivatives of AglA could be useful as prodrugs or alternatively the carbinolamine center could serve as a point of attachment for antibody drug conjugate synthesis if an appropriate pH sensitive alkoxycarbinolamine is identified (Bouchard et al., 2014; Chari et al., 2014). On the other hand, the activity of aminal **18**

was significantly reduced toward HeLa cells (0.084 μM to 17 μM, ~200x) and primary CLL cells (>30 μM) suggestive of the stability of this aminal derivative ($t_{1/2}$ = 7 days at pH = 5 at 37 °C). Introduction of a N9-methyl group in derivative **19** resulted in complete loss of activity (>20 μM against HeLa).

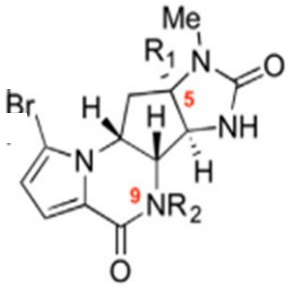

Compd	R_1	R_2	IC_{50} (μM)	
			CLL	HeLa
AglA (**1**)	OH	H	0.71 ± 0.10	0.084 ± 0.05
15	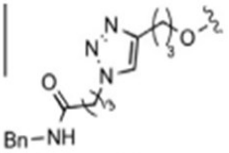	H	>10	>20
17[a]	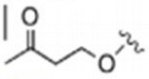	H	5.74 ± 2.99[a]	1.72 ± 0.53[a]
18	NH_2	H	>30	17 ± 2.83
19	OH	Me	NT	>20
20	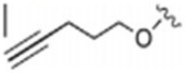	H	>10	>20

[a] AglA (**1**) was released ($t_{1/2}$ = 16 h at 25 °C in water); NT : not tested. Analog **19** is a racemate.

Table 3. Cytotoxicity of AglA derivatives 15–20 with modifications at C5 and N9

Compd	IC_{50}, μM	Human plasma protein binding		
	w/plasma	w/FBS	Fraction bound (%)	Recovery (%)
AglA (**1**)	0.71 ± 0.10	0.93 ± 0.47	23.9	99.2
3	2.82 ± 1.86	2.65 ± 1.22	46.5	102.1

FBS: fetal bovine serum; Fraction bound (%): the portion of the compound that is bound to human plasma; % recovery: the percentage of compound recovered after the incubation period for plasma protein binding analysis.

Table 4. Plasma protein properties of AglA **(1)** and 14-Cl-AglA **(3)**

Protein binding studies

The propensity of AglA **(1)** and 14-Cl-AglA **(3)** to bind to plasma proteins and their stability in these media was investigated with both human plasma and fetal bovine serum (FBS, Table 4). The cytotoxicity of the compounds did not change dramatically when maintained in either human plasma or FBS suggesting that they were not highly protein bound. Further studies were performed to verify these results, and indeed full recovery of these derivatives was possible also pointing to their high stability. Low recovery is often an indication of material loss during the analysis due to compound instability, non-specific binding, or low solubility.

Differential cytotoxicity studies

The toxicity of AglA **(1)** and 14-Cl-AglA **(3)** was compared between CLL cells and normal B and T-lymphocytes (Fig. 2). The study revealed that compared to CLL cells, AglA was less toxic toward B and T cells from healthy donors. The selectivity for CLL leukemia cells was even more apparent for 14-chloro derivative **3**. Although both compounds did demonstrate toxicities toward normal B lymphocytes, this is generally not a concern for future clinical application, as the B cell targeting antibodies rituximab and ofatumumab were proven safe for therapeutic treatment of B cell malignancies (Korycka-Wołowiec et al., 2015).

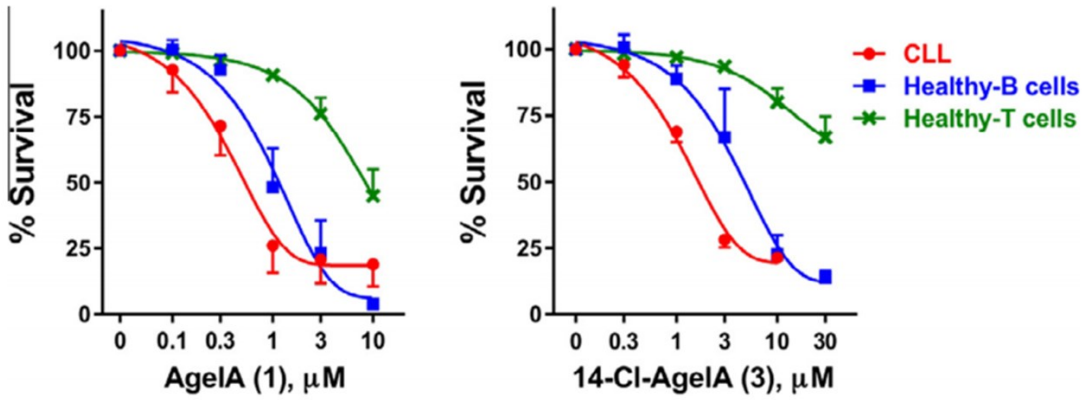

Fig. 2. Effect of AglA **(1)** and 14-Cl-AglA **(3)** on B and T-cells and all plasma cells from healthy donors.

Synthesis of AglA affinity probes

Building on the SAR gathered for the C14-methyl and chloro derivatives **3** and **12**, we targeted a photoaffinity probe that could be useful for affinity chromatography experiments (Leslie and Hergenrother, 2008; Ziegler et al., 2013). Given the low potency exhibited by such derivatives (~0.5-4.5 μM) however, we elected to synthesize a photoaffinity probe to improve the possibility of capturing interacting proteins. Toward this goal, a trifunctional probe **24** containing both a diazirine for covalent capture of putative cellular target(s) through photocrosslinking and an alkyne for subsequent biotin attachment to facilitate purification of covalently modified proteins was synthesized (Scheme 5). Beginning with previously prepared iodide **2**, Stille coupling with a stannyl bis-alkyne gave amine **21**. Acylation of this amine with diaziridine **22** gave amide **23** in modest yield with recovered amine **21**. Oxidation of the diaziridine with I_2 in methanol delivered the trifunctional diazirine probe **24**. We were pleased to find that both diaziridine **23** and diazirine **24** retained activity toward HeLa cells albeit greatly reduced compared to AglA.

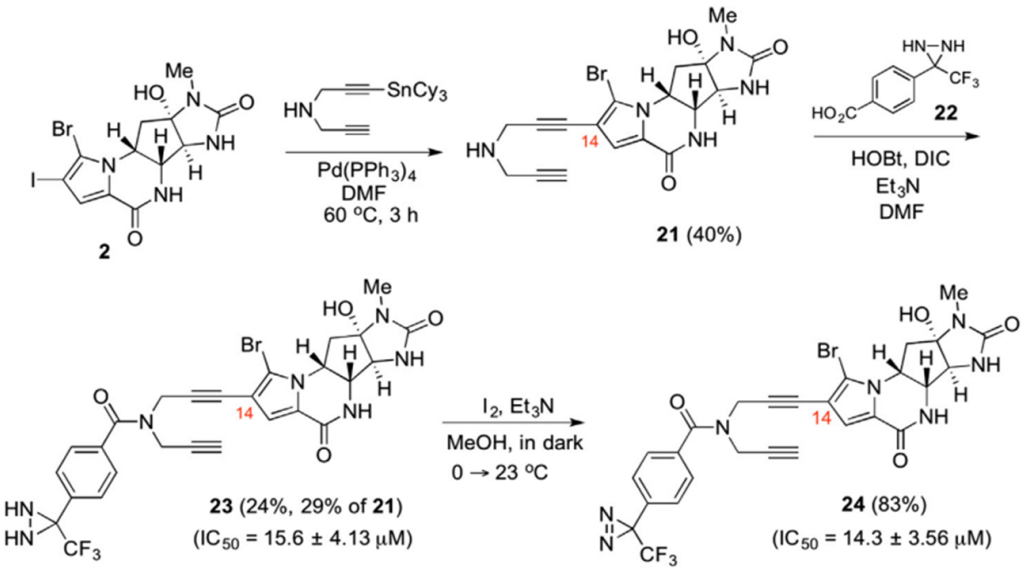

Scheme 5. Synthesis of an AglA trifunctional probe **24.**

Photoaffinity labeling

Photoaffinity labeling allows capture of drug-binding proteins and target identification by mass spectrometry. To ensure covalent crosslinking occurs, a UV light sensitive diazirine derivative is typically incorporated into a probe (Figure 3a, purple), as well as a free alkyne moiety (Figure 3a, blue) that is necessary for click chemistry. For this approach to be successful, a probe must be designed that can bind to the same target proteins and induce the same effects as the parent drug with a similar potency (Figure 3b). Unfortunately, our probe lost significant activity compared to parent AglA, but we still took a gamble to see if any specific proteins were pulled down and competed away in the presence of excess AglA.

Labeling was carried out similar to the methods previously used by our group (Head et al., 2015), but with rabbit reticulocyte lysate and purified ribosomes. These lysates were used because we narrowed down protein translation as the primary target of AglA using phenotypic based approaches, which will be further discussed in Chapter 3. After lysates were treated with the probe, they were placed under a UV lamp for 3 min to activate the photolabile diazirine and covalently crosslink the probe to its potential binding protein(s), after which the samples were denatured by boiling in water. The denatured lysates then were reacted with fluor-azide in the presence of copper, which reacts with the terminal acetylene of the probe to attach the fluorophore covalently via click chemistry. The proteins then were resolved on an SDS/PAGE gel, which was scanned on a fluorescence gel scanner to detect fluorescently labeled proteins. In comparison to the background bands present in the DMSO control sample, no difference was observed with the probe-treated sample (Figure 3c, d).

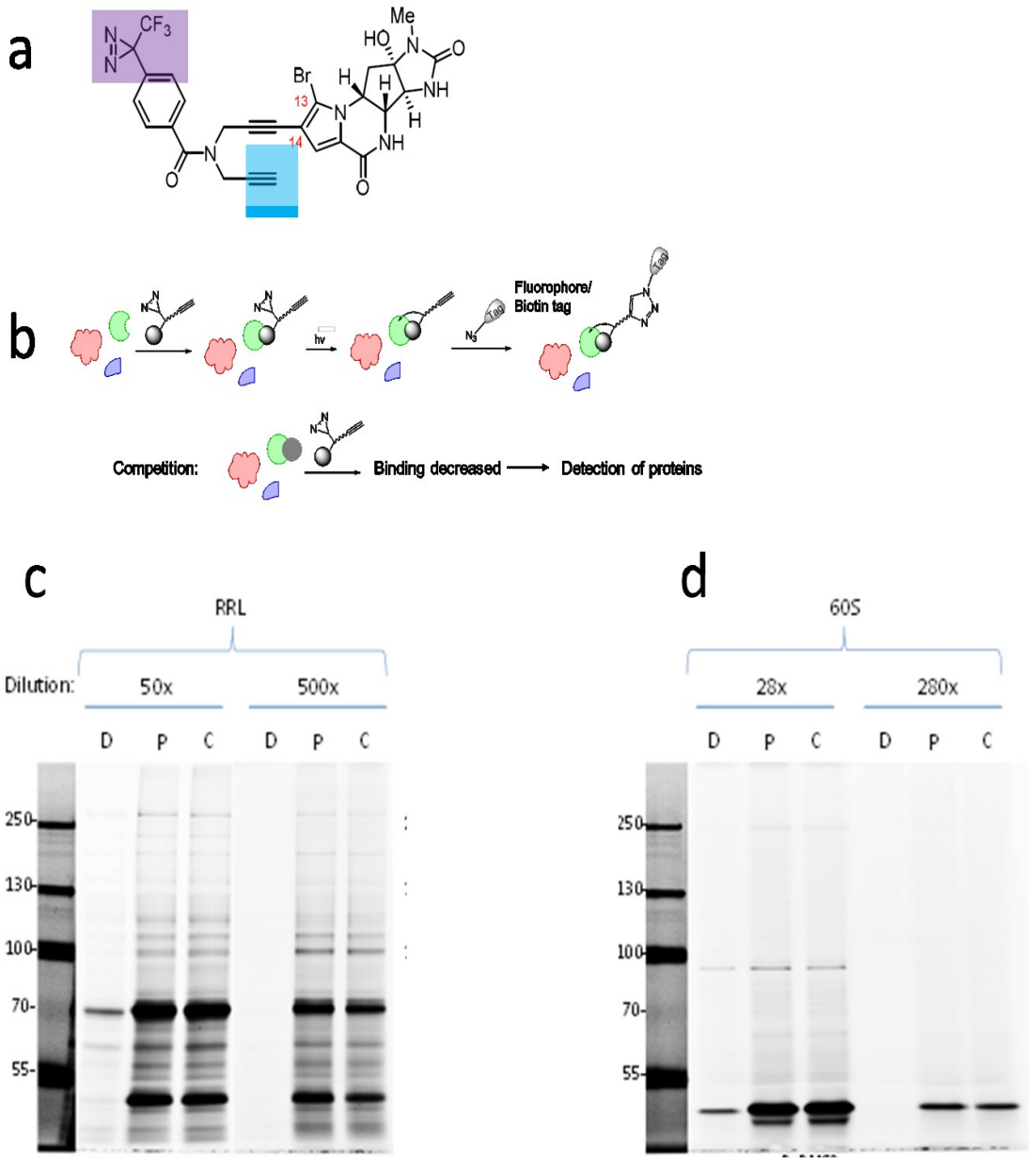

Fig. 3. Photoaffinity labeling. (a) AglA probe **24**. Essential photoaffinity portions highlighted **(*b*)** General schematic summarizing the method. Photoaffinity labeling was conducted using a fluorescent detection tag, and the gel was scanned for fluorescence to detect photolabeled proteins in (**c)** rabbit reticulocyte lysate and (**d)** purified yeast 60S ribosomal subunits

Discussion

In summary, we expanded the SAR profile of the anticancer agent, AglA through further investigations of the C14 position of the pyrrole and positions not previously investigated, C15 and N9. The 14-Cl-AglA **(3)** retained activity against various cancer cell lines including HeLa, CLL and A431. This AglA derivative also showed better selectivity toward CLL cells over B and T-cells than AglA and exhibits low serum protein binding and good stability given that recovery from serum was excellent.

A trifunctional photoaffinity probe of AglA, albeit with low cytotoxic activity relative to AglA, was synthesized. Studies toward cellular target identification, using this probe were conducted. Many proteins were pulled down, which is likely due to nonspecific crosslinking. Unfortunately, no proteins were successfully pulled down and competed away, which is important requirement for drug target candidates. These studies, in conjunction with previous work by others, demonstrate that few modifications of the AglA structure are tolerated while retaining high potency relative to the parent natural product. Finally, we demonstrated that alkoxyaminal derivatives of AglA may prove useful as prodrugs given their ability to regenerate AglA under mild hydrolysis conditions.

Materials and Methods

General Procedures

All reactions were performed under a nitrogen atmosphere in ovendried glassware. N,N-Dimethylformamide was dried over activated molecular sieves (4 Å). Dichloromethane, tetrahydrofuran and methanol were dried by passing through activated molecular sieves or alumina. Triethylamine and diisopropylethylamine were distilled from calcium hydride. N-Bromosuccinimide and N-iodosuccinimide have been recrystallized following reported procedures (Wermuth et al., 2015). Others solvents and reagents were used as received from commercially available sources. Reactions were monitored by LCMS and TLC. Retention times (TR) are reported in minutes. Low-resolution LCMS analyses were conducted in APCI mode with a C18 column (50 x 4.6 mm, 2.7 µm), using a gradient mobile phase (5 → 100% MeCN /H_2O) in 20 min at 0.2 mL/min. All compounds used in biological assays were analyzed by LC-MS and purified to purities of ≥ 95%. Thin layer chromatography was performed using glass-backed 60Å silica gel F-254 (250 µm thickness). Developed plates were visualized by UV light and by immersion in ceric ammonium molybdate (CAM) stain followed by heating. 1 H and 13C NMR spectra were recorded on a 500 MHz (125 MHz) NMR equipped with quad probe for 1 H{31P}{19F} or a 500 MHz (125 MHz) sNMR equipped with a cryoprobe in CD_3OD or $CDCl_3$ and referenced to δ 3.31 and 49.0 ppm, and δ 7.27 and 77.16 ppm respectively for 1 H and 13C NMR. 19F NMR spectra were recorded on a 500 Varian 470 MHz spectrometer. Coupling constants (J) are reported in Hertz (Hz) and multiplicity follows normal convention: s, singlet; d, doublet; t, triplet; q, quartet; quint, quintuplet; dd, doublet of doublets; dt, doublet of triplets; dt, triplet of doublets; m, multiplet; br s, broad

singlet; br dd, broad doublet of doublets; br dt, broad doublet of triplets; (prefix app indicates ‘apparent’). High-resolution mass spectra were obtained through the Center for Chemical Characterization and Analysis (Texas A&M University). Infrared spectra were obtained on a FTIR spectrometer as a thin film on NaCl plates.

(–)-Agelastatin A

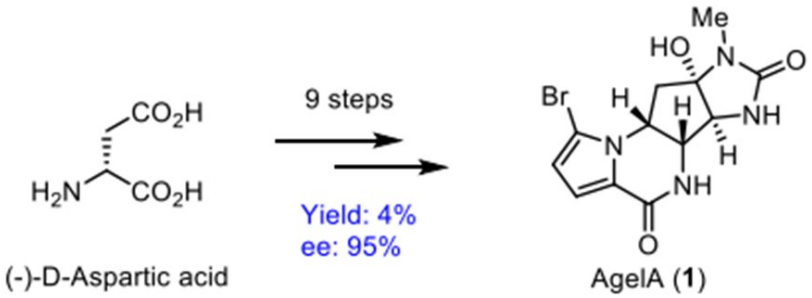

(–)-Agelastatin A **(1)** was synthesized following the procedure described by Movassaghi and co-workers (Movassaghi et al., 2010) in 9 steps from (–)-D-aspartic acid: Rf 0.38 (CH_2Cl_2 / MeOH 9:1) (CAM, UV); 1 H NMR (500 MHz, CD_3OD) δ 6.91 (d, J = 4.1 Hz, 1H), 6.33 (d, J = 4.0 Hz, 1H), 4.60 (app dt, J = 12.0, 6.0 Hz, 1H), 4.09 (d, J = 5.4 Hz, 1H), 3.88 (s, 1H), 2.81 (s, 3H), 2.65 (dd, J = 12.9, 6.4 Hz, 1H), 2.10 (app t, J = 12.6 Hz, 1H); 13C NMR (125 MHz, CD_3OD) δ 161.4, 161.1, 124.1, 116.1, 113.8, 107.3, 95.7, 67.4, 62.2, 54.4, 40.0, 24.2; HRMS (+ESI): m/z calcd for $C_{12}H_{13}BrNaN_4O_3$ [M+Na]+ 363.0068, found 363.0075; Chiral HPLC: (–)-agelastatin A was found to be 95% ee using the following conditions: Chiralpak AD-H, 0.50 mL/min, 30% i-PrOH/hexanes, TR (major) = 11.64 min, TR (minor) = 8.50 min; [α]D 21.4 -90.0 (c = 0.10, MeOH), lit.2 [α]D 22 -87.6 (c = 0.10, MeOH).

*Note: All described AgIA derivatives are expected to have the same absolute configuration and optical purity as the synthetically derived AgIA since no transformations described are expected to lead to inversion of all stereocenters.

14-Iodo Agelastatin A (2)

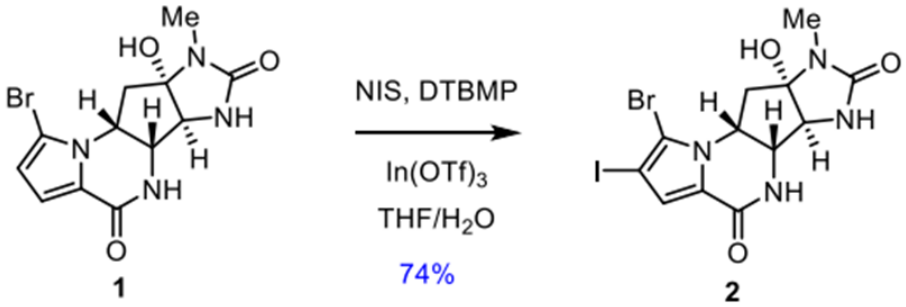

To a solution of (–)-agelastatin A **(1)** (10.0 mg, 0.029 mmol, 1 equiv) in 2:1 THF:H_2O (1.5 mL) at 0 °C was added 2,6-di-t-butyl-4-methylpyridine (12.1 mg, 0.059 mmol, 2 equiv) followed by N-iodosuccinimide (13.2 mg, 0.059 mmol, 2 equiv) and $In(OTf)_3$ (1.6 mg, 0.0029 mmol, 0.1 equiv). After stirring at the same temperature for 3 h, the reaction mixture was quenched by addition of a small crystal of sodium thiosulfate and concentrated *in vacuo*. The residue was purified by flash column chromatography (SiO2, 10% MeOH / CH_2Cl_2) providing 10 mg (74%) of 14-iodo agelastatin A (**2**) as a colorless solid; Rf 0.40 (CH_2Cl_2 / MeOH 9:1) (CAM, UV); 1 H NMR (500 MHz, CD_3OD) δ 7.03 (s, 1H), 4.62 (app dt, J = 11.9, 6.0 Hz, 1H), 4.09 (d, J = 5.6 Hz, 1H), 3.87 (s, 1H), 2.81 (s, 3H,), 2.67 (dd, J = 12.9, 6.4 Hz, 1H), 2.11 (app t, J = 12.7 Hz, 1H); 13C NMR (125 MHz, CD_3OD) δ 161.4, 160.0, 126.1, 122.3, 113.7, 95.5, 69.0, 67.3, 62.1, 55.9, 39.9, 24.2; HRMS (+ESI): m/z calcd for $C_{12}H_{13}BrIN_4O_3$ [M+H]+ 466.9216, found 466.9210.

14-chloro-agelastatin A (3)

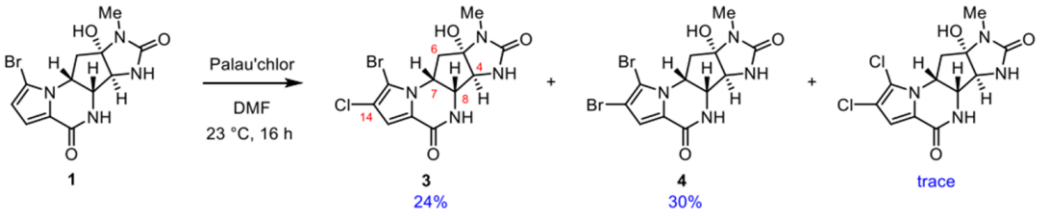

A solution of (–)-agelastatin A **(1)** (5.5 mg, 0.012 mmol, 1 equiv) in DMF (0.5 mL) was degassed by passage of a stream of argon through the solution for 15 min through a stainless steel needle. Palau'chlor® (3.8 mg, 0.018 mmol, 1.5 equiv) was added and the reaction mixture was stirred at 23 °C for 16 h. The reaction mixture was concentrated *in vacuo* and the residue purified by flash column chromatography (SiO_2, 10% MeOH / CH_2Cl_2) and then by semi-preparative reverse-phase HPLC (100 x 21.20 mm, 5 µm; linear gradient, 5 → 95% CH_3CN/H_2O with 0.1% of ammonium bicarbonate over 20 min, 10 mL/min) to yield 14- chloro-agelastatin A **(3)** (TR = 35.2 min, 1.1 mg, 24%) and agelastatin B **(4)** (TR = 37.6 min, 1.5 mg, 30%) both as colorless solids.

14-chloro-agelastatin A **(3)**: Rf 0.39 (CH_2Cl_2 / MeOH 9:1) (CAM, UV); 1 H NMR (500 MHz, CD_3OD) δ 6.91 (s, 1H), 4.58 (app dt, J = 11.9, 6.0 Hz, 1H), 4.11 (d, J = 5.3 Hz, 1H), 3.87 (s, 1H), 2.80 (s, 3H), 2.67 (dd, J = 12.9, 6.4 Hz, 1H,), 2.12 (t, J = 12.6 Hz, 1H); 13C NMR (125 MHz, CD_3OD) δ 161.2, 160.1, 123.7, 116.2, 114.2, 106.2, 95.6, 67.4, 62.0, 55.0, 39.9, 24.2; HRMS (+ESI): m/z calcd for $C_{12}H_{12}BrClNaN_4O_3$ [M+Na]+ 396.9678, found 396.9687.

agelastatin B **(4)**: Rf 0.39 (CH_2Cl_2/ MeOH 9:1) (CAM, UV); 1 H NMR (500 MHz, CD_3OD) δ 6.95 (s, 1H), 4.59 (app dt, J = 11.9, 6.0 Hz, 1H), 4.10 (d, J = 5.4 Hz, 1H), 3.86 (s, 1H), 2.80 (s, 3H), 2.66 (dd, J = 13.2, 6.6 Hz, 1H), 2.11 (t, J = 12.6 Hz, 1H); HRMS

(+ESI): m/z calcd for $C_{12}H_{12}Br_2NaN_4O_3$ [M+Na]+ 440.9174, found 440.9187. Data matched that previously reported (Movassaghi et al., 2010).

15-bromoagelastatin B (5)

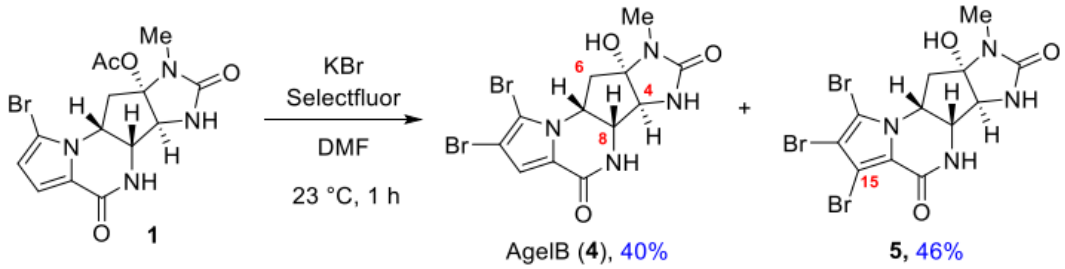

To a solution of (–)-agelastatin A **(1)** (1.1 mg, 0.0032 mmol, 1 equiv) in DMF (0.2 mL) was added potassium bromide (1.5 mg, 0.0128 mmol, 4 equiv) and Selectfluor® (4.5 mg, 0.0128 mmol, 4 equiv). On addition of Selectfluor® the solution turned from colorless to bright yellow. The reaction mixture was stirred at 23 °C for 1 h then concentrated *in vacuo* and the residue was purified by pipette flash column chromatography (SiO_2, 10% of MeOH in MM) and then by semi-preparative reverse-phase HPLC (100 x 21.20 mm, 5µm; linear gradient, from 5 → 95% CH_3CN/H_2O with 0.1% of ammonium bicarbonate over 20 min, 10 mL/min) to yield agelastatin B **(4)** (TR = 10.1 min, 0.53 mg, 40%) and 15-bromoagelastatin A **(5)** (TR =11.2 min, 0.73 mg, 46%) both as colorless solids.

15-bromoagelastatin B **(5)**: Rf 0.39 (CH_2Cl_2 / MeOH 9:1) (CAM, UV); 1 H NMR (500 MHz, CD_3OD) δ 4.64 (app dt, J = 12.0, 5.7 Hz, 1H), 4.09 (d, J = 5.4 Hz, 1H), 3.86 (s, 1H), 2.80 (s, 3H), 2.68 (dd, J = 13.2, 6.6 Hz, 1H), 2.16 (app t, J = 12.6 Hz, 1H); 13C NMR (125 MHz, CD_3OD) δ 161.3, 159.0, 121.5, 109.0, 105.9, 105.6, 95.5, 67.3, 61.5, 56.0, 39.8, 24.2; HRMS (+ESI): m/z calcd for $C_{12}H_{11}Br_3NaN_4O_3$ [M+Na]+ 520.8259, found 520.8275

15-iodo-agelastatin B (6)

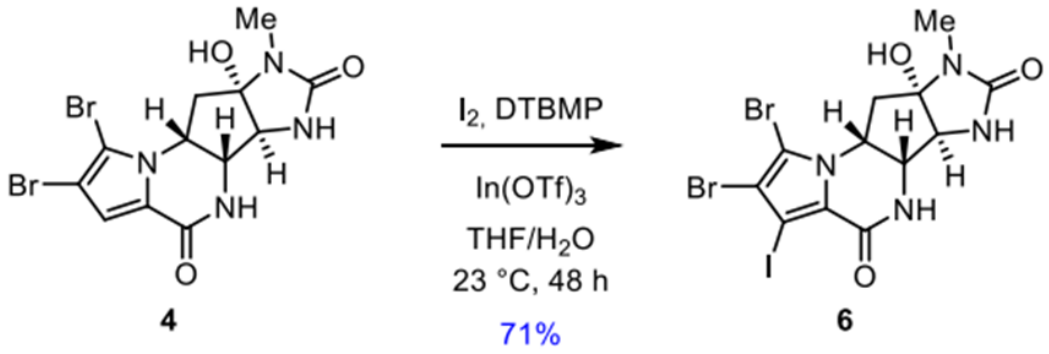

To a solution of agelastatin B **(4)** (1.1 mg, 0.0026 mmol, 1 equiv) in 2:1 THF: H_2O (0.2 mL) at 0 °C was added 2,6-di-t-butyl-4-methylpyridine (3 mg, 0.013 mmol, 5 equiv) followed by I_2 (3 mg, 0.026 mmol, 10 equiv) and $In(OTf)_3$ (0.6 mg, 0.001 mmol, 0.4 equiv). The reaction mixture was stirred at 23 °C for 48 h and after 24 h, additional I_2 (3 mg, 0.026 mmol, 10 equiv) was added. The reaction mixture was quenched by addition of a small crystal of sodium thiosulfate and then concentrated *in vacuo*. The residue was purified by semipreparative reverse-phase HPLC (100 x 21.20 mm, 5µm; linear gradient, 5 → 95% CH_3CN/H_2O with 0.1% of ammonium bicarbonate over 20 min, 8 mL/min) to yield 15- iodoagelastatin B **(6)** (TR = 15 min, 1 mg, 71%) as thin film: Rf 0.40 (CH_2Cl_2 / MeOH 9:1) (CAM, UV); 1 H NMR (500 MHz, CD_3OD) δ 4.65 (app dt, J = 11.9, 6.3 Hz, 1H), 4.08 (br d, J = 5.1 Hz, 1H), 3.86 (s, 1H), 2.80 (s, 3H), 2.68 (br dd, J = 12.8, 6.3 Hz, 1H), 2.16 (br app t, J = 12.6 Hz, 1H); HRMS (+ESI): m/z calcd for $C_{12}H_{12}Br_2IN_4O_3$ [M+H]+ 566.8140, found 566.8186

14,15-dimethyl agelastatin A (8) and 15-methyl agelastatin B (7)

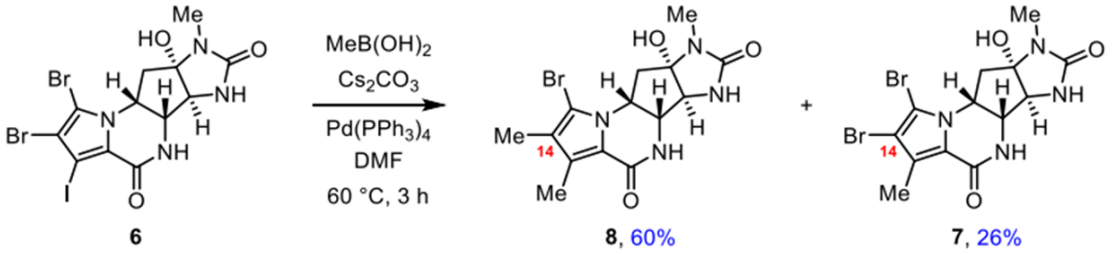

A solution of 15-iodo agelastatin B **(6)** (0.5 mg, 0.9 µmol, 1 equiv) in DMF (0.1 mL) was degassed by passage of a stream of argon through the solution for 15 min through a stainless steel needle. Cs_2CO_3 (2 mg, 0.006 mmol, 6 equiv) and methylboronic acid (0.2 mg, 0.0027 mmol, 3 equiv) were added followed by Pd(PPh3)4 (0.6 mg, 0.6 µmol, 0.6 equiv). The reaction mixture was heated at 60 °C for 3 h. The reaction mixture was filtered, concentrated *in vacuo*, and purified by semi-preparative reverse-phase HPLC (100 x 21.20 mm, 5µm; linear gradient, 5 → 95% CH_3CN/H_2O with 0.1% of ammonium bicarbonate over 20 min, 8 mL/min) to yield 14,15-dimethyl agelastatin A **(8)** (TR = 11.7 min, 0.2 mg, 60%) and 15-methyl-agelastatin B **(7)** (TR = 12.4 min, 0.1 mg, 26%) as thin films.

14,15-bismethyl-agelastatin A **(8)**: Rf 0.41 (CH_2Cl_2 / MeOH 9:1) (CAM, UV); 1 H NMR (500 MHz, CD3OD) δ 4.53 (app dt, J = 12.0, 6.0 Hz, 1H), 3.99 (d, J = 5.4 Hz, 1H), 3.83 (s, 1H), 2.80 (s, 3H), 2.59 (dd, J = 13.3, 6.4 Hz, 1H), 2.29 (s, 3H), 2.25 (s, 3H), 2.09 (app t, J = 12.6 Hz, 1H); 13C NMR (125 MHz, CD_3OD) δ 160.9, 160.4, 129.9, 126.6, 116.4, 100.9, 94.6, 67.1, 61.6, 53.1, 39.7, 23.8, 11.3, 9.9, assignments and correlations were verified by HSQC and HMBC experiments; HRMS (+ESI): m/z calcd for $C_{14}H_{17}BrNaN_4O_3$ [M+Na]+ 391.0381 found 391.0389

15-methyl-agelastatin B **(7)**: Rf 0.41 (CH_2Cl_2 / MeOH 9:1) (CAM, UV); 1 H NMR (500 MHz, CD_3OD) δ 4.57 (app dt, J = 12.0, 6.0 Hz, 1H), 4.03 (d, J = 5.3 Hz, 1H), 3.85 (s, 1H), 2.80 (s, 3H), 2.63 (dd, J = 13.1, 6.4 Hz, 1H), 2.35 (s, 3H), 2.09 (app t, J = 12.6 Hz, 1H); 13C NMR (125 MHz, CD_3OD) δ 160.7, 160.2, 127.7, 119.4, 106.9, 103.7, 94.8, 66.9, 61.3, 54.9, 39.4, 23.6, 11.7, assignments and correlations were verified by HSQC and HMBC experiments; HRMS (+ESI): m/z calcd for $C_{13}H_{14}Br_2NaN_4O_3$ [M+Na]+ 456.9305 found 456.9291

15-methyl-13-debromo-agelastatin A (9)

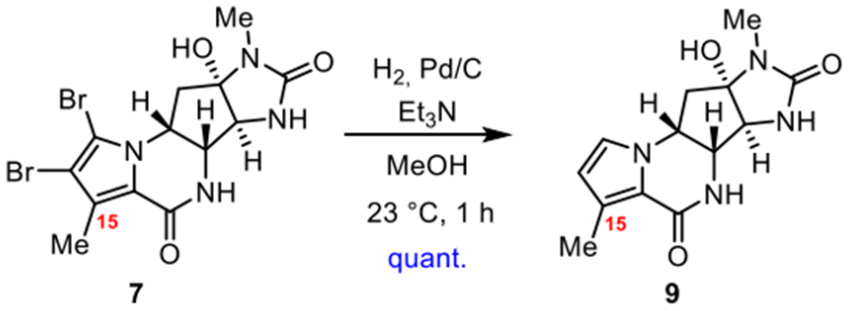

To a solution of 15-methyl-agelastatin B **(7)** (0.5 mg, 0.0011 mmol, 1 equiv) in methanol (0.1 mL) was added Et_3N (1 µL, 0.0055 mmol, 5 equiv) and Pd/C (10% wt). Three cycles of evacuation (aspirator vacuum) and purging with H_2 was followed by stirring at 23 °C for 1 h under 1 atm H2 (balloon) before being filtered and concentrated *in vacuo*. The mixture was purified by semi-preparative reverse-phase HPLC (100 x 21.20 mm, 5µm; linear gradient, 5 → 95% CH_3CN/H_2O with 0.1% of ammonium bicarbonate over 20 min, 8 mL/min) to yield 15-methyl-13-debromo agelastatin A **(9)** (TR = 9.1 min, 0.3 mg, quantitative) as a thin film: Rf 0.39 (CH_2Cl_2 / MeOH 9:1) (CAM, UV); 1

H NMR (500 MHz, CD_3OD) δ 6.88 (d, J = 2.5 Hz, 1H), 6.04 (d, J = 2.2 Hz, 1H), 4.57 (br app dt, J = 11.3, 6.0 Hz, 1H), 3.94 (br d, J = 5.2 Hz, 1H), 3.78 (d, J = 1.0 Hz, 1H), 2.79 (s, 3H), 2.57 (dd, J = 13.3, 6.4 Hz, 1H), 2.35 (s, 3H), 2.26 (dd, J = 13.3, 10.5 Hz, 1H); 13C NMR (125 MHz, CD_3OD) δ 162.8, 161.3, 129.6, 124.3, 118.4, 112.9, 95.7, 67.7, 62.6, 55.5, 41.3, 24.1, 12.6; assignments and correlations were verified by HSQC and HMBC experiments. HRMS (-ESI): m/z calcd for $C_{13}H_{15}N_4O_3$ [M-H]- 275.1144 found 275.1156

14-phenyl-agelastatin A (11) and 13-debromo-13,14-diphenyl-agelastatin A (10)

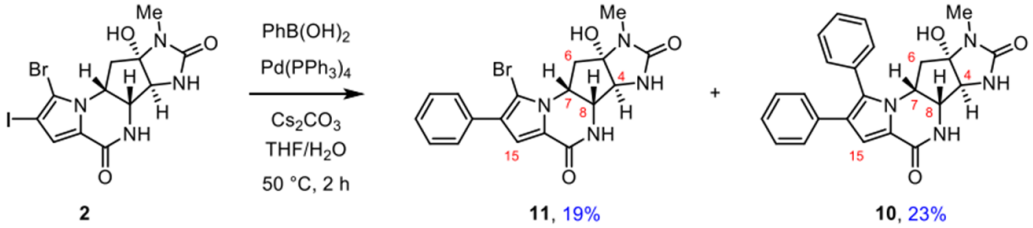

A solution of 14-iodo-agelastatin A **(2)** (8 mg, 0.017 mmol, 1 equiv) in THF/H_2O (0.2: 0.2 mL) was degassed by passage of a stream of argon through the solution for 15 min through a stainless steel needle and phenyl boronic acid (3.1 mg, 0.025 mmol, 1.5 equiv) and cesium carbonate (33 mg, 0.102 mmol, 6 equiv) was added, followed by $Pd(PPh_3)_4$ (3.5 mg, 0.003 mmol, 0.3 equiv). The reaction mixture was heated at 50 °C for 2 h. The reaction mixture was concentrated *in vacuo*. The residue was purified by flash column chromatography (SiO_2, 10% of MeOH in CH_2Cl_2) and then by semi-preparative reverse-phase HPLC (100 x 21.20 mm, 5μm; linear gradient, 5 → 95% CH_3CN/H_2O with 0.1% of ammonium bicarbonate over 20 min, 10 mL/min) to yield 14-

phenyl-agelastatin A **(11)** (TR = 11.5 min, 1.3 mg, 19%) and 13- debromo-13,14-diphenyl agelastatin A **(10)** (TR = 12.4 min, 1.6 mg, 23%) as colorless solids: Rf 0.40 (CH_2Cl_2 / MeOH 9:1) (CAM, UV) for both products.

14-phenyl agelastatin A **(11)**: 1 H NMR (500 MHz, CD_3OD) δ 7.57-7.59 (m, 2H), 7.41 (app t, J = 7.7 Hz, 2H), 7.29-7.33 (m, 1H), 7.14 (s, 1H), 4.70 (app dt, J = 12.0, 6.0 Hz, 1H), 4.16 (d, J = 5.6 Hz, 1H), 3.92 (s, 1H), 2.84 (s, 3H), 2.74 (dd, J = 12.9, 6.3 Hz, 1H), 2.18 (app t, J = 12.7 Hz, 1H); 13C NMR (125 MHz, CD_3OD) δ 161.4, 161.0, 134.9, 129.5, 128.8, 128.1, 127.4, 124.2, 114.9, 105.4, 95.7, 67.4, 67.3, 62.1, 54.7, 45.4, 40.0, 24.2; HRMS (+ESI): m/z calcd for $C_{18}H_{17}BrNaN_4O_3$ [M+Na]+ 439.0381, found 439.0372

13-debromo-13,14-diphenyl agelastatin A **(10)**: 1 H NMR (500 MHz, CD_3OD) δ 7.48-7.51 (m, 3H), 7.38-7.51 (m, 2H), 7.21 (s, 1H), 7.17 (s, 1H), 7.15-7.19 (m, 3H), 7.11-7.13 (m, 1H), 4.28 (app dt, J = 12.0, 6.0 Hz, 1H), 4.10 (d, J = 5.4 Hz, 1H), 3.83 (s, 1H), 2.49 (s, 3H), 2.29 (dd, J = 13.1, 6.3 Hz, 1H), 2.21 (app t, J = 12.7 Hz, 1H); 13C NMR (125 MHz, CD_3OD) δ 161.9, 161.3, 136.1, 135.1, 132.4, 131.8, 130.3, 130.2, 130.1, 129.3, 128.7, 127.1, 126.3, 122.6, 114.7, 95.4, 67.2, 62.4, 53.7, 46.4, 40.6, 23.8; HRMS (+ESI): m/z calcd for $C_{24}H_{22}NaN_4O_3$ [M+Na]+ 464.1589, found 464.1583

14-methyl agelastatin A (12)

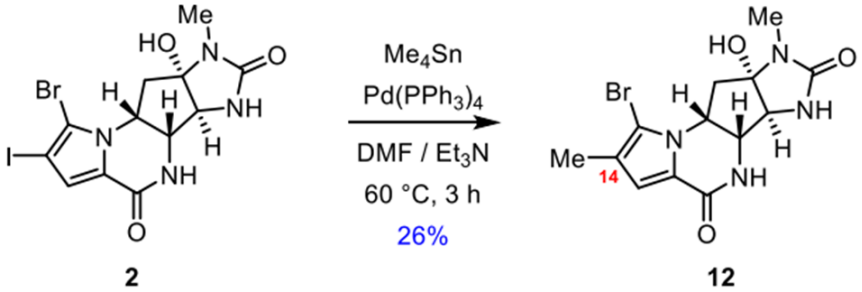

A solution of 14-iodo-agelastatin A **(2)** (3 mg, 0.0065 mmol, 1 equiv) in DMF/Et3N (0.1:0.05 mL) was degassed by passage of a stream of argon through the solution for 15 min through a stainless steel needle and tetramethyl tin (4 µL, 0.026 mmol, 4 equiv) was added, followed by $Pd(PPh_3)_4$ (3.0 mg, 0.0026 mmol, 0.4 equiv). The reaction mixture was heated at 60 °C for 3 h. The reaction mixture was filtered off, concentrated *in vacuo*, and purified by semipreparative reverse-phase HPLC (100 x 21.20 mm, 5µm; linear gradient, 5 → 95% CH_3CN/H_2O with 0.1% of ammonium bicarbonate over 20 min, 8 mL/min) to yield 14- methyl agelastatin A **(12)** (TR = 10.3 min, 0.6 mg, 26%) as thin film: Rf 0.41 (CH_2Cl_2/ MeOH 9:1) (CAM, UV); 1 H NMR (500 MHz, CD_3OD) δ 6.80 (s, 1H), 4.55 (app dt, J = 12.0, 6.0 Hz, 1H), 4.06 (d, J = 5.4 Hz, 1H), 3.86 (s, 1H), 2.80 (s, 3H), 2.62 (dd, J = 13.1, 6.5 Hz, 1H), 2.07 (app t, J = 12.6 Hz, 1H), 2.04 (s, 3H); 13C NMR (125 MHz, CD_3OD) δ 160.7, 160.4, 122.4, 121.2, 116.0, 106.3, 94.8, 67.3, 61.9, 54.4, 39.6, 23.8, 11.2, assignments and correlations were verified by HSQC and HMBC experiments; HRMS (+ESI): m/z calcd for $C_{13}H_{15}BrNaN_4O3$ [M+Na]+ 377.0225, found 377.0245

14-acetyl agelastatin A (13)

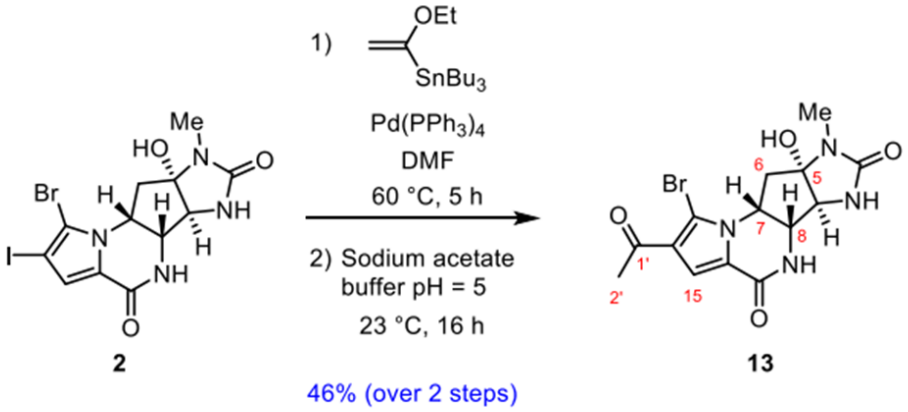

A solution of 14-iodo agelastatin A **(2)** (2 mg, 0.0043 mmol, 1 equiv) in DMF (0.2 mL) was degassed by passage of a stream of argon through the solution for 15 min through a stainless steel needle and the vinyl stannane derivative (6.0 mg, 0.017 mmol, 4.0 equiv) was added, followed by $Pd(PPh_3)_4$ (3.0 mg, 0.0026 mmol, 0.6 equiv). The reaction mixture was heated at 60 °C for 5 h. The reaction mixture was filtered and concentrated *in vacuo*. The residue was dissolved in a 0.2 M solution of sodium acetate buffer (pH = 5) and stirred at 23 °C for 16 h. The reaction mixture was concentrated *in vacuo* and purified by semi-preparative reversephase HPLC (100 x 21.20 mm, 5µm; linear gradient, 5 → 95% CH_3CN/H_2O with 0.1% of ammonium bicarbonate over 20 min, 8 mL/min) to yield 14-acetyl agelastatin A **(13)** (TR = 8.55 min, 0.74 mg, 46%) as a colorless solid: Rf 0.43 (CH_2Cl_2 / MeOH 9:1) (CAM, UV); 1 H NMR (500 MHz, CD_3OD) δ 7.44 (s, 1H), 4.72 (app dt, J = 12.1, 6.1 Hz, 1H), 4.12 (d, J = 5.4 Hz, 1H), 3.90 (s, 1H),

2.82 (s, 3H), 2.73 (dd, J = 13.1, 6.4 Hz, 1H), 2.49 (s, 3H), 2.15 (app t, J = 12.7 Hz, 1H); 13C NMR (125 MHz, CD_3OD) δ 193.2, 160.2, 124.2, 123.9, 116.6, 110.0, 94.3, 67.0, 61.6, 54.3, 39.2, 28.3, 23.9 (due to small quantities obtained, C=O amide not observed), assignments and correlations were verified by HSQC and HMBC experiments; HRMS (+ESI): m/z calcd for $C_{14}H_{15}BrNaN_4O_4$ [M+Na]+ 405.0174, found 405.0177

14-ethynylphenyl agelastatin A (14)

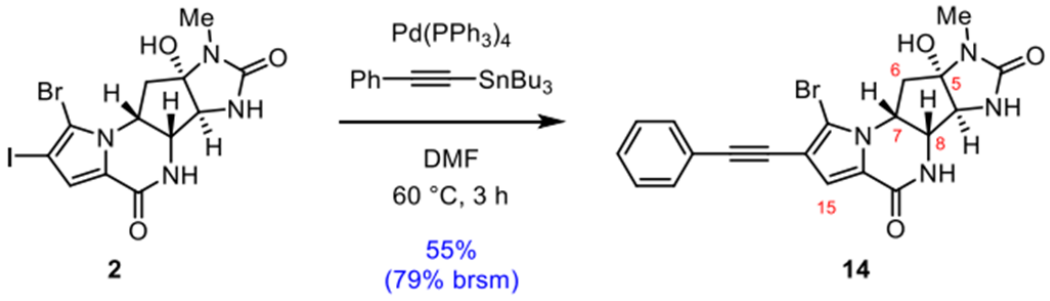

A solution of 14-iodo agelastatin A **(2)** (5 mg, 0.010 mmol, 1 equiv) in DMF (0.5 mL) was degassed by passage of a stream of argon through the solution for 15 min through a stainless steel needle and stannane derivative (10.0 µL, 0.030 mmol, 3 equiv) was added, followed by $Pd(PPh_3)_4$ (3.5 mg, 0.003 mmol, 0.3 equiv). The reaction mixture was heated at 60 °C for 3 h. The reaction mixture was concentrated *in vacuo*. The residue was purified by flash column chromatography (SiO_2, 10% of MeOH in CH_2Cl_2) and by semi-preparative reverse-phase HPLC (100 x 21.20 mm, 5µm; linear gradient, 5 → 95% CH_3CN/H_2O with 0.1% of ammonium bicarbonate over 20 min, 10 mL/min) to yield 14-ethynylphenyl agelastatin A (TR = 12.7 min, 2.4 mg, 55%) and recovered 14-iodo agelastatin A **(2)** (TR = 10.3 min, 1.5 mg) both as colorless solids: Rf 0.39 (CH_2Cl_2 / MeOH 9:1) (CAM, UV); 1 H NMR (500 MHz, CD_3OD) δ 7.48 (m, 2H), 7.35 (m, 3H), 7.05 (s, 1H), 4.63 (app dt, J = 11.9, 6.1 Hz, 1H), 4.13 (d, J = 5.4 Hz, 1H), 3.89 (s, 1H), 2.82 (s,

3H), 2.71 (dd, J = 12.9, 6.3 Hz, 1H), 2.15 (app t, J = 12.6 Hz, 1H); 13C NMR (125 MHz, CD_3OD) δ 161.4, 160.4, 132.3 (2), 129.6, 129.4, 125.4, 124.1, 117.5, 111.9, 110.0, 95.6, 92.8, 82.4, 67.4, 67.3, 62.0, 55.0, 39.9, 24.2; HRMS (+ESI): m/z calcd for $C_{20}H_{17}BrNaN_4O_3$ [M+Na]+ 463.0381, found 463.0390.

4-Azido-N-benzylbutyramide (A)

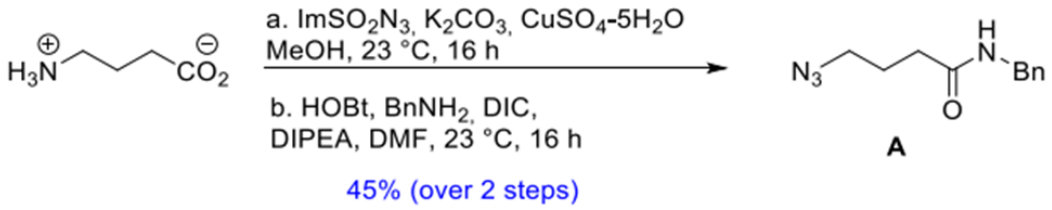

To a solution of 4-azidobutrylamine (Goddard-Borger and Stick, 2007) (500 mg, 3.87 mmol, 1 equiv) was added benzylamine (0.84 mL, 7.75 mmol, 2 equiv), HOBt (1 g, 7.75 mmol, 2 equiv), DIC (1.22 mL, 7.75 mmol, 2 equiv) and DIPEA (2 mL, 11.61 mmol, 3 equiv). The solution was stirred at 23 °C for 16 h and quenched with 0.5 M aqueous solution of HCl. The combined mixture was extracted with diethyl ether (3 x 15 mL). The organic extract was washed with brine (3 x 15 mL), dried over $MgSO_4$, filtered and concentrated under reduced pressure. The resulting colorless solid was purified by flash column chromatography (SiO_2, 20 → 50% EtOAc/hexanes) providing 385 mg (46%) of 4-Azido-N-benzylbutyramide (A) as a colorless solid: m.p. 65-67°C; Rf 0.65 (50% EtOAc /hexanes) (CAM, weak UV active); 1 H NMR (500 MHz, $CDCl_3$) δ 7.34 (dt, J = 6.6, 1.5 Hz, 2H), 7.29 (dd, J = 7.4, 1.4 Hz, 1H), 7.26 (br d, J = 7.8 Hz, 2H), 4.38 (d, J = 5.8 Hz, 2H), 3.29 (br dt, J = 6.6, 1.5 Hz, 2H), 2.29 (br dt, J = 7.4, 1.3 Hz, 2H,), 1.89 (m, 2H); 13C NMR (125 MHz, $CDCl_3$) δ 172.0, 138.3, 128.4 (2), 127.3 (2), 127.1, 50.6, 43.2, 32.8,

24.7; IR (cm-1) 3230, 2105 (N3), 1682 (C=O); HRMS (+ESI): m/z calcd for $C_{11}H_{16}N_4O$ [M+H]+219.1247 found 219.1294

O-Triazole derivative of agelastatin A (15)

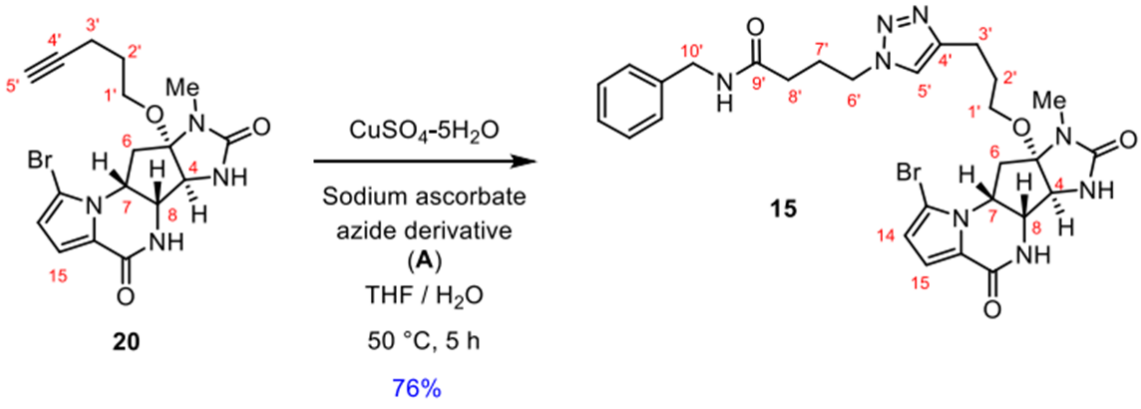

To a solution of O-4'-pentynyl agelastatin A **(20)** (3.0 mg, 7.40 µmol, 1 equiv) and 4-azido-Nbenzylbutyramide (A) (3.22 mg, 14.8 µmol, 2 equiv) in THF (0.2 mL) was added a freshly prepared CuSO4 / sodium ascorbate solution (the solution was made from mixing $CuSO_4$- $5H_2O$, 2.2 µmol, 0.3 equiv and sodium ascorbate, 22.2 µmol, 3 equiv in H2O (0.2 mL) until the initial black color turned yellow). The mixture was stirred at 50 °C for 5 h and concentrated *in vacuo*. The residue was purified by semi-preparative reverse-phase HPLC (100 x 21.20 mm, 5µm; linear gradient, 5 → 70% CH_3CN/H_2O with 0.1% of ammonium bicarbonate over 20 min, 10 mL/min) to yield the O-triazole derivative of agelastatin A 15 (TR = 14.7 min, 3.5 mg, 76%) as a colorless solid: Rf 0.60 (CH_2Cl_2 / MeOH 9:1) (CAM, UV); 1 H NMR (500 MHz, CD_3OD) δ 7.73 (s, 1H), 7.29 (overlapping br app q, J = 7.4 Hz, 2H), 7.27 (overlapping br app d, J = 8.1 Hz, 2H), 7.23 (br app tt, J = 7.1, 1.6 Hz, 1H), 6.91 (d, J = 4.1 Hz, 1H), 6.33 (d, J = 4.1 Hz, 1H), 4.60

(app dt, J = 12.0, 6.1 Hz, 1H), 4.41 (t, J = 6.6 Hz, 2H), 4.35 (s, 2H), 4.09 (d, J = 5.4 Hz, 1H), 4.08 (s, 1H), 3.37 (br dt, J = 9.0, 6.3 Hz, 1H), 3.27 (br dt, J = 9.0, 6.1 Hz, 1H), 2.79 (dt, J = 7.5, 2.6 Hz, 2H), 2.75 (s, 3H), 2.66 (dd, J = 13.3, 6.3 Hz, 1H), 2.26-2.18 (m, 4H), 2.16 (app t, J = 12.7 Hz, 1H), 1.96 (br app quint, J = 6.5 Hz, 1H); 13C NMR (125 MHz, CD_3OD) δ 174.3, 161.6, 161.0, 148.5, 140.0, 129.6 (2), 128.6 (2), 128.2, 124.1, 123.5, 116.1, 113.9, 107.3, 99.8, 62.9, 62.1, 61.5, 53.7, 50.6, 44.2, 39.3, 33.4, 30.2, 27.3, 24.8, 22.9; HRMS (+ESI): m/z calcd for $C_{28}H_{34}BrN_8O_4$ [M+H]+ 625.1887, found 625.1876

O-(butan-3'-one)-agelastatin A (17)

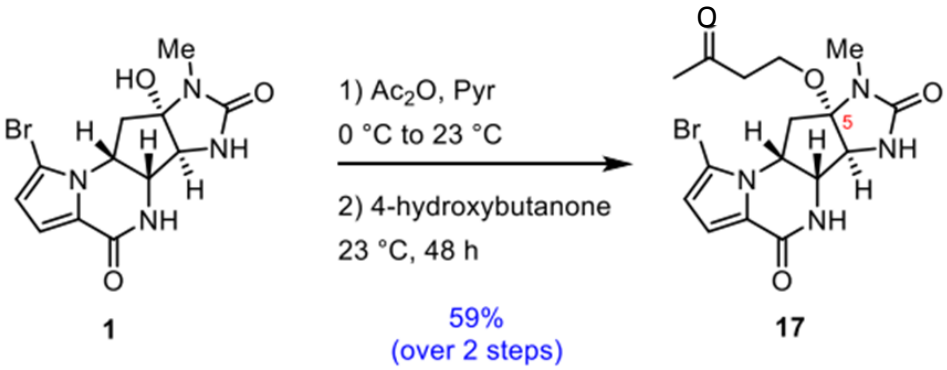

A solution of (–)-agelastatin A **(1)** (1 mg, 0.0029 mmol, 1 equiv) in pyridine (0.1 mL) was cooled at 0 °C and acetic anhydride was added dropwise (0.3 mL). The reaction mixture was slowly allowed to warm up to 23 °C and stirred for 16 h. The reaction mixture was concentrated *in vacuo*. The residue was dissolved in 4-hydroxybutanone (0.1 mL) and stirred at 23 °C for 48 h. The reaction mixture was purified by semi-preparative reverse-phase HPLC (100 x 21.20 mm, 5μm; linear gradient, 5 → 95% CH_3CN/H_2O with 0.1% of ammonium bicarbonate over 20 min, 8 mL/min) to yield O-(butan-3'-one)-agelastatin A (TR = 11.1 min, 0.70 mg, 59%) as a

colorless solid: Rf 0.81 (CH_2Cl_2/ MeOH 9:1) (CAM, UV); 1 H NMR (500 MHz, CD_3OD) δ 6.91 (d, J = 4.1 Hz, 1H), 6.32 (d, J = 4.1 Hz, 1H), 4.60 (app dt, J = 12.1, 6.1 Hz, 1H), 4.15 (s, 1H), 4.11 (d, J = 5.6 Hz, 1H), 3.60 (br dt, J = 9.2, 5.9 Hz, 1H), 3.51 (br dt, J = 9.2, 5.9 Hz, 1H), 2.81 (s, 3H), 2.77 (app t, J = 5.9 Hz, 2H), 2.65 (dd, J = 13.2, 6.4 Hz, 1H), 2.17 (s, 3H,), 2.12 (app t, J = 12.7 Hz, 1H); 13C NMR (125 MHz, CD_3OD) δ 209.7, 161.1, 160.1, 124.1, 116.1, 113.9, 107.3, 99.7, 62.1, 61.5, 58.9, 53.6, 43.1, 39.1, 30.4, 24.7; HRMS (+ESI): m/z calcd for $C_{16}H_{20}BrN_4O_4$ [M+H]+ 411.0668, found 411.0653

5-amino agelastatin A derivative 18

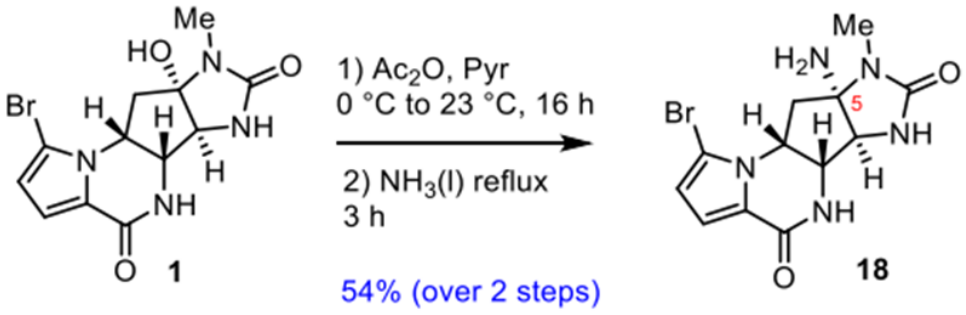

A solution of (–)-agelastatin A **(1)** (0.8 mg, 0.0023 mmol, 1 equiv) in pyridine (0.1 mL) was cooled to 0 °C and acetic anhydride was added dropwise (0.3 mL). The reaction mixture was allowed to slowly warm to 23 °C and stirred for 16 h. The reaction mixture was concentrated *in vacuo* and the residue was dissolved in liquid ammonia (3-5 mL) at -78 °C and stirred at reflux (-30 °C) for 3 h. The reaction mixture was allowed to warm up to 23 °C (to allow ammonia to evaporate) and purified by semi-preparative reverse-phase HPLC (100 x 21.20 mm, 5μm; linear gradient, 5 → 95% CH_3CN/H_2O with 0.1% of ammonium bicarbonate over 20 min, 8 mL/min) to yield 5-amino agelastatin A derivative 18 (TR = 9.0 min, 0.42 mg, 54%) and agelastatin A **(1)** (TR = 10.1 min, 0.35

mg) as thin films: Rf 0.25 (CH_2Cl_2 / MeOH 9:1) (CAM, UV); 1 H NMR (500 MHz, CD_3OD) δ 6.90 (d, J = 4.2 Hz, 1H), 6.32 (d, J = 4.2 Hz, 1H), 4.66 (app dt, J = 12.0, 6.0 Hz, 1H), 4.09 (d, J = 5.5 Hz, 1H), 3.85 (s, 1H), 2.80 (s, 3H), 2.60 (dd, J = 13.2, 6.6 Hz, 1H), 1.98 (app t, J = 12.6 Hz, 1H); 13C NMR (125 MHz, CD_3OD) δ 161.4, 161.1, 124.2, 116.0, 113.8, 107.2, 82.0, 67.9, 63.0, 54.9, 40.8, 24.1; HRMS (+ESI): m/z calcd for $C_{12}H_{16}BrN_5O_3$ [M+H]+ 340.0410, found 340.0401

(±)-9-methyl-agelastatin A (19)

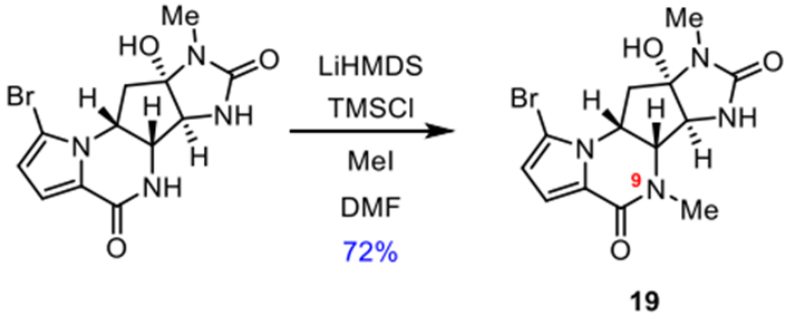

19

To a solution of (±)-agelastatin A (2.0 mg, 5.9 μmol, 1 equiv) in DMF (0.5 mL) was added a 1.0 M solution of LiHMDS in THF (6.4 μL, 6.4 μmol, 1.1 equiv) at 23 °C. After 30 min, a 1.0 M solution of TMSCl in THF (5.9 μL, 5.9 μmol, 1.0 equiv) was added. Following another 30 min of stirring, a 1.0 M solution of LiHMDS in THF (6.4 μL, 6.4 μmol, 1.1 equiv) was added. After an additional 30 minutes of stirring, a 0.5 M solution of MeI in THF (11.7 μL, 5.9 μmol, 1.0 equiv). Following 30 minutes of stirring, TBAF (41 μL, 41.0 μmol, 7.0 equiv) was added and after stirring for 30 min, a 0.5 mL of saturated NH_4Cl solution was added. The reaction mixture was then filtered through a short silica gel plug eluting with 20% MeOH/CH_2Cl_2. The filtrate was concentrated *in vacuo* to give a colorless residue. The residue was purified by preparative TLC eluting and washing with 10% MeOH in CH_2Cl_2 to give 1.5 mg (72%) of (±)-9-methyl agelastatin A **(19)** as a

colorless solid: Rf 0.26 (CH_2Cl_2/ MeOH 9:1) (CAM, UV); 1 H NMR (500 MHz, CD_3OD) δ 6.89 (d, J = 4.0 Hz, 1H), 6.33 (d, J = 4.0 Hz, 1H), 4.70 (dt, J = 12.0, 6.0 Hz, 1H), 4.16 (s, 1H), 4.02 (d, J = 6.0 Hz, 1H), 3.14 (s, 3H), 2.81 (s, 3H), 2.66 (dd, J = 13.0, 6.5 Hz, 1H), 2.10 (dd, J = 13.0, 12.0 Hz, 1H); 13C NMR (125 MHz, CD_3OD) δ 161.7, 159.9, 124.3, 116.1, 114.1, 106.4, 94.8, 68.6, 66.0, 54.2, 41.0, 31.0, 24.2 HRMS (-ESI): m/z calcd for $C_{13}H_{14}BrN_4O_3$ [M-H]- 353.0249 found 353.0233

O-4'-pentynyl agelastatin A (20)

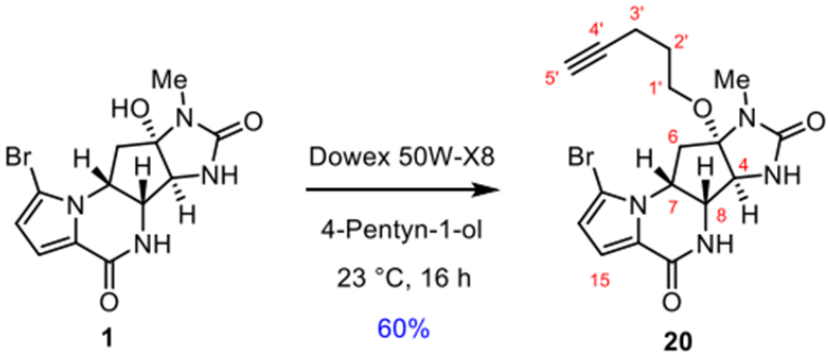

A solution of (–)-agelastatin A **(1)** (5.0 mg, 0.014 mmol, 1 equiv) in 4-pentyn-1-ol (0.3 mL) was stirred with 20 mg of Dowex 50W-8X (200-400 mesh, H+ form, prewashed with 1M HCl, rinsed with distilled H2O and dried under vacuum for 2 days) at 50 °C for 2 h then 16 h at 23 °C. The mixture was filtered and the filtrate concentrated *in vacuo*. The residue was purified by semi-preparative reverse-phase HPLC (100 x 21.20 mm, 5μm; linear gradient, 5 → 95% CH_3CN/H_2O with 0.1% of ammonium bicarbonate over 20 min, 10 mL/min) to yield O-4'- pentynyl agelastatin A **(20)** (TR = 14.3 min, 3.4 mg, 60%) as a colorless solid: Rf 0.75 (CH_2Cl_2 / MeOH 9:1) (CAM, UV); 1 H NMR (500 MHz, CD_3OD) δ 6.92 (d, J = 4.1 Hz, 1H), 6.34 (d, J = 4.1 Hz, 1H), 4.62 (app dt, J = 12.0, 6.1 Hz, 1H),

4.12 (d, J = 5.6 Hz, 1H), 4.09 (s, 1H), 3.46 (dt, J = 9.0, 6.1 Hz, 1H), 3.38 (br dt, J = 8.9, 6.2 Hz, 1H), 2.81 (s, 3H), 2.68 (dd, J = 13.2, 6.5 Hz, 1H), 2.29 (m, 2H), 2.26 (br app t, J = 2.6 Hz, 1H), 2.18 (app t, J = 12.7 Hz, 1H), 1.77-1.80 (m, 2H); 13C NMR (125 MHz, CD_3OD) δ 161.7, 161.0, 124.1, 116.1, 113.9, 107.3, 99.7, 84.1, 70.3, 70.2, 62.2, 61.6, 53.7, 39.2, 29.5, 24.8, 15.8; HRMS (+ESI): m/z calcd for $C_{17}H_{20}BrN_4O_3$ [M+H]+ 407.0719, found 407.0707

N-(prop-2-yn-1-yl)-3-(tricyclohexylstannyl)prop-2-yn-1-amine

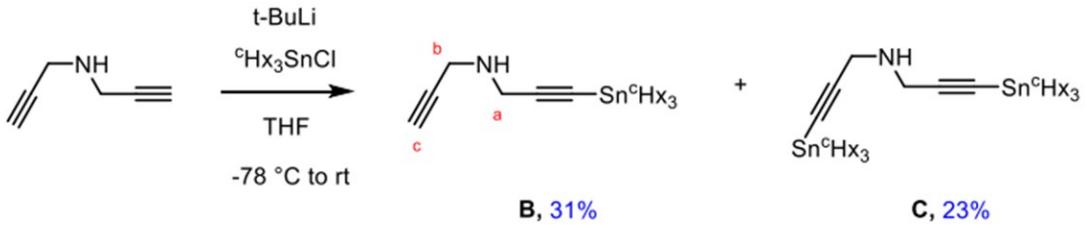

To a solution of dipropargyl amine (100 mg, 1.07 mmol, 1 equiv) in THF (7 mL) at -78 °C was added dropwise a 1.7 M solution of tert-butyllithium in THF (0.63 mL, 1.07 mmol, 1 equiv). The reaction mixture was maintained at -78 °C for 1 h before a pre-cooled solution of c Hx_3SnCl (433 mg, 1.07 mmol, 1 equiv) in THF (3 mL) was added. The reaction mixture was slowly allowed to warm to 23 °C with stirring. The reaction was quenched with saturated aqueous solution of $NaHCO_3$ and extracted with Et_2O (3X). The combined organic layers were washed with brine, dried over $MgSO_4$ and filtered off. The solvent was removed under reduced pressure. The residue was purified by flash column chromatography (SiO_2, 5% EtOAc/hexanes w/ 1% Et_3N → 10% EtOAc/hexanes w/ 2% Et_3N) providing 152 mg (31%) of dipropargylamine stannane (B) as colorless oil and 204 mg (23%) of dipropargylamine distannane (C) as a colorless solid:

Dipropargylamine stannane (B): Rf 0.31 (9:1 EtOAc/hexanes) (CAM); 1 H NMR (300 MHz, $CDCl_3$) δ 3.53-3.56 (m, 4H), 2.21 (t, J = 2.4 Hz, 1H), 1.86-1.90 (m, 6H), 1.60-1.70 (m, 12H), 1.56-1.58 (m, 6H), 1.22-1.36 (m, 9H); 13C NMR (74.5 MHz, $CDCl_3$) δ 108.1, 86.7, 81.7, 71.6, 38.5, 36.9, 32.3, 32.2, 32.0, 29.5, 29.1, 28.7, 27.9, 27.1; HRMS (+ESI): m/z calcd for $C_{24}H_{40}NSn$ [M+H]+ 462.2183, found 462.2172

Dipropargylamine distannane (C): Rf 0.53 (9:1 EtOAc/hexanes) (CAM) 1 H NMR (300 MHz, $CDCl_3$) δ 3.57 (app t, J = 2.4 Hz, 4H), 1.82-1.91 (m, 12H), 1.61-1.70 (m, 24H), 1.57 (br s, 12H), 1.24-1.34 (m, 18H); HRMS (+ESI): m/z calcd for $C_{42}H_{72}NSn_2$ [M+H]+ 830.3709, found 830.3715

14-dipropargylamine agelastatin A derivative 21

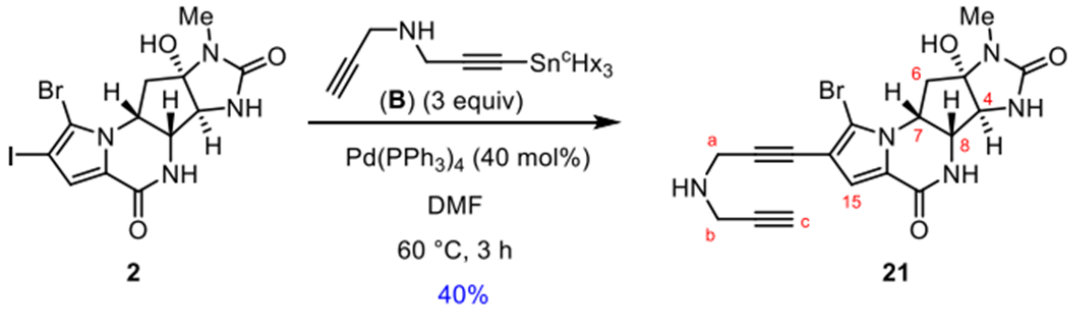

To a solution of 14-iodo-agelastatin A (7 mg, 0.015 mmol, 1 equiv) in DMF (0.4 mL) was added stannane derivative (B) (21 mg, 0.045 mmol, 3 equiv). The reaction mixture was degassed by passage of a stream of argon through the solution for 15 min through a stainless steel needle and then $Pd(PPh_3)_4$ (7.0 mg, 0.084 mmol, 0.4 equiv) was added and the reaction mixture was heated at 60 °C for 3 h. The reaction mixture

was allowed to cool to 23 °C and charcoal (200 mg) was added. After 10 min at 23 °C, the reaction mixture was filtered and concentrated *in vacuo*. The residue was purified by flash column chromatography (SiO2, 10% MeOH/CH_2Cl_2 w/ 1% Et_3N) providing 2.5 mg (40%) of 14-dipropargylamine agelastatin A derivative **21** as a colorless solid: Rf 0.36 (CH_2Cl_2 / MeOH 9:1) (CAM, UV); 1 H NMR (500 MHz, CD_3OD) δ 6.96 (s, 1H), 4.59 (app dt, J = 11.9, 6.0 Hz, 1H), 4.10 (d, J = 5.3 Hz, 1H), 3.87 (s, 1H), 3.70 (s, 2H), 3.54 (br d, J = 2.7 Hz, 2H), 2.80 (s, 3H), 2.67 (br dd, J = 13.2, 6.6 Hz, 1H), 2.64 (br t, J = 2.5 Hz, 1H), 2.10 (app t, J = 12.7 Hz, 1H); 13C NMR (125 MHz, CD_3OD) δ 161.4, 160.4, 123.9, 117.7, 111.7, 109.8, 95.6, 89.6, 81.3, 77.2, 73.6, 67.4, 62.0, 54.9, 39.8, 37.8, 37.0, 24.2; HRMS (+ESI): m/z calcd for $C_{18}H_{19}BrN_5O_3$ [M+H] + 432.0672, found 432.0674.

4-(3-(trifluoromethyl)diaziridin-3-yl)benzoic acid (22)

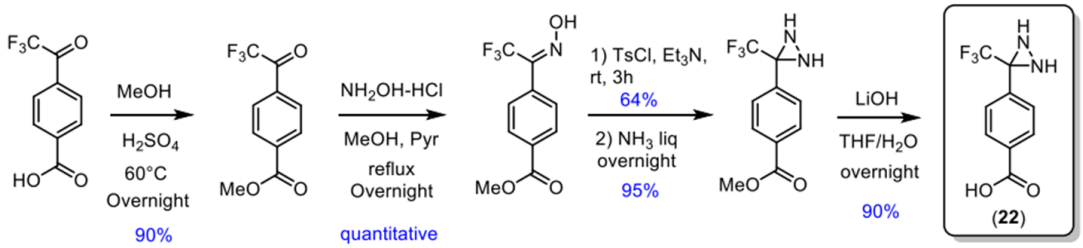

The diaziridine **22** was prepared according to published procedures (Bender et al., 2007; Rennhack et al., 2012).

Diaziridine agelastatin A derivative 23

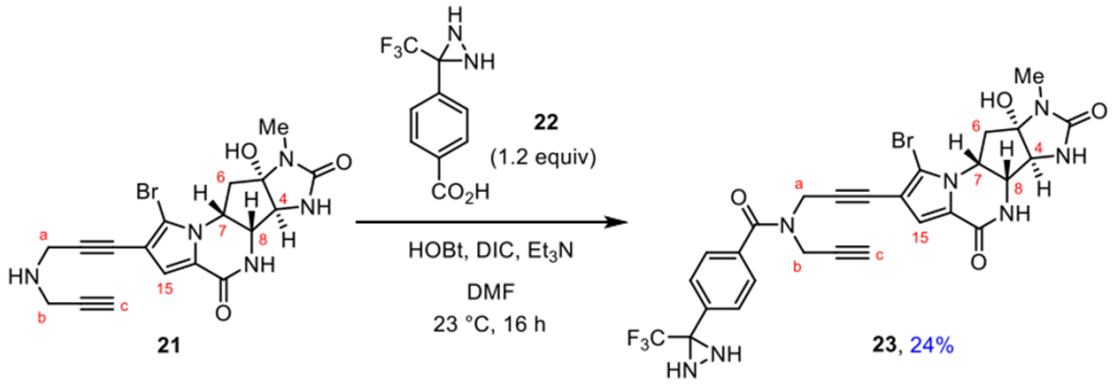

To a solution of 14-dipropargylamine-agelastatin A **(21)** (3.0 mg, 0.007 mmol, 1.0 equiv) in DMF (0.4 mL) at 0 °C was added trifluoromethyldiaziridine carboxylic acid **22** (1.9 mg, 0.008 mmol, 1.2 equiv), HOBt (1.0 mg, 0.007 mmol, 1.0 equiv), Et_3N (2 µL, 0.011 mmol, 1.5 equiv) and DIC (1.3 µL, 0.008 mmol, 1.2 equiv). The mixture was stirred at 0 °C and allowed to warm to 23 °C overnight. The reaction mixture was concentrated *in vacuo* and the residue was purified by pipette flash column chromatography (SiO_2, 10% of MeOH in CH_2Cl_2 with 1% of NH_4OH) and then by semi-preparative reverse-phase HPLC (100 x 21.20 mm, 5µm; linear gradient, 5 → 95% CH_3CN/H_2O with 0.1% of ammonium bicarbonate over 20 min, 10 mL/min) to deliver the diaziridine agelastatin A probe 23 (TR = 11.0 min, 1.1 mg, 24%) as a 1:1 mixture of amide rotamers and as a thin film.

Diaziridine agelastatin A derivative (**23**): Rf 0.35 (CH_2Cl_2 / MeOH 9:1) (CAM, UV); 1 H NMR (500 MHz, CD_3OD) δ 7.77 (br d, J = 7.1 Hz, 2H), 7.65 (br s, 2H), 7.01 (s, 1H), 4.68 (m, 1H), 4.61 (app ddd, J = 12.9, 12.2, 6.1 Hz, 1H), 4.49 (m, 1H), 4.39 (m, 1H), 4.23 (m, 1H), 4.11 (d, J = 5.4 Hz, 1H), 6.88 (s, 1H), 2.81 (s, 3H), 2.68 (br dd, J = 13.0, 6.5 Hz, 1H), 2.13 (app t, J = 12.6 Hz, 1H); 13C NMR (125 MHz, CD_3OD) δ 161.3, 160.8, 137.5,

130.4, 129.7, 127.8, 124.9, 124.0, 117.2, 112.3, 95.7, 67.5, 66.9, 66.4, 61.5, 54.4, 39.3, 35.2, 23.6 (due to small quantities and slow relaxation time, 8 carbons were not observable; extended reaction times were precluded due to instability concerns), assignments and correlations were verified by HSQC and HMBC experiments; ^{19}F NMR (470 MHz, CD_3OD) δ -76.67; HRMS (+ESI): m/z calcd for $C_{27}H_{24}BrF_3N_7O_4$ [M+H]+ 646.1025, found 646.1041.

Diazirine Agelastatin A derivative 24

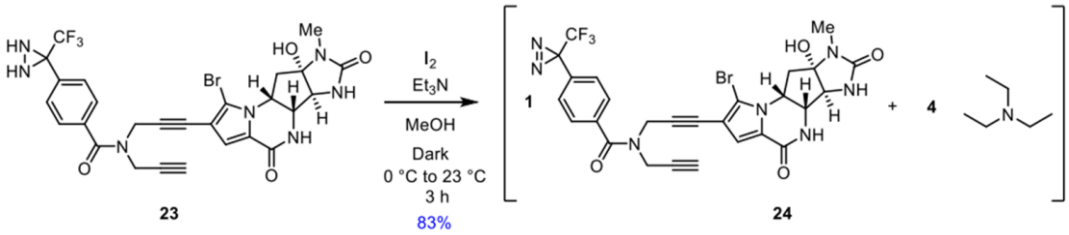

To a solution of the diaziridine agelastatin A derivative **23** (1 mg, 0.0015 mmol, 1 equiv) in MeOH (0.1 mL) protected from light at 0 °C was added Et_3N (1.3 µL, 0.009 mmol, 6 equiv) and I2 (0.6 mg, 0.0023 mmol, 1.5 equiv). The mixture was allowed to warm to 23 °C for 3 h and concentrated *in vacuo*. The residue was purified by pipette flash column chromatography protected from light (SiO_2, 9% MeOH, 1% NH_4OH in CH_2Cl_2) to yield diazirine agelastatin A derivative 24 (1.14 mg as a mixture of 1:4 probe/Et_3N; 0.800 mg, 83% estimated by NMR of free probe) as a thin film: Rf 0.40 (9% MeOH, 1% NH_4OH in CH_2Cl_2) (CAM, UV); 1 H NMR (500 MHz, CD_3OD) δ 7.68 (br d, J = 7.6 Hz, 2H), 7.40 (d, J = 8.1 Hz, 2H), 7.00 (s, 1H,), 4.60 (app dt, J = 11.9, 6.3 Hz, 1H) overlap with 4.60 (m, 1H), 4.49 (m, 1H), 4.37 (m, 1H), 4.22 (m, 1H), 4.10 (d, J = 5.4 Hz, 1H), 3.88 (s, 1H), 2.81 (s, 3H,), 2.69 (br dd, J = 13.3, 6.2 Hz, 1H), 2.13 (app t, J = 12.6

Hz, 1H); 19F NMR (470 MHz, CD_3OD) δ -66.9; HRMS (+ESI): m/z calcd for $C_{27}H_{21}BrLiF_3N_7O_4$ [M+Li]+ 650.0951, found 650.0933

13-debromo-13-methyl-agelastatin A (25)

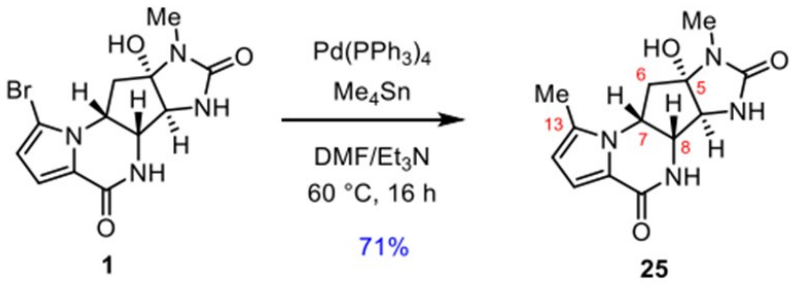

A solution of (–)-agelastatin A **(1)** (5 mg, 0.015 mmol, 1 equiv) in DMF/Et_3N (0.3/0.1 mL) was degassed by passage of a stream of argon through the solution for 15 min through a stainless steel needle and tetramethyltin (9.0 µL, 0.06 mmol, 4 equiv) was added, followed by $Pd(PPh_3)_4$ (7.0 mg, 0.006 mmol, 0.4 equiv). The reaction mixture was heated at 60 °C for 16 h. The reaction mixture was concentrated *in vacuo*. The residue was purified by flash column chromatography (SiO_2, 10% of MeOH in CH_2Cl_2) and then by semi-preparative reverse-phase HPLC (100 x 21.20 mm, 5µm; linear gradient, 5 → 95% CH_3CN/H_2O with 0.1% of ammonium bicarbonate over 20 min, 10 mL/min) to yield 13-debromo-13-methyl-agelastatin A (**25**) (TR = 8.0 min, 3.0 mg, 71%) as a colorless solid: Rf 0.35 (CH_2Cl_2 / MeOH 9:1) (CAM, UV); 1 H NMR (500 MHz, CD_3OD) δ 6.83 (d, J = 3.6 Hz, 1H), 6.01 (d, J = 3.6 Hz, 1H), 4.54 (app dt, J = 12.0, 6.1 Hz, 1H), 4.03 (d, J = 5.3 Hz, 1H), 3.87 (s, 1H), 2.80 (s, 3H), 2.60 (dd, J = 13.0, 6.4 Hz, 1H), 2.28 (s, 3H), 2.09 (app t, J = 12.6 Hz, 1H); 13C NMR (125 MHz, CD_3OD) δ 162.3, 161.5, 134.7, 121.6,

115.5, 110.4, 95.9, 67.5, 62.5, 52.8, 40.2, 24.2, 11.4; HRMS (+ESI): m/z calcd for $C_{13}H_{17}N_4O_3$ [M+H]+ 277.1301, found 277.1290.

Photoaffinity labeling

Photoaffinity labeling was performed as described (Head et al., 2015), with modifications. Lysates were diluted to 200 ul, in ice cold 1x PBS (pH 8.5), followed by pretreatment with 100 uM competitor (AglA (**1**)) or an equal volume of DMSO vehicle for 30 min, before the addition of 1 uM probe or DMSO. After 1-h incubation with the probe, lysates were placed 3 cm below a Spectroline FC100 365 nm UV lamp for 1 min on ice to minimize heating from the lamp. After irradiation, samples were incubated at 95 °C for 5 min to denature all the proteins. For the click reaction with fluor-azide, 40 µL of lysate was removed and transferred to a new tube, and 0.2 µL Alexa Fluor 647 azide (1 mM stock solution in DMSO), 0.58 µL TCEP (100 mM stock with four equivalents NaOH added), and 3.38 µL TBTA (1.7 mM stock in a 4:1 ratio of t-butanol to DMSO) were added sequentially and vortexed to mix. Then $CuSO_4$-$5H_2O$ (1.14 µL, 50 mM stock in water) was added to start the reaction. The samples were vortexed again briefly and were incubated at room temperature for 30 min in the dark. Then aliquots of 50 µL 2× SDS sample buffer were added, and samples were subjected to SDS/PAGE before being scanned on a Typhoon FLA 9500 gel scanner (GE Healthcare Life Sciences) using a red excitation laser

Cell proliferation assay

HeLa cells were seeded at 3000 cells per well in 96-well plates and cultured in DMEM plus 10% FBS and 1% Penicillin Streptomycin at 37 °C with 5% CO_2. Twenty four hours after seeding, drugs were added and incubation was continued for an additional 24 h. An aliquot of 1 μCi of [3H]-thymidine (Perkin Elmer) was added per well and incubation was continued for an additional 6 h. Cells were harvested onto a Printed Filtermat A glass fiber filter (Perkin Elmer) using Tomtec Harvester 96 Mach III and filters were immersed in Betaplate Scint (Perkin Elmer) scintillation fluid, followed by scintillation counting on 1450 Microbeta JET (Perkin Elmer).

Patients

Samples from 12 CLL patients and three normal donors were used in this study. Median age of the patient was 65.5 (52 to 78) with 7 male patients and 5 female patients. Their median white blood cell count was 67.7 (14.6 to 214.6). The median lymphocyte percentage was 88% (73 to 94%). Majority of the patients was untreated. Approval was obtained from the University of Texas M. D. Anderson Cancer Center Institutional Review Board for this investigation, and all patients and donors agreed to participate and provided informed consent for use of their cells for in vitro studies.

CLL cells isolation and culture

Peripheral blood from the CLL patients were collected in heparin vacutainer tubes and centrifuged at 1500 rpm for 15 min to separate the plasma (upper layer), which was removed and saved for cell culture. The lower layer was diluted with phosphate-buffered saline (PBS), and the mononuclear cells were isolated by Ficoll density gradient centrifugation. The isolated CLL cells were cultured at 1 × 107 cells/mL in RPMI 1640 medium containing 10% of autologous plasma or 10% fetal bovine serum (FBS).

Quantitation of cell death

The CLL cells or normal lymphocytes were incubated with increasing concentrations of AglA or analogues for 24h, in RPMI 1640 media supplemented with either 10% patient plasma or 10% FBS. Cell viability was measured by Annexin V/propidium iodide double staining followed by flow cytometry. After the drug treatment, CLL cells (1x106 cells) were incubated in dark for 15 min at room temperature in 200 μL binding buffer with 5 mL annexin V-Cy5. After staining, 300 μL binding buffer with 5 μL of 50 μg/mL PI were added to each tube. Samples were analyzed immediately with a Becton Dickinson C6 flow cytometer. Cells stained positive for either annexin V or PI were considered dead cells. Normal B and T cells were identified by their positive staining for CD19 (B cells) or CD3 (T cells).

Plasma protein binding analysis

Plasma protein binding of the compounds was analyzed by equilibrium dialysis followed by liquid chromatography-mass spectrometry, in the Pharmaceutical Science Facility in the Institute for Applied Cancer Science, M. D. Anderson Cancer Center. All measurements were performed in triplicates.

SJSA1, A431, A3, Ovcar3 and Igrov cells isolation and culture

SJSA1, A431 and Ovcar3 cells were from ATCC. Igrov cells were a gift from National Cancer Institute on behalf of Dr. J. Benard. A3 was the A431 cells expressing the mesothelin protein, generated at Morphotek. Igrov, SJSA1, A431 and Ovcar3 cells were cultured in RPMI-1640 medium supplemented with 10% heat inactivated fetal bovine serum, 2 mM glutamine, 1X MEM. Non-essential amino acids, 50 unit/mL penicillin, and 50 mg/mL streptomycin. A3 cells were cultured in the same medium with 10 mg/mL zeocin. Cells were seeded at 10,000 cells/well in 96 well tissue culture plates, incubated at 37°C, 5% CO2 for overnight. All the compounds were dissolved in DMSO at 6 mM. Then compounds were serial diluted in the medium and added to the cells, incubated for additional 48 hours. At the end of the assay, discarded the medium, washed the plates with 200 mL DPBS, stained with 0.2% crystal violet solution for 15 minutes at room temperature, then washed with tap water, air dried, and dissolved with 200 mL of 1% SDS. Read the plates at 570 nm.

Chapter 3. Elucidation of the molecular target of Agelastatin A

Introduction

We show that AglA selectively inhibits protein synthesis, using a “top-down” target elucidation approach as described previously (Titov and Liu, 2012). By taking advantage of the extensive prior knowledge of eukaryotic translation, we systematically examined the effects of AglA on multiple steps of protein synthesis and determined that AglA inhibits translation elongation by binding within the ribosome, the heart of protein translation. Composed of an intricate complex of ribosomal RNA (rRNA) and proteins, the ribosome acts in conjunction with protein factors to catalyze templated peptide formation (Fig. 4). Each ribosome is composed of two subunits: The small 40S subunit (30S in bacteria and archaea) and the large 60S (50S) complex. (Cannone et al., 2002; Jenner et al., 2012)

The structure and sequence of ribosomal RNA have changed only little in the course of billions of years; the overall tertiary folds of the ribosomal components have been retained over the course of evolution. Because of its strong sequence conservation and slow mutation rate, ribosomal RNA presents an excellent evolutionary clock, though eukaryotic and prokaryotic ribosomes do differ from one another in a number of ways. Compared to its bacterial counterpart, the size of eukaryotic ribosomes is larger. The small bacterial subunit entails one molecule of rRNA (16S) and 21 proteins, while eukaryotes typically contain some 30 proteins and a longer (18S) rRNA molecule. The large bacterial subunit is composed of 5S and 23S rRNA and 34 proteins, which expanded to three species of rRNA (5S, 5.8S and 28S) and over 40 ribosomal proteins in eukaryotes (Lecompte et al., 2002). The core of the ribosome is very well conserved, though eukaryotic ribosomes have acquired expansion segments, insertions of often several hundred nucleotides in both 18S and 28S rRNA.

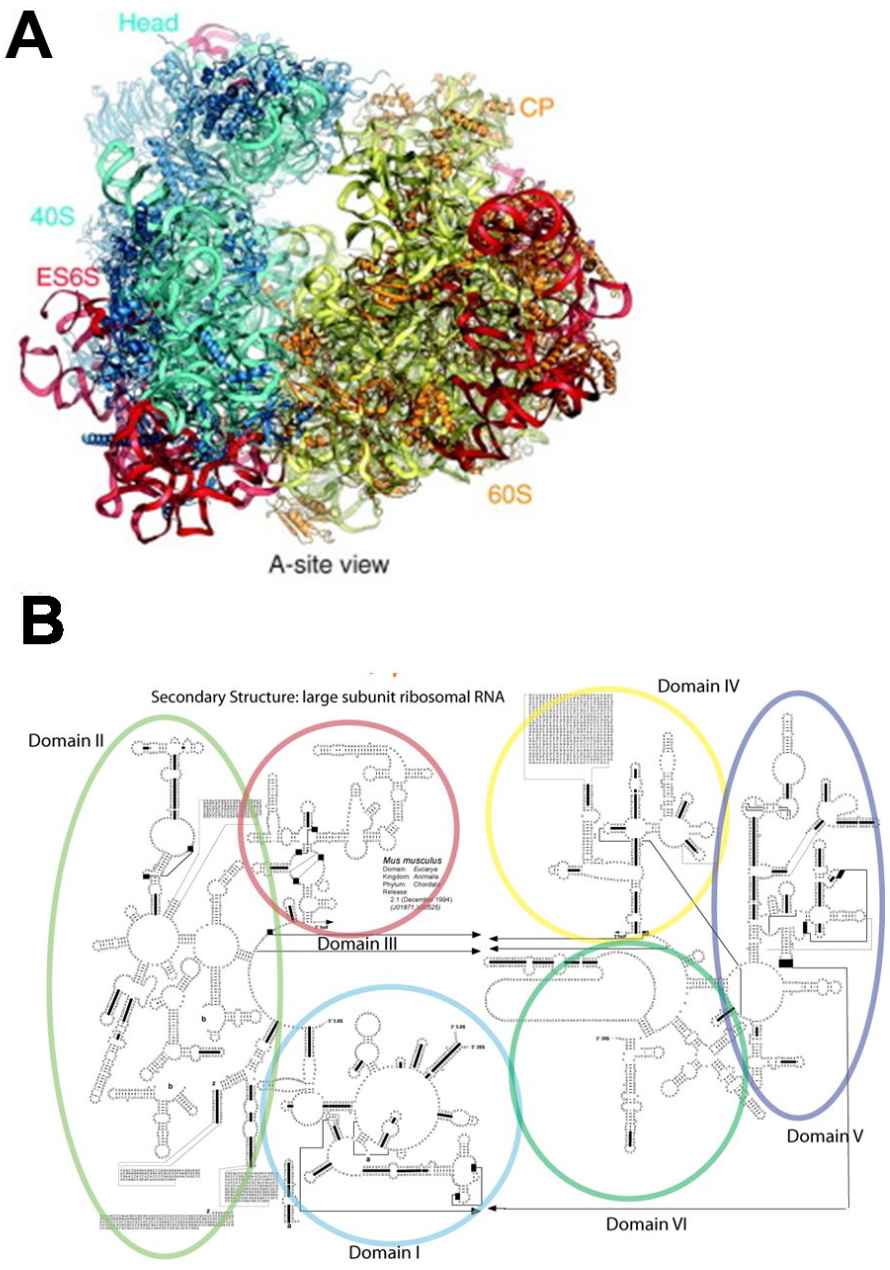

Fig. 4. Structure of the 60S ribosomal subunit. A) Crystal structure of the S. cerevisiae 80S ribosome, viewed from the A site and large subunit side. Polypeptide exit tunnel, mRNA entry and exit tunnels are indicated. The large subunit is shown in yellow with orange proteins and the small subunit in cyan with blue proteins. Eukaryote expansion segments (ES) are shown in red (adapted from Jenner et al., 2012). **B)** Secondary Structure of 28S rRNA with domains outlined (adapted from Cannone et al. 2002).

The 18S rRNA of the small subunit coordinates tRNA binding and codon recognition, while the 28S rRNA of the 60S subunit catalyzes peptide bond formation. Transfer RNAs (tRNA) are key players involved with the ribosome and formation of peptides. They are 74-95 nucleotide long polynucleotides, folding into characteristic cloverleaf secondary structures. Carrying an amino acid on their 3' end, they provide the large subunit with substrates for peptide formation while their anticodon loop interacts with the small subunit and its bound mRNA to ensure incorporation of the correct building blocks. Additional contacts to the ribosome are formed by the D and T-loops of tRNA (Agrawal et al., 2000).

While both eukaryotic and prokaryotic ribosomes carry out the same function, they work in very different environments. In bacteria, translation proceeds co-transcriptionally and because of the operon organization of prokaryotic genes, re-initiation on one transcript occurs regularly. In contrast, transcription and translation occur in two separate cellular compartments in eukaryotes. Eukaryotic translation of mRNAs begins with initiation (Fig. 5). During the initiation phase, the 40S ribosomal subunit is associated with initiator tRNA, and associated initiation factors; this complex unites with mRNA bound to a separate group of initiation factors. The 60S large ribosomal subunit is later recruited to form an 80S ribosome, marking the end of initiation and the beginning of elongation (Jackson et al., 2010). Elongation begins with the delivery of aminoacyl-tRNA into the ribosomal A-site (aminoacyl), mediated by the GTPase activity of eEF1A (Fig. 6).

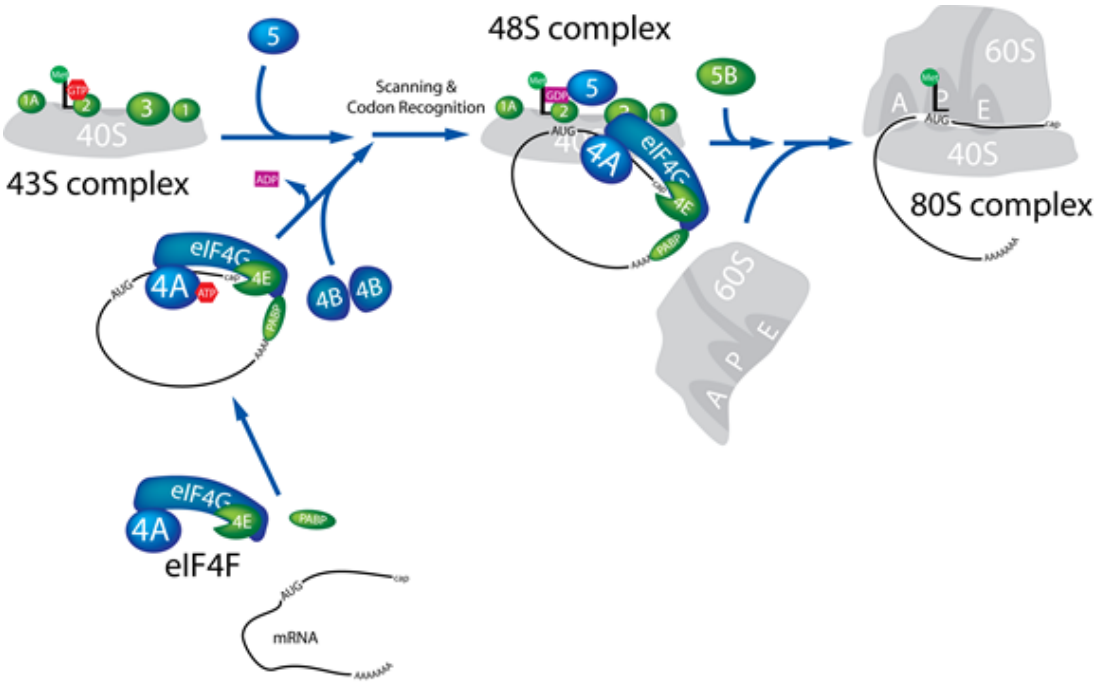

Fig. 5. A simplified overview of eukaryotic translation initiation. The eIF2-tRNA-GTP ternary complex binds the small ribosomal subunit before recruitment of the mRNA message. After localization of the start codon to the ribosomal P-site and dissociation of the initiation factors, the large ribosomal subunit can bind and elongation begin (Created by T. Schneider-Poetsch).

This is followed by peptidyl transfer and the eEF2-mediated peptidyl-tRNA translocation from A-site to P-site (peptidyl-site) while deacyltated tRNA is simultaneously transferred from the P- to E-site (exit). The highly conserved peptidyl transferase center (PTC) resides in the 60S subunit of the ribosome and is the epicenter of peptide bond formation. In order for peptide bonds to form, aminoacyl-tRNA and peptidyl-tRNA must to be properly aligned in the A-site and P-site of the PTC (Merrick, 1992; Polacek and Mankin, 2005).

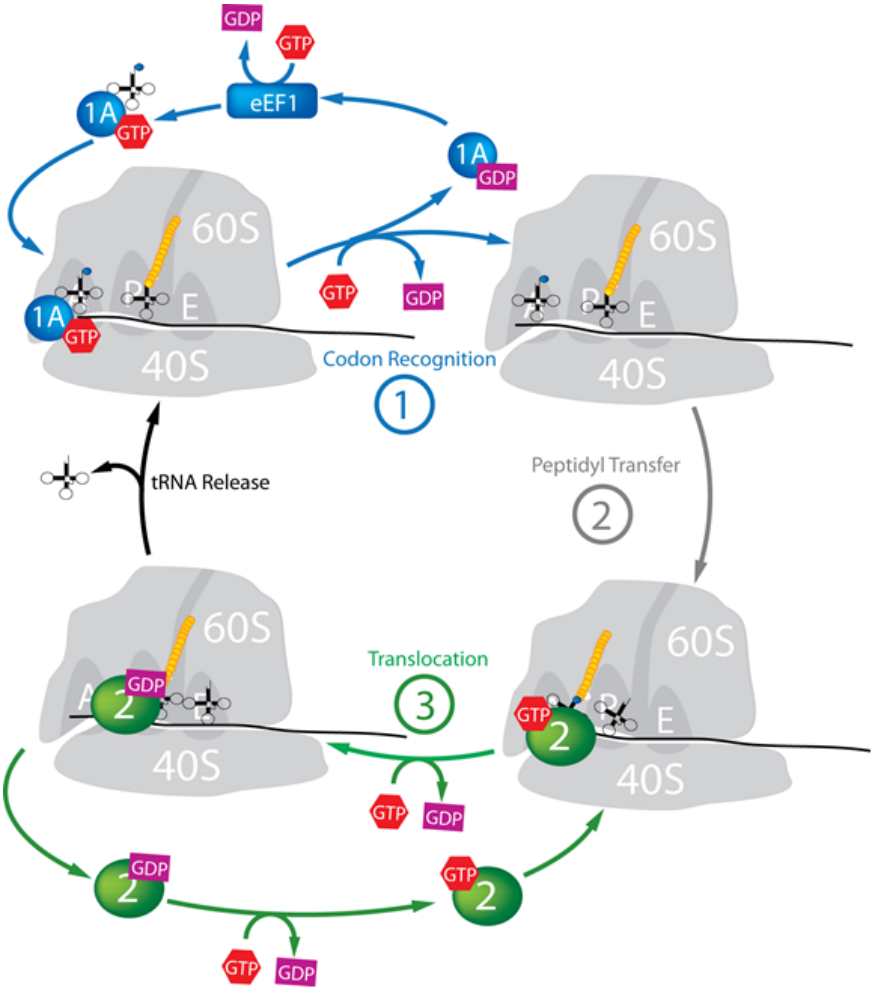

Fig. 6. The Eukaryotic Elongation Cycle. eEF1A delivers its acylated tRNA cargo into the A-site of the 80S ribosome. Upon codon recognition eEF1A hydrolyzes GTP and recycles, leaving the tRNA behind. The ribosome catalyzes peptidyl transfer, thereby attaching the nascent peptide to the A-site tRNA. eEF2 translocates the deacylated P-site tRNA into the E-site and the A-site tRNA into the P-site, thereby clearing the A-site for the next round of elongation (Adapted from Merrick 1992 and created by T. Schneider-Poetsch).

Regulation of protein translation plays an essential role in cell survival, especially in fast-proliferating cancer cells (Bhat et al., 2015). Inhibitors of eukaryotic protein synthesis, including the translation elongation inhibitor homoharringtonine, have entered the clinic, establishing translation as a promising target for chemotherapy (Gandhi et al., 2014). Not only is this promising for future cancer therapeutics; perturbation of translation by new small molecules will allow us to dissect minute molecular details of the process, providing valuable insight into the eukaryotic ribosome and its function. These insights will allow us to establish further contrasts between prokaryotic ribosomes, facilitating the development of new antibiotics.

Results

Inhibition of protein synthesis by Agelastatin A

As an initial approach to elucidating the mechanism of the antitumor action of AglA, we began by investigating its cellular effects (Fig. 7A) using a phenotype-based approach, determining whether AglA has a specific effect on three major cellular processes: DNA replication, transcription, or translation. The effects of AglA on DNA synthesis, RNA synthesis, and global protein synthesis were determined using incorporation of [^{3}H]-thymidine, [^{3}H]-uridine, and [^{35}S]-methionine and cysteine as readouts, respectively. Treatment of HeLa cells with AglA for 1 hour led to a dose-dependent inhibition of incorporation of [^{3}H]-thymidine with an IC_{50} of 0.39 μM, and of [^{35}S]-methionine with an IC_{50} of 0.29 μM. In contrast, RNA synthesis as judged by incorporation of [^{3}H]-uridine was not significantly affected (Fig. 7B). As a positive control, treatment with CHX led to inhibition of [^{3}H]-thymidine with an IC_{50} of 0.059 μM, and [^{35}S]-methionine with an IC_{50} of 0.045 μM (Fig. 7C). Both AglA and CHX inhibited DNA synthesis and translation, although CHX is ~6 fold more potent than AglA (Fig. 7D). As

observed in previous work with translation inhibitors differences in the observed IC_{50} values between cell proliferation and translation assays may be attributed to the different drug incubation times and intrinsic sensitivity of the different assays (Dang et al., 2011; Schneider-Poetsch et al., 2010).

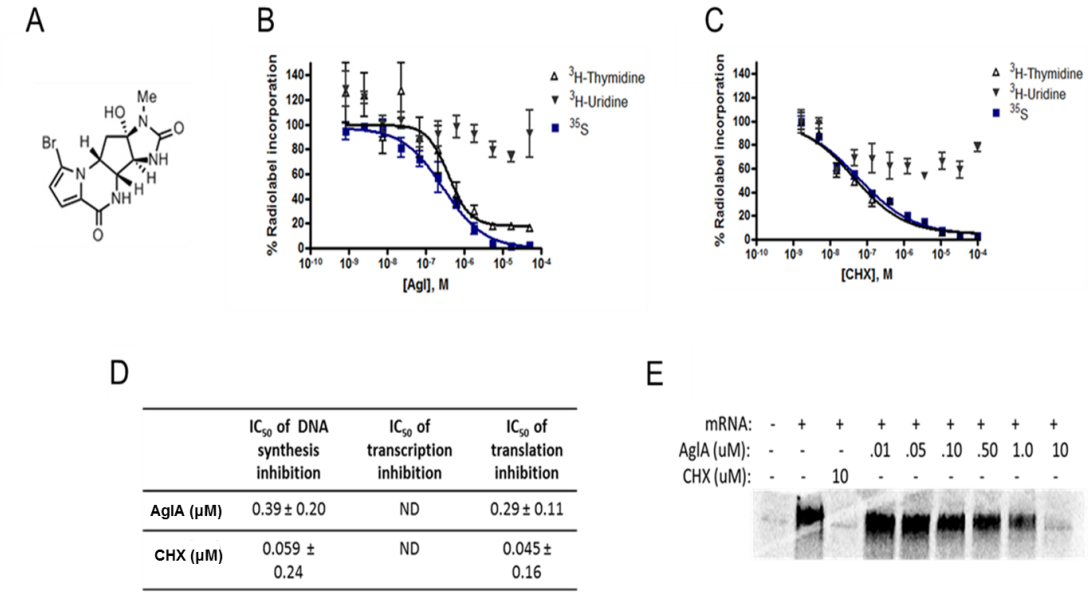

D

	IC_{50} of DNA synthesis inhibition	IC_{50} of transcription inhibition	IC_{50} of translation inhibition
AglA (μM)	0.39 ± 0.20	ND	0.29 ± 0.11
CHX (μM)	0.059 ± 0.24	ND	0.045 ± 0.16

E

Fig. 7. Inhibition of protein synthesis by AglA. **A).**Chemical Structure of Agelastatin A **B).** Dose-dependent inhibition of translation by AglA. HeLa cells were incubated with varying concentrations of each compound in the presence of either [^{3}H]-thymidine, [^{3}H]-uridine, or [^{35}S]-cysteine/methionine for 1 hr. Protein synthesis was measured by scintillation counting of trichloroacetic acid (TCA)-precipitated proteins on a filter. DNA synthesis and transcription were monitored by scintillation counting of nucleic acids bound to a filter. **C).** Mean values ± SEM (error bars) from 3 independent experiments are shown. IC_{50} values are listed ± SE. **D).** Drugs were added to a rabbit reticulocyte lysate (RRL) cocktail that included a control luciferase poly(A) mRNA (supplied by Promega) and [^{35}S]-methionine was added for 1 hr.

To verify that AglA directly blocked translation, protein synthesis from luciferase mRNA templates in rabbit reticulocyte lysate (RRL) and [^{35}S]-methionine was used. AglA also inhibited protein synthesis in a dose-dependent manner in the RRL system (Fig. 7E). The lysate contains the cytosolic components necessary for protein synthesis, eliminating the possibility of downstream signaling effects on protein translation (Beckler et al., 1995).

Agelastatin A inhibits translation elongation

To distinguish between the possibilities of AglA interfering with the initiation or elongation phase of protein synthesis, a dual luciferase assay was conducted. Many viral mRNAs and a relatively small number of cellular mRNAs are translated through an internal ribosome entry site (IRES). HCV IRES-mediated translation initiation does not require the 5' 7meG-cap structure. By recruiting initiation factors directly to the AUG start codon, HCV can bypass the eIF4F complex, which contains cap-binding factors eIF4E, and initiation factors eIF4A and eIF4G (Otto and Puglisi, 2004). The dual luciferase reporter assay uses bicistronic *in vitro* reporters with a conventional capped firefly luciferase, followed by renilla luciferase under the translational control of an HCV IRES element, which is resistant to inhibitors of translation initiation. Transcribed HCV IRES dual luciferase reporters were used to perform in vitro translation assays with RRL. AglA dose-dependently inhibited both cap-dependent and IRES-dependent translation of both luciferase reporters. As a control, CHX was found to inhibit both cap- and HCV IRES-dependent translation. In contrast, Pateamine A (PatA), a translation initiation inhibitor, only inhibited cap-dependent translation (Fig. 8A). These results suggested that AglA's involvement in translation initiation is unlikely.

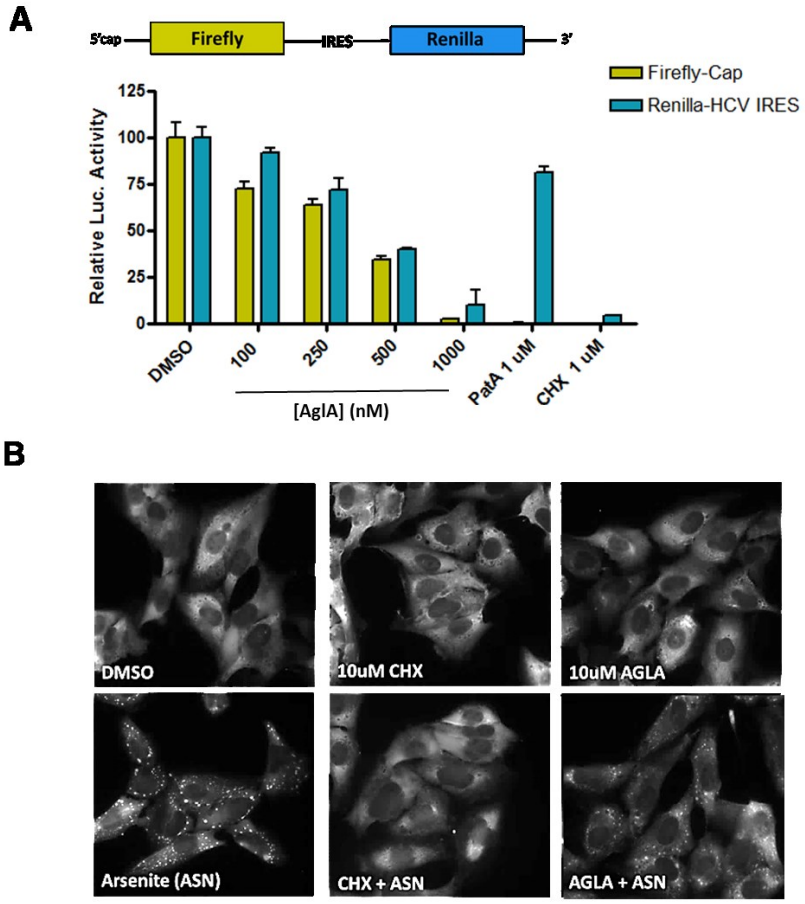

Fig. 8. AglA inhibits translation elongation. A) Dual reporters with a conventional capped firefly luciferase followed by renilla luciferase under the translational control of HCV IRES were used in *in vitro* RRL translation assays in the presence of different concentrations of AglA , 4 μM PatA, and 4 μM CHX. **B)** Stress grandule induction performed in U2OS cells stably expressing GFP-G3BP in the presence of different compounds as indicated. Images (40x objective) were captured using an Olympus B X61 fluorescence microscope. Abbreviations: PatA, pateamine A.

To further verify that AglA inhibited translation elongation rather than initiation, we determined its effect on stress granule formation in cells. Translation initiation inhibitors are known to trigger stress granule formation. In contrast, translation elongation inhibitors prevent the formation of stress granules (Dang et al., 2011). The induction of stress granules was performed in U2OS cells stably expressing GFP-G3BP, a stress-granule marker. Upon AglA treatment, no stress granule formation was observed, similar to results obtained in the presence of CHX (Fig. 8B). Arsenite, a known inducer of stress granules, was also used. As expected, pretreatment with CHX prevented stress granule formation induced by arsenite. Pretreatment with AglA also blocked stress granule formation in response to arsenite, albeit slightly less potently than CHX.

Translation elongation can be further subdivided into three major steps. First, aminoacyl-tRNA is delivered to the ribosomal A-site by eEF1A. Second, peptide bond formation occurs. Finally, eEF2 mediates peptidyl-tRNA translocation from A-site to P-site, and deacylated-tRNA is transferred from the P to E-site. Using a reconstituted system consisting of ribosomes, a poly (U) template, eEF1A, GTP, and aminoacyl-tRNA, we assayed the effects of AglA on dipeptide bond formation, and the products of the reaction were separated using an electrophoretic cellulose thin-layer chromatography plate. AglA clearly inhibited the rate of dipeptide bond formation (Fig. 9A).

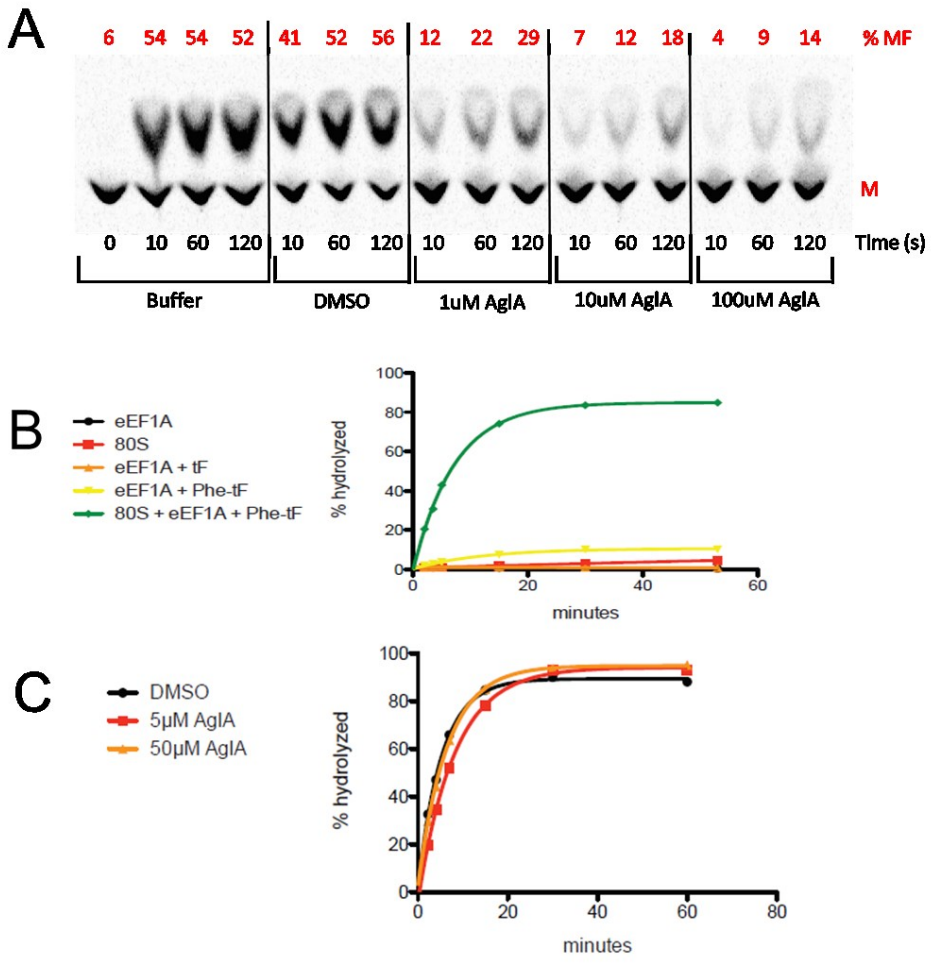

Fig. 9. Effects of AglA on translation peptidyl transfer. **A).** AglA decreased the rate of dipeptide formation. Radiolabeled methionine with initiation complexes mixed with drug and pre-incubated for 5min. eEF1A, tRNA-Phenylalanine, and GTP were mixed with complexes and incubated at given time points. Aliquots were quenched in 250mM KOH then run on TLC plates for analysis of dipeptides. **B,C).** AglA does not inhibit eEF1A's ribosome-dependent GTPase activity. Yeast eEF1A, phenylalanyl tRNA-Phe and 80S ribosomes were incubated in 1X buffer E with α-32P GTP, and aliquots were quenched at the indicated timepoints. TLC assay was quantified, showing no difference in GTP hydrolysis in the presence of AglA.

We next assessed whether AglA could affect the GTPase activity of eEF1A. GTP hydrolysis by eEF1A is highly dependent on both ribosomes and aa-tRNA (Fig. 9B). In the presence of these factors, AglA had no effect on the rate of GTP hydrolysis (Fig. 9C), suggesting that eEF1A-mediated tRNA loading is not affected and ruling out eEF1A as a likely binding target of AglA, which leaves the ribosome itself as the potential target.

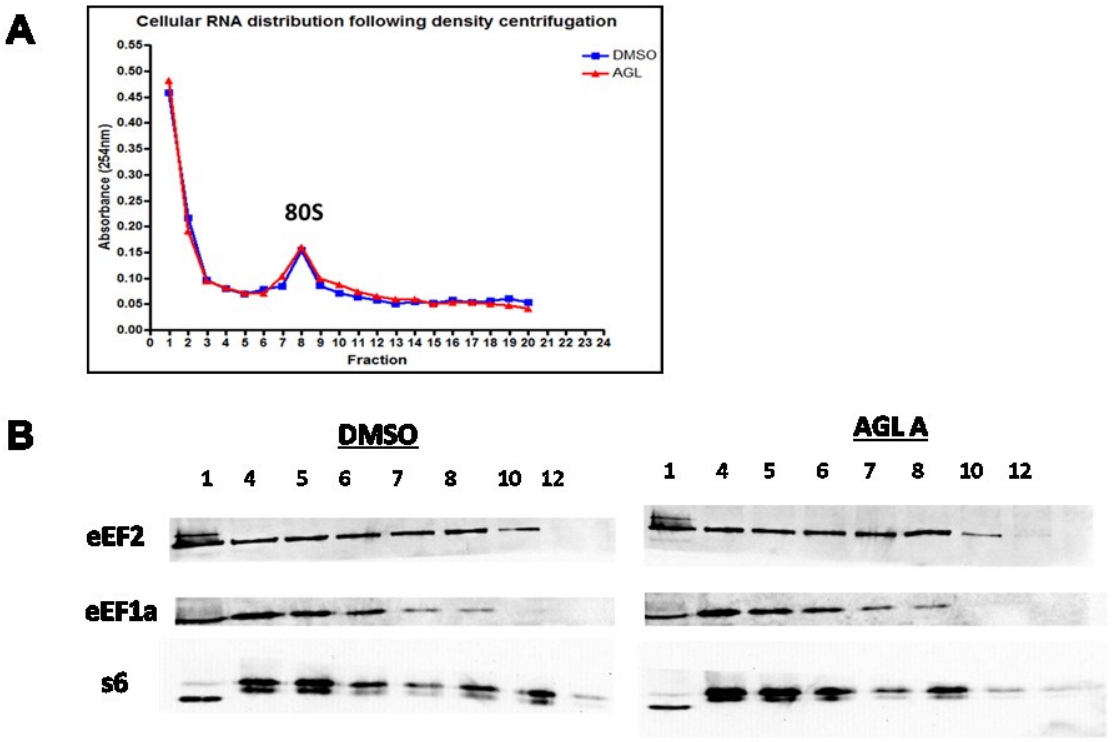

Fig. 10. AglA does not alter elongation factor distribution. A). Lysates of treated 293T cells were separated by density centrifugation and fractionated. Each fraction's RNA concentration was measured by absorbance **B)**. Each fraction's elongation factor and ribosomal content was observed by immuno-blotting. S6 denotes ribosomal protein rps6.

As further support of the conclusion that eIF1A is not a target of AglA, the association of eEF1A across a sucrose gradient was observed. Several known translation inhibitors, such as didemnin B, exert their effect by arresting eEF1A on the ribosome(Ahuja et al., 2000; Gomez-Lorenzo, 2000). Should AglA have a similar effect, then one would expect a change in its distribution on a density gradient. 293T cells were treated with inhibitors and their lysates were centrifuged across sucrose density gradients. Fractions were collected by hand and the optical density of each fraction was determined. Aliquots were run on polyacrylamide gels and transferred onto nitrocellulose membranes. Each membrane was probed against eEF1A, eEF2 and the small ribosomal subunit protein S6, which served as an indicator of ribosome content. No clear change in eEF1A or eEF2 was observed in the presence of AglA (Fig 10). If AglA had caused tighter association of ribosomes and elongation factors, one would have expected either factor to concentrate in the 80S fraction. If eEF1A had bound more strongly, eEF2 should have associated less because the binding sites for both elongation factors overlap at the ribosomal A- site.

Footprinting analysis reveals binding site of Agelastatin A

Based on AglA's strong effect on the accumulation of dipeptides, we hypothesized that binding was occurring near the peptidyl transferase center. We performed molecular docking to assess the potential binding site and binding mode of AglA in the yeast ribosomal peptidyl transferase center (PTC). According to the docking model, AglA docks well into the PTC (Fig. 11A). The pyrrole ring of AglA was predicted to form a π–π stacking with C2821 and A2820 of the yeast 25S rRNA. In order to validate this model and confirm the binding site of AglA on the ribosome, we performed a whole-ribosome dimethyl sulfate (DMS) protection assay with a modified form of DMS-seq (Ding et al., 2013; Rouskin et al., 2013). Purified yeast ribosomes were pre-

incubated with AglA, and probed with 90 mM DMS, which methylates adenine and cytosine residues. Instead of the classic method of looking for reverse transcriptase (RT) stops by gel (Moazed et al., 1986) or sequencing (Ding et al., 2013; Rouskin et al., 2013), we used a thermostable group II intron RT(Siegfried et al., 2014) which proceeds past DMS-modified nucleotides, but incorporates mismatches at these methylated positions at high frequency. Counting these mismatches by high-throughput sequencing produces a quantitative readout (Siegfried et al., 2014) of the extent of DMS modification.

Treatment of ribosomes with cycloheximide (CHX) produced dose-dependent protection exclusively at 25S rRNA nucleotide C2764, where CHX was previously shown to bind (Garreau de Loubresse et al., 2014; Schneider-Poetsch et al., 2010) (Fig. 12A, 12B). Treatment with 0.5 mM or 1.0 mM AglA produced strong (~30-fold) and specific protection at the PTC nucleotide 25S C2821 (Fig. 11B, 11C), consistent with computational modeling. The neighboring nucleotides, A2820, A2941, and C2942 were also protected by AglA treatment, but to a lesser extent (Fig. 11D). However, the level of modification at these nucleotides was lower than for C2821 in the absence of AglA. A2820 specifically showed about 2-fold reduction in DMS signal upon AglA treatment; however, the signal is ~25 fold lower than for C2821. Thus, it did not pass cutoffs for statistical significance in our assay.

Crystal Structure of 80S/Agelastatin A complex

In collaboration with Dr. Marat Yusupov, we determined the X-ray crystal structure of AglA bound to the yeast ribosome. AglA binds to the PTC and precisely at the A-site on the large ribosomal subunit (LSU). Upon binding of AglA, the residue U-2875 of the 80S ribosome undergoes a major rearrangement and it flips up compared to what is seen in the structure of vacant 80S ribosome (Ben-Shem et al., 2011) (Fig. 13).

Additionally, the inhibitor induces the displacement of A-2819, A-2820, and C-2821 in order to create stable contacts with the LSU A-site pocket, through the formation of stacking interactions. Moreover, the flipping-up of uracil 2875 induces the displacement of A-2404, probably due to steric hindrance between these two residues. AglA forms two additional hydrogen bonds with the rRNA surrounding the A-site and, more specifically, with U-2869 and U-2873. Such rearrangements are common for inhibitors binding. LSU A-site pocket, and show how natural compounds can develop to accommodate in the eukaryotic ribosome. Similarly to this, the base of rRNA C-2821 flips out compared to the vacant 80S structure, establishing an additional bond with an Mg^{2+} ion; this agrees with the large accessibility change in the footprint data. Finally, the essential bromide group of AglA forms a π-stacking interaction with U-2875, a quite unusual feature for inhibitors binding to the A-site of the PTC.

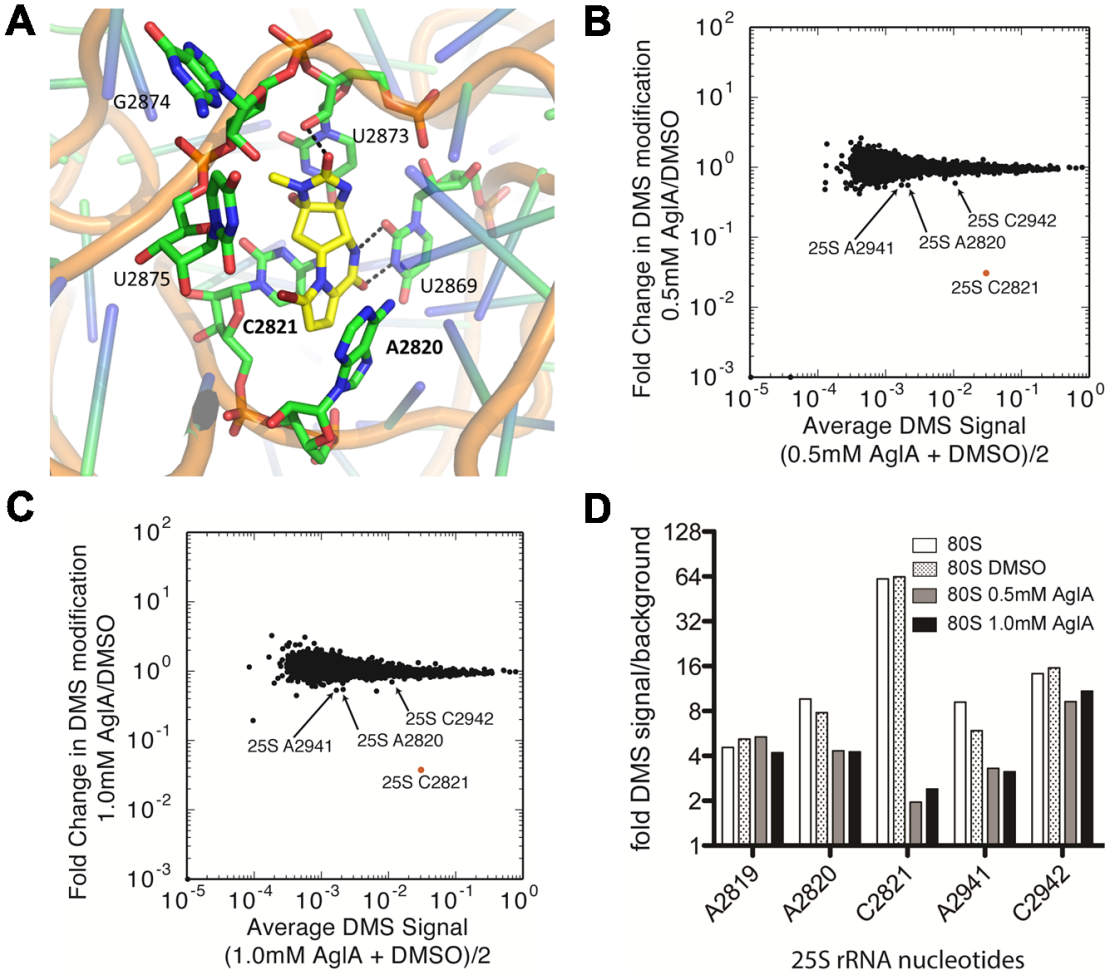

Fig. 11. AglA is bound within the PTC of the larger ribosomal subunit. A). Molecular docking model of the interaction of AglA with the *Saccharomyces cerevisiae* ribosome (PDBID: 4U52). The numberings correspond to the 25S yeast ribosome sequence. **B,C).** MA plots showing, for each rRNA nucleotide, the average DMS-dependent mutation rate on the x axis, against the fold change upon AglA treatment on the y axis. Nucleotides passing significance and fold-change cutoffs are orange, and changing nucleotides from panel C are labeled. **D).** Fold change in mutation rate, relative to a no-DMS control, for an unaffected nucleotide (A2819), and 4 AglA-protected nucleotides near the P site in the 25S rRNA.

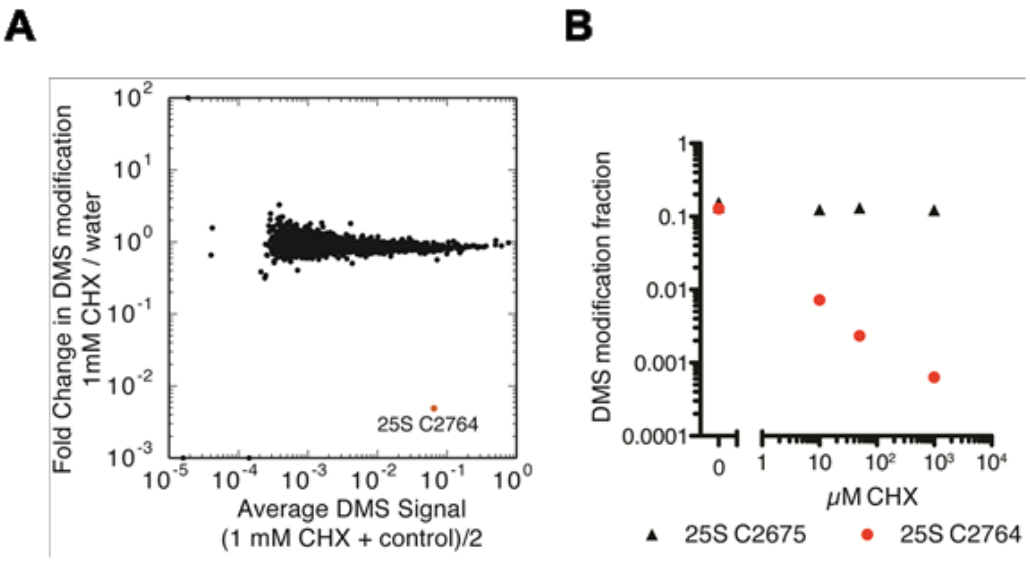

Fig. 12. *in vitro* DMS-seq can specifically identify known drug binding sites in rRNA. A). MA plot showing, for each rRNA nucleotide, the average DMS-dependent mutation rate against the fold change upon CHX treatment. The shape of this plot is typical of methods where the noise decreases with increasing signal. The unique protection at 25S C2764 demonstrates the extraordinary sensitivity and specificity of the method. **B)**. Titration curve of CHX concentration vs. DMS-dependent mutation rate for the CHX target site (25S C2764) and a control nucleotide with similar DMS modification, demonstrating the quantitative nature of DMS-seq.

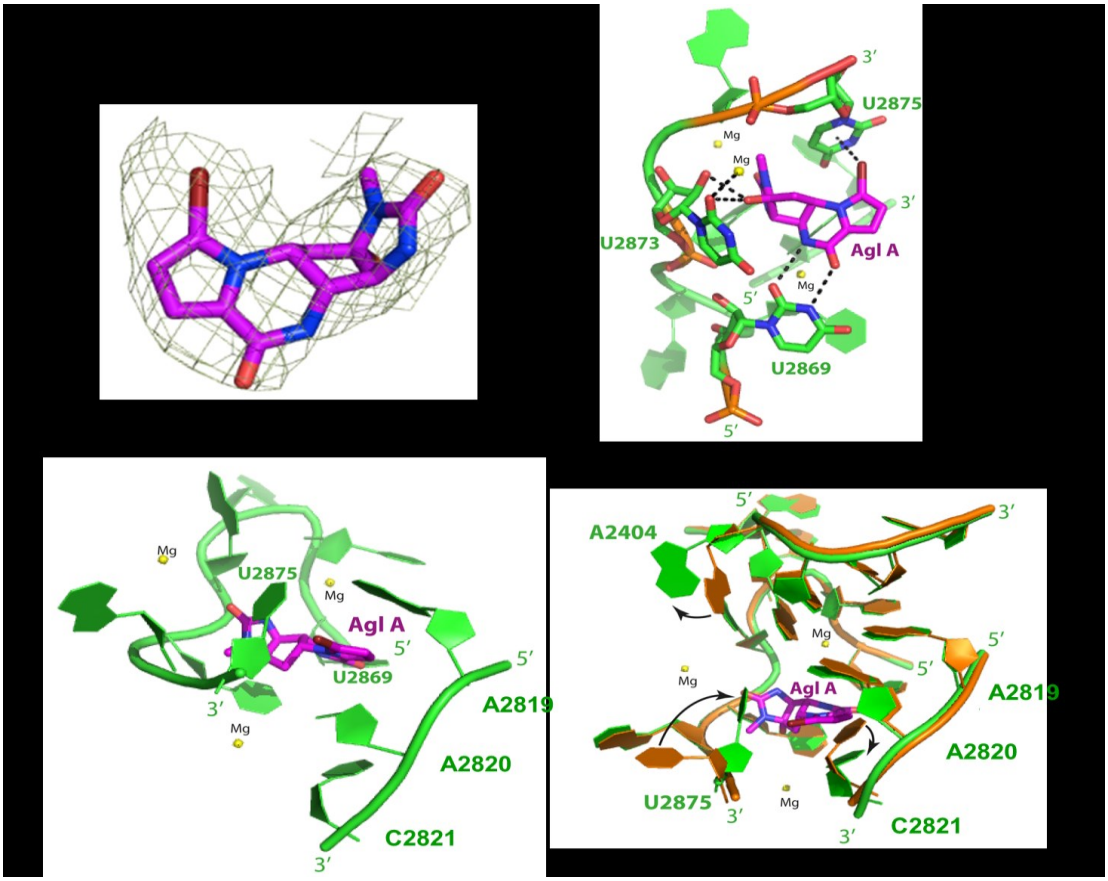

Figure 13. Crystal structure of A-site bound AglA. A) AglA (pink) fitted in the difference map (mFO-DFc). Structure has been determined to the resolution of 3.5 Å. See table 5 for statistics of data collection and processing. B) AglA (pink) forms hydrogen bonds with U2869 and U2873 and π-stacking interaction with U2875 of 25S rRNA (green) and electrostatic interaction with a magnesium ion (yellow). C) Stacking interactions between A2819, A2820, and C2821 of 25S rRNA (green) at A-site and AglA (pink). D) superposition of vacant ribosome structure (orange; PDB code: 4V88) and ribosome bound to AglA structure (green) displaying major movements of nucleotides A2404, C2821, and U2875 (black arrows) induced by the binding of AglA (pink) to A-site.

	AglA/80S complex
Data collection	
Space group	$P2_1$
Cell dimensions	
a, *b*, *c* (Å)	304.08, 286.55, 436.55
α, β, γ (°)	90.00, 99.05, 90.00
Resolution (Å)	100.00 – 3.50 (3.60 – 3.50) *
R_{meas} (%)	59.7 (242.5)
$I/\sigma I$	5.56 (1.00)
$CC_{1/2}$ (%)	98.5 (32.2)
Completeness (%)	100.0 (99.9)
Redundancy	10.55 (7.42)
Refinement	
Resolution (Å)	98.38 – 3.50
No. reflections	925645
R_{work}/ R_{free}	0.1963 / 0.2363
No. atoms	
Protein	178135
RNA	222512
Ions/ligands	8896
B-factors	
Protein	82.74
RNA	80.58
Ions/ligands	151.94
R.m.s deviations	
Bond lengths (Å)	0.008
Bond angles (°)	1.128

Table 5. Data collection and refinement statistics of ribosome bound AglA crystals. 13 crystals were used. *Highest resolution shell is shown in parenthesis.

Discussion

Although AglA has been an attractive natural product for biological studies for the past two decades since its first isolation, its underlying cause of antiproliferative effects in cells and molecular target(s) have remained a mystery. In this study, we identified the ribosomal peptidyl transferase center as the key target of AglA. It has previously been reported that AglA down-regulates β-catenin expression, causing repression of OPN and inhibition of OPN-mediated malignant cell migration (Mason et al., 2008). We surmise that this is most likely due to AglA causing reduced levels of the protein to be translated by interfering with peptide chain elongation.

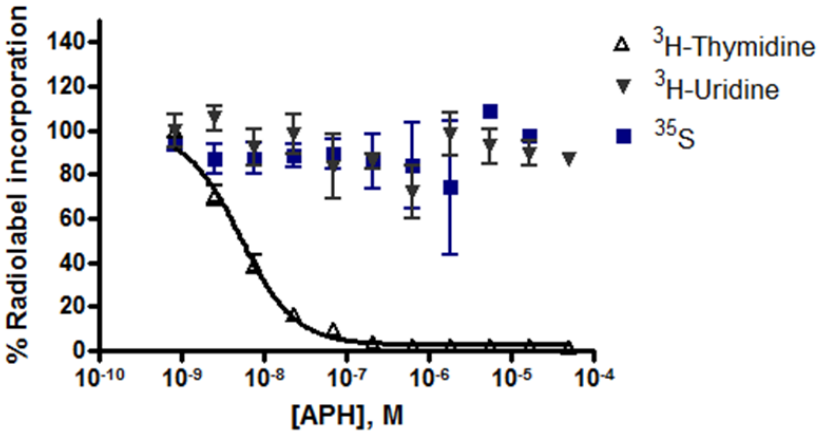

	IC_{50} of DNA synthesis inhibition
APH (nM)	5.2 ± .058 nM

Fig. 14: Inhibition of DNA replication by aphidicoline. HeLa cells were incubated with varying concentrations of each compound in the presence of either [^{3}H]-thymidine, [^{3}H]-uridine, or [^{35}S]-cysteine/methionine for 1 hr. Protein synthesis was measured by scintillation counting of trichloroacetic acid (TCA)-precipitated proteins on a filter. DNA synthesis and transcription were monitored by scintillation counting of nucleic acids bound to a filter.

AglA inhibited both protein synthesis and DNA replication in HeLa cells. As a comparison, we also tested the incorporation of [^{3}H]-thymidine, [^{3}H]-uridine, and [^{35}S]-methionine and cysteine in the presence of aphidicolin, an inhibitor of DNA polymerase α (Oguro et al., 1979; Spadari et al., 1982). Only DNA replication was inhibited (Figure 14). Interestingly, CHX similarly affects both protein synthesis and DNA replication, and the same phenomenon has been reported for a number of other translation inhibitors (Chan, 2004). It is possible that this is the result of a primary effect on the synthesis of fast-turnover proteins necessary for DNA replication, suggesting the existence of a mechanism directly coupling DNA replication and translation (Abid et al., 1999; Berthon et al., 2009).

Three independent pieces of evidence allowed us to rule out the possibility that AglA was inhibiting translation initiation. First, AglA inhibited both cap-dependent and initiation factor-independent HCV IRES reporter translation. Second, AglA does not induce stress granule formation in cells. Finally, because the eukaryotic ribosome's highly conserved nature, we were able to take advantage of a yeast system to further dissect the mechanism of AglA. Initially, we tested the effects of AglA on yeast culture growth; however, there was no strong effect (Fig. 15). This may be attributed to AglA's inability to penetrate the yeast cell wall. Fortunately, in an *in vitro* semi purified system, AglA strongly inhibited dipeptide bond formation, suggesting that AglA was either inhibiting eEF1A, or directly binding within the ribosome itself. AglA caused no effect on eEF1A-dependent GTP hydrolysis, suggesting to us that peptide bond formation itself was affected.

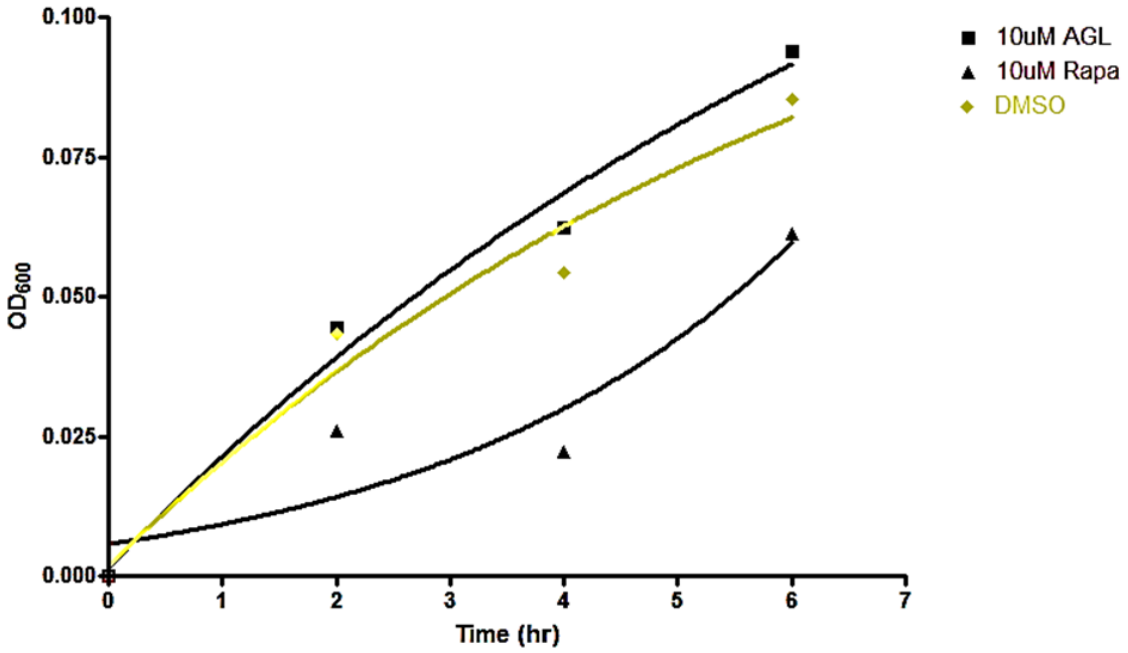

Fig. 15. Effect of AglA on the growth of *Saccharomyces cerevisiae*. AglA and rapamycin were added at 10 μM each.

Molecular docking predicted that AglA could bind within the peptidyl transferase center of the ribosome, with the pyrrole ring predicted to form a pi-pi stacking with C2821 and A2820 in the PTC, positioned near P-site and A-site tRNAs (Fig. 16).

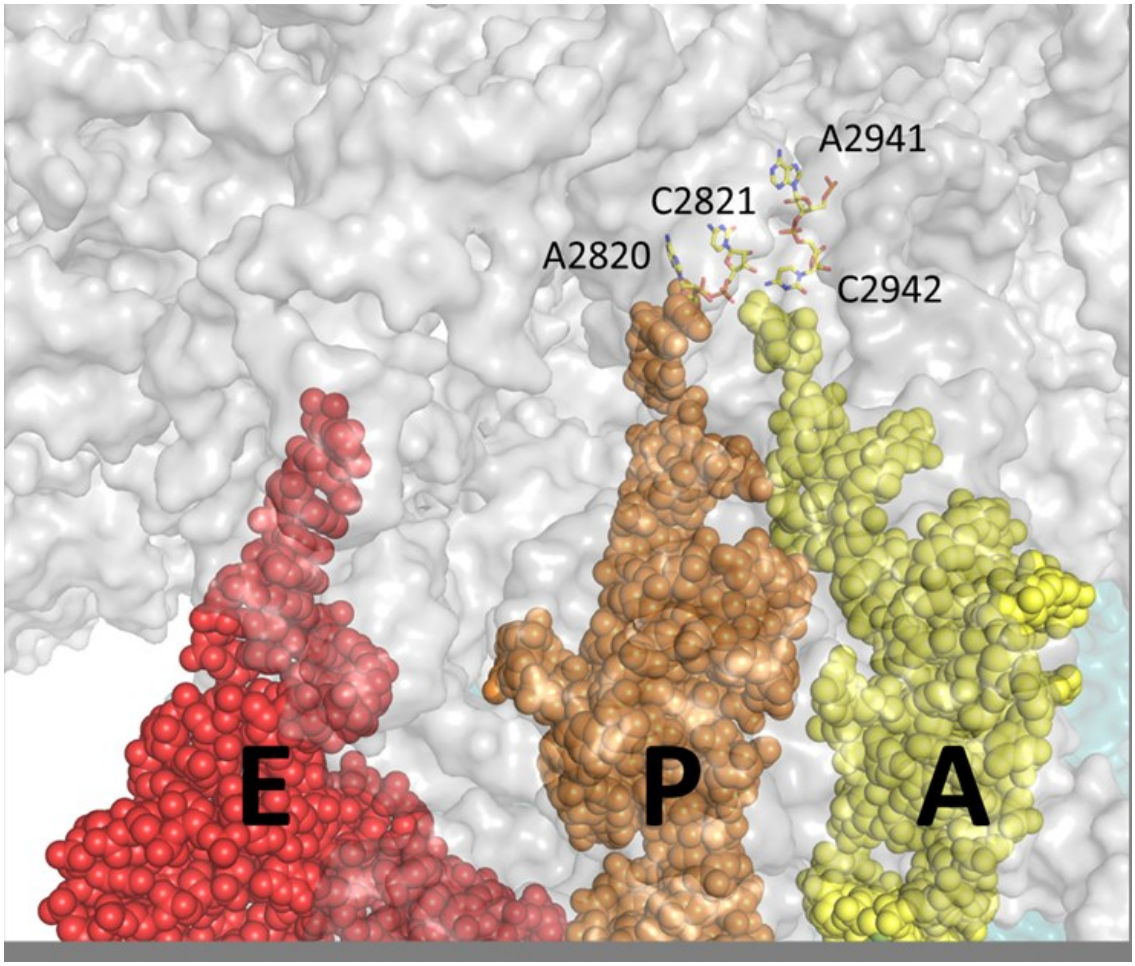

Fig. 16. tRNA binding sites. *Thermus thermophilus* tRNAs aligned onto the yeast structure[59]. tRNAs are positioned in the E/P/A sites from the left: A2820, C2821, A2941, C2942.

We were extremely surprised to find how closely the molecular docking model predicted the binding site of AglA, which was validated by both the DMS-Seq footprint and crystal structure. These findings provide a potential clue for future analogs with improved potency; consistent with our predication, previously reported SAR studies (Jouanneau et al., 2016) show a gradual loss in activity as the size of the C14 substituent increases, as larger substituents at this position may bump into A2820 that forms π–π interaction with AglA. The PTC of the ribosome was also found to be the binding site of several other translation inhibitors, including anisomycin, which has been reported to form a hydrogen bond with C2821, thus allowing protection from chemical modification at this position (Garreau de Loubresse et al., 2014; Rodriguez-Fonseca et al., 1995). Although they occupy a similar binding pocket in the PTC, the structures of these compounds are quite distinct (Fig. 17) and show a distinct interaction pattern with nearby nucleotides. Flipping of residues C-2821, U-2875 and A-2404 seems to be dependent on the chemical structure of the inhibitor rather than the accommodation of the inhibitor itself, as shown in our comparison with narciclasine (NAR) and ANI (Fig. 18). In the case of NAR, for instance, U-2875 adopts a conformation close to the vacant 80S while ANI causes this residue to flip up in a manner similar to the AglA structure. A-2404, by contrast, is very mobile and rearranges in different positions when comparing the inhibitors' bound and the vacant ribosome.

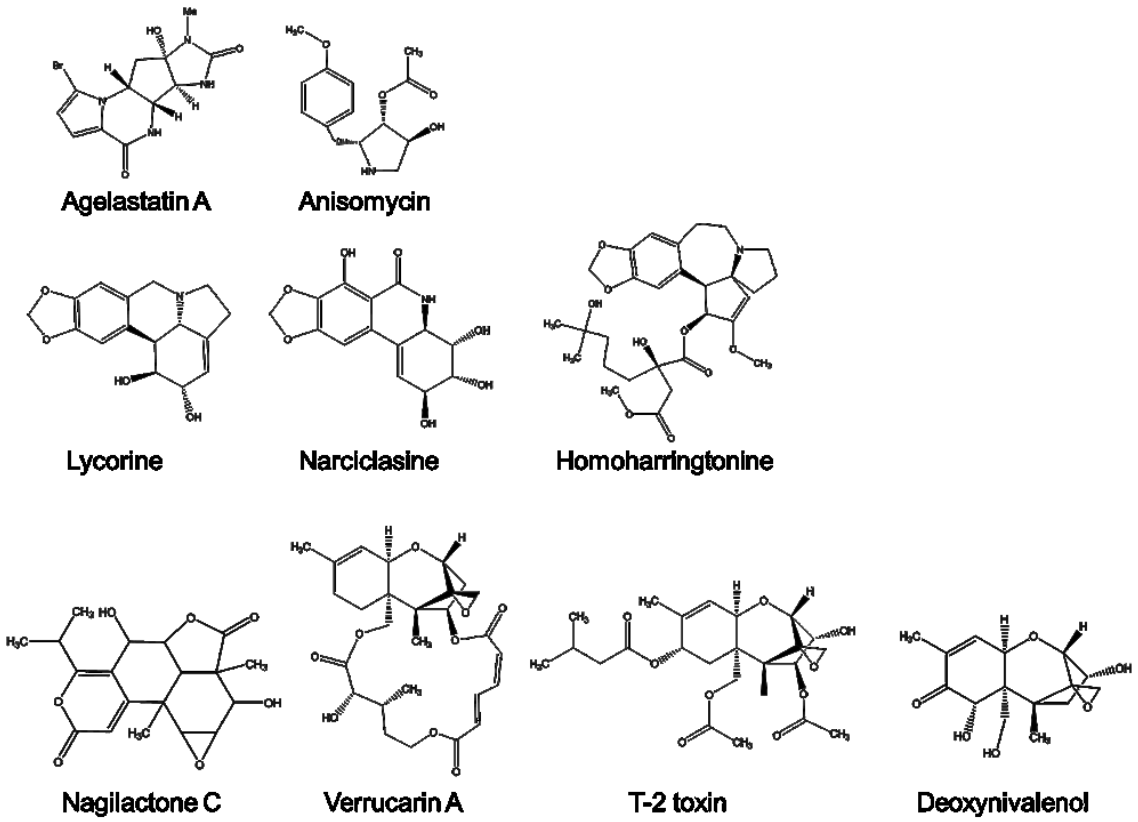

Fig.17. Chemical structures of current eukaryotic translation inhibitors that target the PTC.

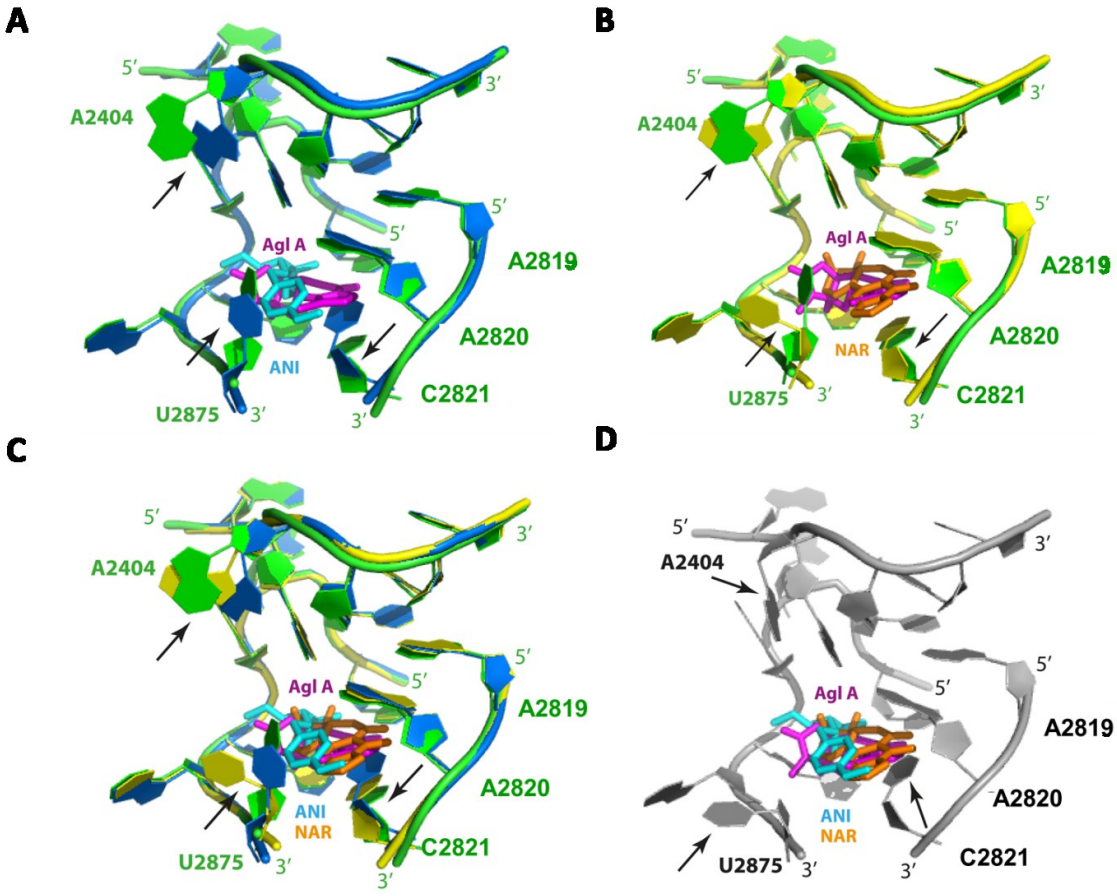

Fig.18. **Structural comparison of AglA and other A-site inhibitors.** A) Superposition of ribosome bound to anisomycin (ANI) structure (blue; PDB code: 4U3M) and ribosome bound to AglA structure (green) displaying differences in movements of nucleotides A2404, C2821, U2875 (black arrows) induced upon binding of ANI (cyan) or AglA (pink) to A-site. B) Superposition of ribosome bound to narciclasine (NAR) structure (yellow; PDB code: 4U51) and ribosome bound to AglA structure (green) displaying differences in movements of nucleotides A2404, C2821, U2875 (black arrows) induced upon binding of NAR (orange) or AglA (pink) to A-site. C) Superimposition of ribosome bound to NAR structure (yellow; PDB code: 4U51), ribosome bound to ANI structure (blue; PDB code: 4U3M) and ribosome bound to AglA structure (green) displaying differences in movements of nucleotides A2404, C2821, U2875 (black arrows) induced upon binding of NAR (orange) or ANI (cyan) or AglA (pink) to A-site. D) Binding pocket of AglA (pink), ANI (cyan; PDB code: 4U3M) and NAR (orange; PDB code: 4U51) in vacant ribosome structure (grey; PDB code: 4V88). Nucleotides pointed by black arrows are the ones that are the most displaced upon binding of these inhibitors to the A-site.

Among the compounds identified as inhibitors of peptide bond formation, Homoharringtonine was approved in 2012 for use as a treatment for patients with chronic myeloid leukemia who are resistant to tyrosine kinase inhibitors such as imatinib (Moen et al., 2007). These recent developments strongly highlight the need for further evaluation of translation inhibitors for use against cancers. In particular, AglA and its analogues have displayed admirable blood-brain barrier penetration and potent activity against CNS related tumors in murine models, making it an excellent candidate for brain cancer studies.

Naturally, translation inhibitors will always remain generally toxic due to the requirement of protein turnover in fast growing cells. However, quickly proliferating cells such as aggressively growing tumors should suffer more strongly from translation inhibition compared to normal somatic cells. Besides their overall antiproliferative effects, translation inhibitors may also prevent the cell from producing anti-apoptotic proteins, which could aid the development of resistance against other chemotherapeutic agents. In combination with a proven first-line chemotherapeutic, translation inhibition may act synergistically to enhance the primary drug's effect and prevent the development of additional chemo-resistance.

Materials and Methods

Reagents and cell lines

AglA was synthesized as reported (Reyes and Romo, 2012) and dissolved in DMSO. CHX, and GMPNP were purchased from Sigma. HEK293T and HeLa cells were cultured in DMEM medium supplemented with 10% FBS and were maintained in a 5% CO2 atmosphere.

Metabolic labeling

HeLa cells were used for cellular metabolic labeling experiments. HeLa cells (20,000 per well) were seeded in 96-well plates. Twenty four hours after seeding, drugs were added at the indicated concentrations, followed by addition of an aliquot of 1 µCi of [^{3}H]-uridine or [^{35}S]-methionine (Perkin Elmer) for 1 h. Cells were washed twice with 200 µl of cold PBS and lysed by addition of 100 µl lysis buffer [20 mM Tris-HCl, pH 7.4, 1% SDS, 100 µg/ml yeast tRNA (for [^{3}H]-uridine incorporation) or 25 mM Tris-HCl, pH 7.6, 150 mM NaCl, 1% NP-40, 1% deoxycholate, 0.1% SDS, 100 µg/ml BSA (for [^{35}S]-methionine incorporation)]. After a 20-minute incubation at 4 °C, 100 µl of 20% trichloroacetic acid (TCA) was added and the resulting mixtures were transferred to Millipore MSFCN6B10 filter plates. After 2 hours incubation at 4 °C, the mixtures were filtered under vacuum, and the plates were washed twice with 100 µl 5% TCA and twice with 100 µl ethanol. The plates were dried overnight, and 50 µl of Optiphase Supermix was added to each well and incorporation of ^{3}H or ^{35}S was quantified by scintillation counting on 1450 Microbeta JET instrument (Perkin Elmer).

Dual luciferase reporter assay

HCV IRES dual luciferase reporter vector was linearized with BamHI (NEB) and transcribed using T7 polymerase (Promega). Reactions were carried out as previously described (Dang et al., 2011), using the Dual-Luciferase reporter assay system (Promega).

Induction of stress granules

U2OS cells stably expressing GFP-G3BP were treated with the indicated compounds for 1 hour. Cells were pretreated with either CHX or AglA for 30 minutes before arsenite addition for 1 hour. Cells were then fixed with 4% paraformaldehyde for 10 minutes, and washed twice with PBS. Images were captured using an Olympus B X61 fluorescence microscope, equipped with a Roper Photometrics CoolSnap HQ CCD camera.

Elongation factor distribution

Fifteen centimeter culture dishes of human embryonic kidney (HEK) 293T cells were grown to confluency. Drugs were added at the indicated concentrations and incubated with the cells for 30 min. Cells were lyzed in 0.5 ml 30 mM Tris-HCl, pH 7.4, 100 mM KCl, 5 mM $MgCl_2$, 2 mM DTT, and 1% Triton-X 100. After clearing the lysate of debris by centrifugation at 13,000 rpm, 4˚C for 10 min, aliquots containing the same amount of RNA (measured by OD_{254}) were loaded onto linear 15-45% sucrose density gradients in 20 mM Hepes-KOH, pH 7.4, 100 mM KCl, 5 mM $MgCl_2$ and 2 mM DTT. Gradients were fractionated in 500 µl aliquots by hand. The optical density at 254 nm was determined for each fraction. Aliquots of each fraction were boiled with 2x SDS

loading buffer and run on 10% SDS-PAGE gels. Protein was transferred onto nitrocellulose membranes at 4 ˚C and 20 V overnight or at 90 V for 2 h. Membranes were blocked for at least one hour in 5% milk in TBS-T (50 mM Tris-HCl, pH 7.0, 150 mM NaCl, and 0.5% Tween-20) buffer and then probed with primary antibodies against ribosomal proteins or elongation factors for 3 h to overnight at 1:500-1:1000 dilution. Membranes were washed 3 times with TBS-T buffer before application of secondary antibody in 5% milk at 1:2000 dilution, followed by 3 washes with buffer and addition of 2 ml of horseradish-peroxidase substrate per membrane. Luminescence was detected on a Kodak Image Station 440 camera system.

In vitro peptidyl transfer assays

Ribosome initiation complexes were assembled and purified as previously described (Eyler and Green, 2011), containing Met-tRNA^{IMT} in the P site and a phe codon (UUC) in the A site. The open reading frame of the mRNA used was Met-Phe-Stop (AUG-UUC-UAA). For peptidyl transfer, Phe-tRNA^{Phe} ternary complex was prepared by mixing 1μM Phe-tRNA^{Phe}, 2uM eEF1A and 1mM GTP in buffer E (20 mM Tris-Cl, pH 7.5, 100 mM potassium acetate, 2.5 mM magnesium acetate, 0.25 mM spermidine, 2 mM DTT) at 26 °C for 15 min. During this time, initiation complexes (20 nM) were incubated with either drug or DMSO for 5 minutes at 26 °C. Ternary complex was then added to each initiation complex: drug mixture to initiate the reaction. Time points were taken after 10, 60, and 120 seconds and quenched in 250 mM KOH. Samples were run on electrophoretic TLCs (Millipore) at 1200V for 24min, developed using a Typhoon FLA 9500 Phosphorimager system, and quantified using ImageQuantTL (GE Healthcare Life Sciences).

Yeast growth assay

WT yeast cultures were grown in yeast peptone dextrose (YPD) medium. Saturated starter cultures were diluted to 0.05 OD_{600} units and plated at 1 ml each into 24 well plates. Increasing concentrations of AglA were added in triplicate and the cells were incubated at 30 ˚C for 6 hours to monitor initial log phase growth.

eEF1A GTPase assay

S. cerevisiae ribosomes (Acker et al., 2007) and eEF1A (Eyler and Green, 2011) were purified as previously described. Yeast phenylalanine tRNA (chemblock) was charged by incubation with phenylalanine and S. cerevisiae S100 extract (Eyler and Green, 2011), and recovered by phenol extraction and ethanol precipitation. eEF1A GTPase assays were assembled in 10µl reactions containing 1x buffer E by addition, in order, of S. cerevisiae eEF1A (0.25µM), charged phenylalanine tRNA (Eyler and Green, 2011) (0.25µM), 40S ribosomal subunits(0.20µM), 60S ribosomal subunits(0.20µM) and 0.5ul AglA in DMSO. Reactions were started by addition of α-32P GTP (Perkin Elmer) to 0.133µM.From each reaction, 1.5µl aliquots were quenched in an equal volume of 60% formic acid at the indicated time points. GTP and GDP were separated on PEI cellulose F TLC plates (Millipore) with 0.5M KH2PO4 pH 3.5. The dried plates were developed using a Typhoon 9410 phosphorimager system (GE Healthcare Life Sciences) and quantified using ImageQuantTL (GE Healthcare Life Sciences).

Computational Modeling

The receptor model used for molecular docking was derived from the crystal structure of yeast 80s ribosome bound to a small molecular inhibitor Nagilactone C (PDBID: 4U52). Because the whole 80s ribosome structure is too large for the docking study, the nucleotides and amino acids that were 10Å away from the ribosomal peptidyl

transferase center (PTC) were deleted. Water molecules, ions and nagilactone C were also removed. After the addition of hydrogen atoms and charges, a brief relaxation of the receptor structure was performed by using the Protein Preparation module in Maestro v7.5 (Schrödinger Inc. NY). LigPrep module in Maestro v7.5 (Schrödinger Inc. NY) was used to prepare the 3D structure of AglA. Afterwards, AglA was docked into the PTC by using Glide v4.0 (Schrödinger Inc. NY) in the extra-precision (XP) mode. Finally, the predicted binding mode between AglA and yeast 80s ribosome PTC were visualized and analyzed in Pymol 0.99rc (www.pymol.org).

DMS modification

DMS treatment was performed in a final volume of 25ul, containing 30mM K-HEPES (pH 7.5), 3mM MgOAc2, 100mM KCl, 2mM DTT, 0.5μM each of 40S and 60S yeast ribosomal subunits. For AglA treatment, 10% of AglA in DMSO was added. For CHX treatment, a 10% volume of CHX in water was added. Reactions were brought to 24μl, and pre-incubated at 26°C for 5 minutes. 1μl of 2.25M dimethyl sulfate (sigma D186309, use within 6 months) diluted in ethanol (to 90mM final concentration) was added, reactions mixed by pipetting, and incubated at 26°C for 8 minutes. Reactions were quenched by addition of 475μl of (30% 2-mercaptoethanol, 0.3M sodium acetate, pH 5.5). Reactions were isopropanol precipitated, resuspended in 200μl of 0.3M sodium acetate, pH 5.2 and extracted twice with acid phenol-chloroform-isoamyl alcohol (thermo-fisher AM9722). Reactions were ethanol precipitated with 10ug glycogen, washed with 80% ethanol, resuspended in 40μl water, and RNA concentrations quantified by NanoDrop.

Library Preparation

4µg of RNA was fragmented by incubation at 95°C for 5 minutes with 10mM ZnCl2, quenched by addition of EDTA to 20mM on ice. RNA was precipitated and 3' ends were dephosphorylated by incubating in 12.5µl reactions of 1x PNK buffer (NEB), 1.25ul T4 PNK (NEB) and 0.5ul SUPERase-In (Thermo-Fisher) at 37°C for 1 hour. Reactions were run on a 10% TBE-Urea PAGE gel (Bio-Rad), alongside 10bp DNA ladder (Invitrogen) and a slice was cut from the gel between the 60 and 70bp markers. From this point, the library preparation proceeded essentially as previously described (Rouskin et al., 2013) with the following modifications. For linker ligation, 10 picomoles of pre-adenylated miRNA cloning liker 2 was used, [IDT , AppCACTCGGGCACCAAGGA/3ddC/, pre-adenylated in-house based on (Pfeffer et al., 2005) for its higher annealing temperature. 10µl Reverse transcription (RT) reactions were performed with half of the gel-purified ligated product, 1x first stand buffer (Invitrogen), 0.5mM dNTPs, 0.5µl SUPERase-In (Thermo-Fisher) 100nM of complementary circularizeable RT primer (IDT, /5Phos/AGATCGGAAGAGCGTCGTGTAGGGAAAGAGTGTAGATCTCGGTGGTCGC/iSP18/CACTCA/iSp18/TTCAGACGTGTGCTCTTCCGATCTGTCCTTGGTGCCCGAGTG), 5mM DTT and 0.5µM TGIRTIII RT (InGex) for 1 hour at 60°C. Instead of truncated RT products, full-length RT products were gel-purified. Circularized cDNA was prepared for Illumina sequencing with 11-13 cycles of PCR with forward primer (IDT, AATGATACGGCGACCACCGAGATCTACAC) and barcoded reverse primer (IDT,CAAGCAGAAGACGGCATACGAGATxxxxxxGTGACTGGAGTTCAGACGTGTGCTCTTCC, where xxxxxx was one of 24 base-balanced barcodes). Data generated by these experiments is deposited in Gene Expression Omnibus (Gene accession GSE85619. Full-length libraries were gel-purified from a 10% TBE-

PAGE gel (Bio-Rad) quantified by bioanalyzer (Agilent), pooled, and sequenced on an Illumina HiSeq 2000 in 100nt single-end rapid mode.

Sequencing data analysis

The linker sequence for all reads was trimmed using cutadapt (Martin, 2011), and the 5'-most 3 nucleotides were removed with FASTX trimmer. Any reads without an identifiable 3' linker sequence were discarded. The trimmed reads were fed into the ShapeMapper package (Siegfried et al., 2014) to further trim the reads based on quality, and to count mismatches relative to the yeast rDNA sequence (from the UCSC genome browser, August 29th, 2011 version). The mutation rate was defined as the ratio of the number of sequence mismatches at an rRNA position, divided by the total number of trimmed reads overlapping a position. The error at a position was defined by the Poisson sampling error as previously described (Siegfried et al., 2014). Several rRNA nucleotides have in vivo methylations on their Watson-Crick face (18S 1191; 25S 645,2142,2634,2843), and reproducibly have up to 50-90% mutation rates, even in the absence of DMS treatment. These nucleotides demonstrate the quantitative nature of the mismatches introduced by the RT, but are excluded from downstream analysis. Log10 fold changes in DMS-induced mutations between treatment and control were computed, and the errors for the two datasets were propagated through the division and log transformation. To determine if any of these changes constituted significant protections or deprotections, z scores were computed from these means and standard errors, based on a distribution with a mean of 0, the normal distribution integrated from the z score to positive or negative infinity, and tested against a p-value of 0.01, with bonferroni correction. A 3-fold change cutoff was also instituted, based on analysis of cycloheximide titrations. The analysis software, which produces quality control

information, wig files, output tables, and plots from FASTQ files is freely available at https://github.com/borisz264/mod_seq/.

Ribosome purification, complex formation, crystallization and crystal treatment

80S ribosomes from the yeast *S. cerevisiae* were purified and crystals were prepared as described previously(Ben-Shem et al., 2011; Garreau de Loubresse et al., 2014). Crystals were grown at 4°C by hanging-drop vapor diffusion and then treated based on the previously described protocol(Ben-Shem et al., 2011; Garreau de Loubresse et al., 2014) maintaining an increased glycerol concentration to 20% in all intermediate solutions. AglA was added at a final concentration of 250 µM in the last treatment solution, where crystals of the 80S ribosome were finally soaked in for 60 minutes prior to freezing in liquid N_2.

Data collection, processing and structure determination

Data of the 80S/AglA complex have been collected at the X06SA beamline at the PSI-SLS (Switzerland) and at the PROXIMA-1 beamline at SOLEIL (France), finally yielding a complete dataset at maximal resolution of 3.5 Å (Table 5). Data were processed using XDS and scaled with XSCALE [73]. The resulting file was converted into mtz format with the XDSCONV tool and then submitted for a first cycle of rigid-body refinement in phenix.refine (PHENIX suite(Adams et al., 2010)) using, as initial model, the *Saccharomyces cerevisiae* vacant 80S ribosome (PDB code: 4V88). Inspection of the resulting map allowed to detect positive difference density ($F_{obs} – F_{calc}$) close to the A-site peptidyl-transferase center (PTC) and to place the AglA into it. Drawing of the chemical structure of AglA was performed using MarvinSketch suite (ChemAxon, http://www.chemaxon.com/), which resulted in the 3D coordinates of the compound. Dictionary of restraints for the AglA was generated by submitting the 3D coordinates to

the GradeWebServer (http://grade.globalphasing.org). Iterative model building and refinement were performed using Coot (Emsley and Cowtan, 2004) and phenix.refine respectively. A protocol of positional, grouped isotropic B-factor and TLS refinement using a strong weight for geometry restraints yielded the final statistics presented in Table 1. Structure validation was performed using Molprobity (Chen et al., 2010). Ramachandran plot resulted in 85.8% favored, 10.3% allowed and 3.9% outliers.

References

Abid, M.R., Li, Y., Anthony, C., and De Benedetti, A. (1999). Translational Regulation of Ribonucleotide Reductase by Eukaryotic Initiation Factor 4E Links Protein Synthesis to the Control of DNA Replication. J. Biol. Chem. *274*, 35991–35998.

Acker, M.G., Kolitz, S.E., Mitchell, S.F., Nanda, J.S., and Lorsch, J.R. (2007). Reconstitution of Yeast Translation Initiation. In Methods in Enzymology, (Elsevier), pp. 111–145.

Adams, P.D., Afonine, P.V., Bunkóczi, G., Chen, V.B., Davis, I.W., Echols, N., Headd, J.J., Hung, L.-W., Kapral, G.J., Grosse-Kunstleve, R.W., et al. (2010). *PHENIX* : a comprehensive Python-based system for macromolecular structure solution. Acta Crystallogr. D Biol. Crystallogr. *66*, 213–221.

Agrawal, R.K., Spahn, C.M., Penczek, P., Grassucci, R.A., Nierhaus, K.H., and Frank, J. (2000). Visualization of tRNA movements on the Escherichia coli 70S ribosome during the elongation cycle. J. Cell Biol. *150*, 447–460.

Ahuja, D., Vera, M.D., SirDeshpande, B.V., Morimoto, H., Williams, P.G., Joullié, M.M., and Toogood, P.L. (2000). Inhibition of protein synthesis by didemnin B: how EF-1alpha mediates inhibition of translocation. Biochemistry (Mosc.) *39*, 4339–4346.

Al-Mourabit, A., Zancanella, M.A., Tilvi, S., and Romo, D. (2011). Biosynthesis, asymmetric synthesis, and pharmacology, including cellular targets, of the pyrrole-2-aminoimidazole marine alkaloids. Nat. Prod. Rep. *28*, 1229.

Beckler, G.S., Thompson, D., and Van Oosbree, T. (1995). In Vitro Translation Using Rabbit Reticulocyte Lysate. In In Vitro Transcription and Translation Protocols, (New Jersey: Humana Press), pp. 215–232.

Beghyn, T., Deprez-Poulain, R., Willand, N., Folleas, B., and Deprez, B. (2008). Natural compounds: leads or ideas? Bioinspired molecules for drug discovery. Chem. Biol. Drug Des. *72*, 3–15.

Bender, T., Huss, M., Wieczorek, H., Grond, S., and von Zezschwitz, P. (2007). Convenient Synthesis of a [1-14C]Diazirinylbenzoic Acid as a Photoaffinity Label for Binding Studies of V-ATPase Inhibitors. Eur. J. Org. Chem. *2007*, 3870–3878.

Ben-Shem, A., Garreau de Loubresse, N., Melnikov, S., Jenner, L., Yusupova, G., and Yusupov, M. (2011). The Structure of the Eukaryotic Ribosome at 3.0 A Resolution. Science *334*, 1524–1529.

Berthon, J., Fujikane, R., and Forterre, P. (2009). When DNA replication and protein synthesis come together. Trends Biochem. Sci. *34*, 429–434.

Bhat, M., Robichaud, N., Hulea, L., Sonenberg, N., Pelletier, J., and Topisirovic, I. (2015). Targeting the translation machinery in cancer. Nat. Rev. Drug Discov. *14*, 261–278.

Cannone, J.J., Subramanian, S., Schnare, M.N., Collett, J.R., D'Souza, L.M., Du, Y., Feng, B., Lin, N., Madabusi, L.V., Müller, K.M., et al. (2002). The comparative RNA web (CRW) site: an online database of comparative sequence and structure information for ribosomal, intron, and other RNAs. BMC Bioinformatics *3*, 2.

Chan, J. (2004). Eukaryotic protein synthesis inhibitors identified by comparison of cytotoxicity profiles. RNA *10*, 528–543.

Chen, V.B., Arendall, W.B., Headd, J.J., Keedy, D.A., Immormino, R.M., Kapral, G.J., Murray, L.W., Richardson, J.S., and Richardson, D.C. (2010). *MolProbity* : all-atom structure validation for macromolecular crystallography. Acta Crystallogr. D Biol. Crystallogr. *66*, 12–21.

D'Ambrosio, M., Guerriero, A., Debitus, C., Ribes, O., Pusset, J., Leroy, S., and Pietra, F. (1993). Agelastatin a, a new skeleton cytotoxic alkaloid of the oroidin family. Isolation from the axinellid sponge Agelas dendromorpha of the coral sea. J. Chem. Soc. Chem. Commun. 1305.

Dang, Y., Schneider-Poetsch, T., Eyler, D.E., Jewett, J.C., Bhat, S., Rawal, V.H., Green, R., and Liu, J.O. (2011). Inhibition of eukaryotic translation elongation by the antitumor natural product Mycalamide B. RNA *17*, 1578–1588.

Ding, Y., Tang, Y., Kwok, C.K., Zhang, Y., Bevilacqua, P.C., and Assmann, S.M. (2013). In vivo genome-wide profiling of RNA secondary structure reveals novel regulatory features. Nature *505*, 696–700.

Domostoj, M.M., Irving, E., Scheinmann, F., and Hale, K.J. (2004). New Total Synthesis of the Marine Antitumor Alkaloid (−)-Agelastatin A. Org. Lett. *6*, 2615–2618.

Dong, G. (2010a). Recent advances in the total synthesis of agelastatins. Pure Appl. Chem. *82*.

Dong, G. (2010b). A Historical Story on the Synthesis of Agelastatin. Pure Appl. Chem. 2231–2314.

Duspara, P.A., and Batey, R.A. (2013). A Short Total Synthesis of the Marine Sponge Pyrrole-2-aminoimidazole Alkaloid (±)-Agelastatin A. Angew. Chem. Int. Ed. *52*, 10862–10866.

Emsley, P., and Cowtan, K. (2004). *Coot* : model-building tools for molecular graphics. Acta Crystallogr. D Biol. Crystallogr. *60*, 2126–2132.

Eyler, D.E., and Green, R. (2011). Distinct response of yeast ribosomes to a miscoding event during translation. RNA *17*, 925–932.

Forte, B., Malgesini, B., Piutti, C., Quartieri, F., Scolaro, A., and Papeo, G. (2009). A Submarine Journey: The Pyrrole-Imidazole Alkaloids. Mar. Drugs *7*, 705–753.

Gandhi, V., Plunkett, W., and Cortes, J.E. (2014). Omacetaxine: A Protein Translation Inhibitor for Treatment of Chronic Myelogenous Leukemia. Clin. Cancer Res. *20*, 1735–1740.

Garreau de Loubresse, N., Prokhorova, I., Holtkamp, W., Rodnina, M.V., Yusupova, G., and Yusupov, M. (2014). Structural basis for the inhibition of the eukaryotic ribosome. Nature *513*, 517–522.

Goddard-Borger, E.D., and Stick, R.V. (2007). An efficient, inexpensive, and shelf-stable diazotransfer reagent: imidazole-1-sulfonyl azide hydrochloride. Org. Lett. *9*, 3797–3800.

Gomez-Lorenzo, M.G. (2000). Three-dimensional cryo-electron microscopy localization of EF2 in the Saccharomyces cerevisiae 80S ribosome at 17.5 A resolution. EMBO J. *19*, 2710–2718.

Guerriero, A., D'Ambrosio, M., Chiasera, G., and Pietra, F. (1994). Conformational Preferences and Absolute Configuration of Agelastatin A, a Cytotoxic Alkaloid of the Axinellid SpongeAgelas dendromorpha from the Coral Sea,via combined molecular modelling, NMR, and exciton splitting for diamide and hydroxyamide derivatives. Helv. Chim. Acta *77*, 1895–1902.

Han, S., Siegel, D.S., Morrison, K.C., Hergenrother, P.J., and Movassaghi, M. (2013). Synthesis and Anticancer Activity of All Known (−)-Agelastatin Alkaloids. J. Org. Chem. *78*, 11970–11984.

Head, S.A., Shi, W., Zhao, L., Gorshkov, K., Pasunooti, K., Chen, Y., Deng, Z., Li, R., Shim, J.S., Tan, W., et al. (2015). Antifungal drug itraconazole targets VDAC1 to modulate the AMPK/mTOR signaling axis in endothelial cells. Proc. Natl. Acad. Sci. *112*, E7276–E7285.

Hong, T.W., Jímenez, D.R., and Molinski, T.F. (1998). Agelastatins C and D, New Pentacyclic Bromopyrroles from the Sponge *Cymbastela* sp., and Potent Arthropod Toxicity of (−)-Agelastatin A. J. Nat. Prod. *61*, 158–161.

Hunter, P. (2008). Harnessing Nature's wisdom. Turning to Nature for inspiration and avoiding her follies. EMBO Rep. *9*, 838–840.

Jackson, R.J., Hellen, C.U.T., and Pestova, T.V. (2010). The mechanism of eukaryotic translation initiation and principles of its regulation. Nat. Rev. Mol. Cell Biol. *11*, 113–127.

Jenner, L., Melnikov, S., de Loubresse, N.G., Ben-Shem, A., Iskakova, M., Urzhumtsev, A., Meskauskas, A., Dinman, J., Yusupova, G., and Yusupov, M. (2012). Crystal structure of the 80S yeast ribosome. Curr. Opin. Struct. Biol. *22*, 759–767.

Jouanneau, M., McClary, B., Reyes, J.C.P., Chen, R., Chen, Y., Plunkett, W., Cheng, X., Milinichik, A.Z., Albone, E.F., Liu, J.O., et al. (2016). Derivatization of agelastatin A leading to bioactive analogs and a trifunctional probe. Bioorg. Med. Chem. Lett.

Kabsch, W. (2010). *XDS*. Acta Crystallogr. D Biol. Crystallogr. *66*, 125–132.

Koehn, F.E., and Carter, G.T. (2005). The evolving role of natural products in drug discovery. Nat. Rev. Drug Discov. *4*, 206–220.

Korycka-Wołowiec, A., Wołowiec, D., and Robak, T. (2015). Ofatumumab for treating chronic lymphocytic leukemia: a safety profile. Expert Opin. Drug Saf. *14*, 1945–1959.

Lecompte, O., Ripp, R., Thierry, J.-C., Moras, D., and Poch, O. (2002). Comparative analysis of ribosomal proteins in complete genomes: an example of reductive evolution at the domain scale. Nucleic Acids Res. *30*, 5382–5390.

Leslie, B.J., and Hergenrother, P.J. (2008). Identification of the cellular targets of bioactive small organic molecules using affinity reagents. Chem. Soc. Rev. *37*, 1347.

Li, Z., Shigeoka, D., Caulfield, T.R., Kawachi, T., Qiu, Y., Kamon, T., Arai, M., Tun, H.W., and Yoshimitsu, T. (2013). An integrated approach to the discovery of potent agelastatin A analogues for brain tumors: chemical synthesis and biological, physicochemical and CNS pharmacokinetic analyses. MedChemComm *4*, 1093.

Martin, M. (2011). Cutadapt removes adapter sequences from high-throughput sequencing reads. EMBnet.journal *17*, 10.

Mason, C.K., McFarlane, S., Johnston, P.G., Crowe, P., Erwin, P.J., Domostoj, M.M., Campbell, F.C., Manaviazar, S., Hale, K.J., and El-Tanani, M. (2008). Agelastatin A: a novel inhibitor of osteopontin-mediated adhesion, invasion, and colony formation. Mol. Cancer Ther. *7*, 548–558.

Meijer, L., Thunnissen, A.-M., White, A., Garnier, M., Nikolic, M., Tsai, L.-H., Walter, J., Cleverley, K., Salinas, P., Wu, Y.-Z., et al. (2000). Inhibition of cyclin-dependent kinases, GSK-3β and CK1 by hymenialdisine, a marine sponge constituent. Chem. Biol. *7*, 51–63.

Merrick, W.C. (1992). Mechanism and regulation of eukaryotic protein synthesis. Microbiol. Rev. *56*, 291–315.

Moazed, D., Stern, S., and Noller, H.F. (1986). Rapid chemical probing of conformation in 16 S ribosomal RNA and 30 S ribosomal subunits using primer extension. J. Mol. Biol. *187*, 399–416.

Moen, M.D., McKeage, K., Plosker, G.L., and Siddiqui, M.A.A. (2007). Imatinib: a review of its use in chronic myeloid leukaemia. Drugs *67*, 299–320.

Montaser, R., and Luesch, H. (2011). Marine natural products: a new wave of drugs? Future Med. Chem. *3*, 1475–1489.

Movassaghi, M., Siegel, D.S., and Han, S. (2010). Total synthesis of all (−)-agelastatin alkaloids. Chem. Sci. *1*, 561.

Oguro, M., Suzuki-Hori, C., Nagano, H., Mano, Y., and Ikegami, S. (1979). The Mode of Inhibitory Action by Aphidicolin on Eukaryotic DNA Polymerase alpha. Eur. J. Biochem. *97*, 603–607.

Ortholand, J.-Y., and Ganesan, A. (2004). Natural products and combinatorial chemistry: back to the future. Curr. Opin. Chem. Biol. *8*, 271–280.

Otto, G.A., and Puglisi, J.D. (2004). The Pathway of HCV IRES-Mediated Translation Initiation. Cell *119*, 369–380.

Pfeffer, S., Lagos-Quintana, M., and Tuschl, T. (2005). Cloning of Small RNA Molecules. In Current Protocols in Molecular Biology, F.M. Ausubel, R. Brent, R.E. Kingston, D.D. Moore, J.G. Seidman, J.A. Smith, and K. Struhl, eds. (Hoboken, NJ, USA: John Wiley & Sons, Inc.), p.

Polacek, N., and Mankin, A.S. (2005). The Ribosomal Peptidyl Transferase Center: Structure, Function, Evolution, Inhibition. Crit. Rev. Biochem. Mol. Biol. *40*, 285–311.

Rennhack, A., Jumpertz, T., Ness, J., Baches, S., Pietrzik, C.U., Weggen, S., and Bulic, B. (2012). Synthesis of a potent photoreactive acidic γ-secretase modulator for target identification in cells. Bioorg. Med. Chem. *20*, 6523–6532.

Reyes, J.C.P., and Romo, D. (2012). Bioinspired Total Synthesis of Agelastatin A. Angew. Chem. Int. Ed. *51*, 6870–6873.

Rodriguez, R.A., Pan, C.-M., Yabe, Y., Kawamata, Y., Eastgate, M.D., and Baran, P.S. (2014). Palau'chlor: A Practical and Reactive Chlorinating Reagent. J. Am. Chem. Soc. *136*, 6908–6911.

Rodriguez-Fonseca, C., Amils, R., and Garrett, R.A. (1995). Fine Structure of the Peptidyl Transferase Centre on 23 S-like rRNAs Deduced from Chemical Probing of Antibiotic-Ribosome Complexes. J. Mol. Biol. *247*, 224–235.

Rouskin, S., Zubradt, M., Washietl, S., Kellis, M., and Weissman, J.S. (2013). Genome-wide probing of RNA structure reveals active unfolding of mRNA structures in vivo. Nature *505*, 701–705.

Schneider-Poetsch, T., Ju, J., Eyler, D.E., Dang, Y., Bhat, S., Merrick, W.C., Green, R., Shen, B., and Liu, J.O. (2010). Inhibition of eukaryotic translation elongation by cycloheximide and lactimidomycin. Nat. Chem. Biol. *6*, 209–217.

Siegfried, N.A., Busan, S., Rice, G.M., Nelson, J.A.E., and Weeks, K.M. (2014). RNA motif discovery by SHAPE and mutational profiling (SHAPE-MaP). Nat. Methods *11*, 959–965.

Spadari, S., Sala, F., and Pedrali-Noy, G. (1982). Aphidicolin: a specific inhibitor of nuclear DNA replication in eukaryotes. Trends Biochem. Sci. *7*, 29–32.

Stien, D., Anderson, G.T., Chase, C.E., Koh, Y., and Weinreb, S.M. (1999). Total Synthesis of the Antitumor Marine Sponge Alkaloid Agelastatin A. J. Am. Chem. Soc. *121*, 9574–9579.

Stout, E.P., Choi, M.Y., Castro, J.E., and Molinski, T.F. (2014). Potent Fluorinated Agelastatin Analogues for Chronic Lymphocytic Leukemia: Design, Synthesis, and Pharmacokinetic Studies. J. Med. Chem. *57*, 5085–5093.

Syvret, R.G., Butt, K.M., Nguyen, T.P., Bulleck, V.L., and Rieth, R.D. (2002). Novel process for generating useful electrophiles from common anions using Selectfluor fluorination agent. J. Org. Chem. *67*, 4487–4493.

Tilvi, S., Moriou, C., Martin, M.-T., Gallard, J.-F., Sorres, J., Patel, K., Petek, S., Debitus, C., Ermolenko, L., and Al-Mourabit, A. (2010). Agelastatin E, Agelastatin F, and Benzosceptrin C from the Marine Sponge *Agelas dendromorpha*. J. Nat. Prod. *73*, 720–723.

Titov, D.V., and Liu, J.O. (2012). Identification and validation of protein targets of bioactive small molecules. Bioorg. Med. Chem. *20*, 1902–1909.

Wehn, P.M., and Du Bois, J. (2009). A Stereoselective Synthesis of the Bromopyrrole Natural Product (−)-Agelastatin A. Angew. Chem. Int. Ed. *48*, 3802–3805.

Wermuth, C.G., Aldous, D., Raboisson, P., and Rognan, D. (2015). The Practice of Medicinal Chemistry, fourth ed. (Elsevier).

Ye, C., and Shreeve, J.M. (2004). Structure-dependent oxidative bromination of unsaturated C-C bonds mediated by selectfluor. J. Org. Chem. *69*, 8561–8563.

Zhou, C.-Y., Li, J., Peddibhotla, S., and Romo, D. (2010). Mild Arming and Derivatization of Natural Products via an In(OTf) $_3$ -Catalyzed Arene Iodination. Org. Lett. *12*, 2104–2107.

Ziegler, S., Pries, V., Hedberg, C., and Waldmann, H. (2013). Target Identification for Small Bioactive Molecules: Finding the Needle in the Haystack. Angew. Chem. Int. Ed. *52*, 2744–2792.

(2007). All natural. Nat. Chem. Biol. *3*, 351–351.

CURRICULUM VITAE FOR Ph.D. CANDIDATES

The Johns Hopkins University School of Medicine

Brandon T. McClary October 1, 2016

Education History:

Ph.D. expected 2016; Program in Biochemistry Cellular and Molecular Biology-Pharmacology; Johns Hopkins School of Medicine
Mentor: Jun O. Liu, Ph.D.

B.S. 2010; Biological Sciences, minor in Psychology; University of Maryland, Baltimore County (UMBC)

Professional Experience:

Doctoral Candidate, Aug 2010-Present, Lab of Jun O. Liu, Ph.D., Department of Pharmacology and Molecular Sciences, Johns Hopkins School of Medicine

Coursera Online Certification, Sept 16 2016-Oct 2016, Design and Interpretation of Clinical Trials by Janet Holbrook, Ph.D., MPH and Lea Drye, Ph.D., Johns Hopkins University

UNCF Merck Summer Intern, Jun 2010-Aug 2010 and Jun 2009-Aug 2009, Research Advisor: Rene Bartz, Ph.D., Merck Research Labs, RNA Therapeutics Department, West Point, PA

UMBC Student Events Board President, Apr 2009-Apr 2010, Event Programmer, Apr 2007-Apr 2009, University of Maryland, Baltimore County

Research Assistant, Aug 2008-May 2010, Research Advisor: Dr. Charles Bieberich, University of Maryland, Baltimore County

Summer Intern, May 2008-Aug 2008, Research Advisor: Dr. Richard Bodnar, Summer Undergraduate Research Program, University of Pittsburgh

Summer Intern, Jun 2007- Aug 2007, Research Advisor: Dr. Nancy Colburn, NIH Summer Internship Program, National Cancer Institute, Frederick, MD

Scholarships and Fellowship Awards

F31 Predoctoral National Research Service Grant Award Recipient, 5F31AT008324-02/AT/NCCIH, 2014-2016

UNCF/Merck Science Initiative Undergraduate Fellow; 2009-2010

UMBC Meyerhoff Scholar; 2006-2010

Publications

Jouanneau, M., **McClary, B**., Reyes, J.C.P., Chen, R., Chen, Y., Plunkett, W., Cheng, X. Milinichik, A.Z., Albone, E.F., Liu, J.O., et al. (2016). Derivatization of agelastatin A leading to bioactive analogs and a trifunctional probe. Bioorg. Med. Chem. Lett.

McClary, B., Zinshteyn, B., Meyer, M., Pellegrino, S., Yusupova, G., Schuller, A., Jouanneau, M., Reyes, J.C.,Yu J., Luo, C., Dang Y., Romo, D.,Yusupov, M., Green R., Liu, J.O., Inhibition of Eukaryotic Translation by the Antitumor Natural Product Agelastatin A (*In preparation).*

Presentations

McClary, B., Jouanneau, M., Schuller, A., Dang, Y., Green, R., Romo, D.,Liu, J.O. Inhibition of Eukaryotic Translation by Antitumor Marine Natural Product Agelastatin A. Poster: Gordon Research Seminar and Conference: Marine Natural Products; Mar 6-11, 2016; Ventura, CA.

McClary, B., Schuller, A., Jouanneau, M., Romo, D., Green, R., Liu J.O. Elucidating the Molecular Mechanism of Action of Agelastatin A. MedImmune Day of Science; Sep 24, 2015. Gaithersburg, MD (Poster).

McClary B., Bodnar R.J., Identifying Communication Pathways between Pericyte and Endothelial Cells in Angiogenesis Using an in vitro Vasculature Model. ABRCMS; Nov 6, 2008. Orlando, Florida (Talk).

Honors and Activities

Regulatory Affairs Professionals Society; 2015-present

Judge, Annual Biomedical Conference for Minority Students; 2015

American Society for Cell Biology Member; 2014

Biomedical Careers Initiative; 2014-2015

Hopkins Biotech Network; 2013-2015

AAAS/Science Program for Excellence in Science Member; 2013

UMBC Chapter of Young Alumni; 2011-2014

Incentive Mentoring Program; 2011-2014

VP of Events, Johns Hopkins Biomedical Scholars Association; 2010-2011